

Nanoparticles for drug delivery to ocular neovascularizations

Dissertation to obtain the Degree of Doctor of Natural Sciences

(Dr. rer. nat.)

from the Faculty of Chemistry and Pharmacy

Universität Regensburg



Presented by

Alexandra Ławrowska, née Haunberger

from Pfarrkirchen

July 2021

This dissertation was supervised by Prof. Dr. Achim Göpferich.

Doctoral application submitted on:	22 nd July 2021
Date of examination:	21 st October 2021
Examination board:	
Chairman:	Prof. Dr. Jens Schloßmann
First referee:	Prof. Dr. Achim Göpferich
Second referee:	Prof. Dr. Miriam Breunig
Third examiner:	Prof. Dr. Rainer Müller

To my Family

Table of Contents

Chapter 1	Introduction	1
Chapter 2	Goals of the thesis	23
Chapter 3	New approaches for the fine tuning of size and surface charge of lipid nanocapsules	27
Chapter 4	Modification of LNC with an integrin-binding peptide for endothelial cell targeting	49
Chapter 5	Antiproliferative effect of cyclosporin A and itraconazole loaded LNC on microvascular endothelial cells	75
Chapter 6	Antiproliferative effect of drug-loaded LNC in a mouse model of retinal neovascularization	105
Chapter 7	Summary and conclusion	123
Appendix	Abbreviations	128
	Curriculum Vitae	132
	List of Publications	133
	Acknowledgements	134
	Statement in Lieu of an Oath	137

Introduction

Our eyes are our windows to the world. Therefore, for most people vision is their highest health priority [1] and they are less afraid of death from cancer, stroke or heart attack than of losing their vision [2]. But pathological neovascularizations severely threaten our sense of sight. In the following, the anatomy of the retina, its blood supply and the pathogenesis of retinal and choroidal neovascular diseases are reviewed.

1.1 Anatomy of the retina

1.1.1 The retina

The retina is a multi-layer neuronal tissue inside the posterior eye globe. In humans, it has a thickness of 0.4 mm at the border of the optic nerve head and is thinning toward the periphery with approximately 0.14 mm at the ora serrata and in the area of the foveola with 0.18 mm [3].

The different layers and cell types of the retina are shown in Figure 1. The outermost layer of the neural retina is built by the outer and inner segments of the photoreceptors (rods and cones). The photoreceptor nuclei are located in the outer nuclear layer (ONL) and the outer plexiform layer (OPL) is mainly formed by the axons of the photoreceptor cells and their synapses with bipolar cells. The inner nuclear layer (INL) is composed of the nuclear bodies of Müller cells and the major classes of interneurons: bipolar cells, amacrine cells and horizontal cells [3,4]. These interneurons and their microcircuits act as image processor, regulating photoreceptor sensitivity, analyzing various facets of their signals and modulating their signal transduction. The neuronal impulses are forwarded to ganglion cells, which transmit them to the lateral geniculate nucleus in the brain [2]. The axons of the bipolar and amacrine cells and their connection to the dendrites of ganglion cells constitute the inner plexiform layer (IPL). The nuclei of ganglion cells are located in the ganglion cell layer (GCL) and their axons traverse the nerve fiber layer (NFL) to the optic disk from where they leave the eye. The NFL is lined by the inner limiting membrane, a basement membrane structure formed by the footpads of Müller cells, that adjoins the vitreous body [3].

On the outer part of the neural retina, the photoreceptor layer is separated from the vessels of the choriocapillaris by the retinal pigment epithelium (RPE) and Bruch's membrane. The RPE is a monolayer of highly pigmented cuboidal cells that, on the one hand, form a tight barrier between the retina and the choroid, but on the other hand facilitate the diffusion and selective transport of nutrients and signal molecules from the choroid to the retina and the removal of waste from the

photoreceptor layer toward the choroid. The basolateral membrane of the RPE constitutes the inner layer of Bruch's membrane. The remainder is composed of two collagenous zones, an elastin layer in between them, and the basement membrane of the choriocapillaris [3,5].

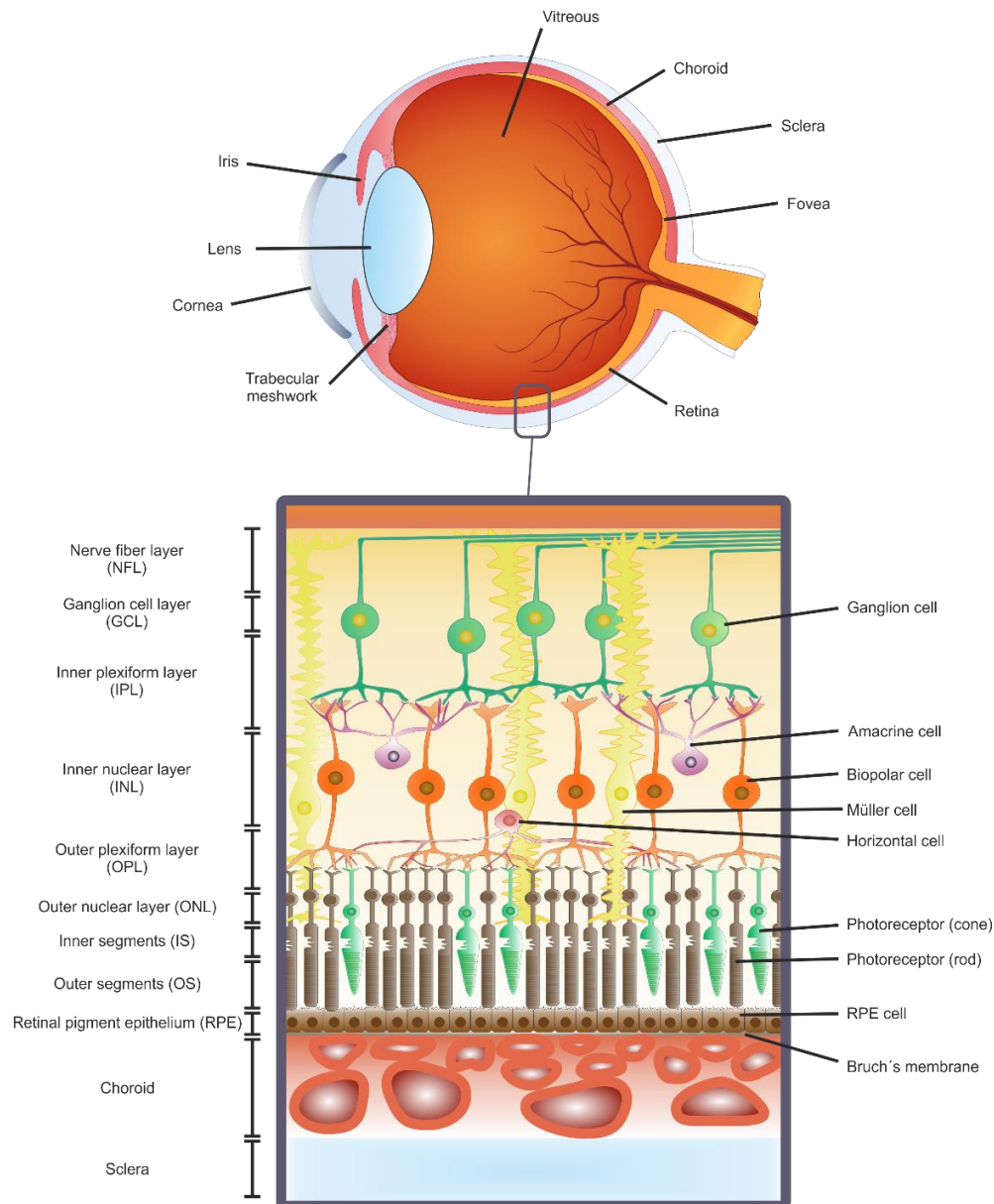


Figure 1: The anatomy of the eye with focus on the retinal layers and cell types. The light enters the eye globe through the lens and initiates neuronal impulses in the photoreceptors. The signals are forwarded via the interneurons to the ganglion cells, which finally transmit the information to the brain.

Besides the different types of neuronal cells, glia represent another cell population that is crucial for retinal function. Microglia are the primary resident innate immune cells of the retina acting as defense against pathogens and initiators of inflammation, but they also exhibit neuroprotective effects and promote tissue repair. Müller cells and astrocytes constitute the group of macroglia. They play an important role in the transport of nutrients, waste products, ions, water and other molecules between vessels and neurons. Müller cells span the entire thickness of the neuroretina while their nuclei are located in the inner nuclear layer [6]. They also function as scaffold for the retina and support the inner segments of photoreceptors [3]. Astroglia are mainly found in the NFL and the ganglion cell layer [6] and play a crucial role in the developmental vascularization of the retina [6–8].

1.1.1 Retinal blood supply

During fetal development, the retina is mostly supplied by the hyaloid, an arterial network which originates from the hyaloid artery in the optic nerve, spanning the vitreous and leaving the eye through an annular collection vessel at the front of the eye to the venous choroidal net. The choroid and the hyaloid develop early in the gestation, while the retinal vessel development starts later around the 15th week of gestation. The retinal vasculature starts to form around the optic nerve head, spreads in a primary plexus along the NFL towards the outer parts of the retina, before the vessels sprout deeper into the retina to form a secondary plexus. In humans, retinal vessels replace the hyaloid vasculature around mid-gestation, in mice in contrast, this switch takes place only around birth [8,9]. After the vascular development is completed, the inner two thirds of the retina are nourished by intra-retinal vessels, while the photoreceptors in the avascular outer one third are supplied by the choriocapillaris [10,11].

The central retinal artery branches off the ophthalmic artery and, at the optic disk, divides into four arteriole branches, which run through the NFL right below the internal limiting membrane [3]. These arterioles belong to the superficial vascular complex (SVC), which also contains venules and capillaries and is located in the NFL and GCL [10]. Another vascular complex, which is sometimes assigned to the superficial vascular complex [12,13], is the radial peripapillary capillary plexus (RPCP), which can be found in the NFL in a small rim around the optic nerve head [10,13]. The intermediate capillary plexus (ICP) is located at the boundary between the IPL and the INL and the deep capillary plexus perfuses the region between the INL and the OPL. The ICP and the

DCP can be summarized to the deep vascular complex (DVC) and merge into one network in the periphery of the retina, where the INL is too thin to separate them [13]. They are predominantly formed by capillary-sized vessels. The vascular plexuses run in parallel laminar planes in most of the retina, but are interconnected vertically with each other [10,13]. The choroidal and retinal vessels are schematically shown in Figure 2.

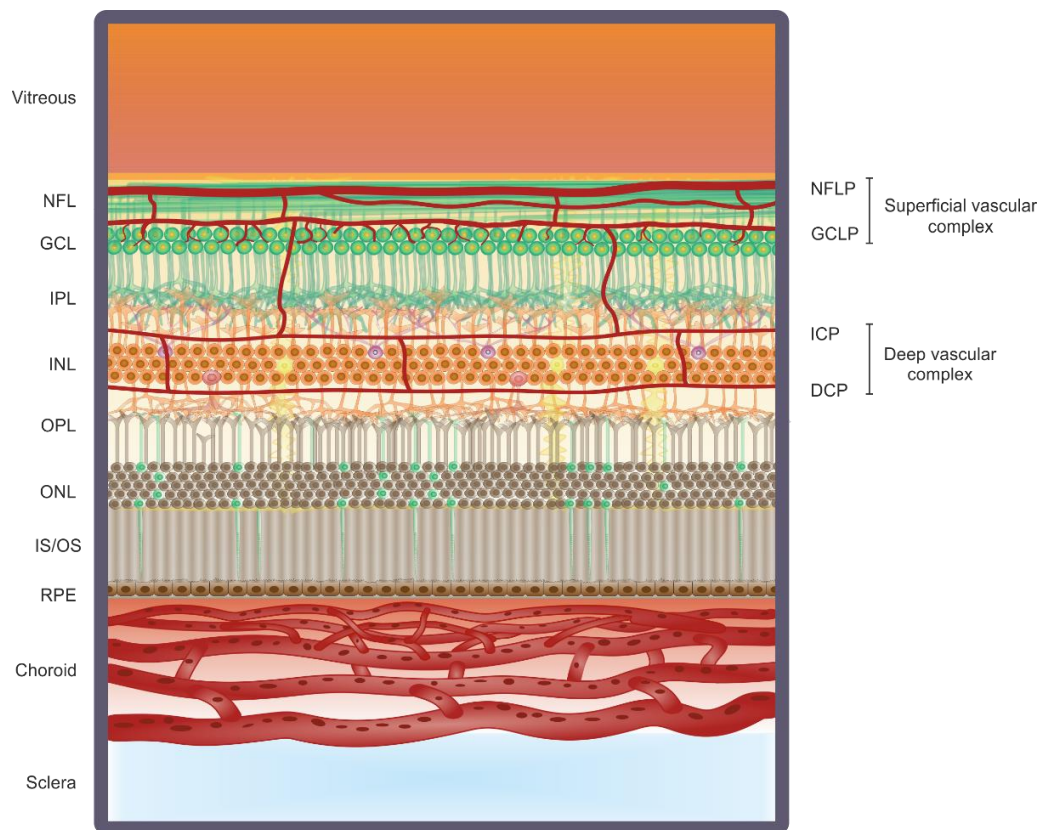


Figure 2: Schematic depiction of the vascular layers in the posterior eye. While the photoreceptors are supplied by the fenestrated vessels of the choroid, the inner layers of the retina are nourished by the intraretinal vessels of the nerve fiber layer plexus (NFLP), ganglion cell layer plexus (GCLP), intermediate capillary plexus (ICP) and deep capillary plexus (DCP). The horizontal vascular layers in the retina are connected by vertically orientated vessels.

Situated around the foveola is a capillary-free area with about 400 μm diameter [3]. This enables an unobstructed passage of light to the photoreceptors within this region of best visual acuity [10]. In the foveola, the retina is completely supplied by the choroidal circulation, which is possible due to the thinness of the retina in this area [10].

The retinal vessels are lined by continuous endothelium with tight junctional complexes forming the inner blood retinal barrier (iBRB). Intramural pericytes are found almost in a one to one ratio with endothelial cells and share a common basal lamina with them. Pericytes together with smooth muscle cells provide structural support for the vessels and play an important role in the autoregulation of retinal blood flow [14]. The iBRB is impermeable to even small molecules like glucose or amino acids so that transport systems are required for them to cross the endothelium [5].

The outer blood retina barrier (oBRB) is formed by the RPE and Bruch's membrane together with the endothelium of choriocapillaris [10]. A high gradient of oxygen tension is required to uphold a sufficient diffusion through this barrier for the supply of photoreceptors. This gradient is maintained by the extraordinarily high blood flow in the choroid, which is probably the highest of any tissue in the body in relation to the tissue weight [5]. The choroid exerts multiple tasks besides supplying oxygen and nutrients to the retina. It removes phototoxic metabolic waste products [5,10], drains aqueous humor from the anterior chamber, regulates the temperature of the retina and it even helps to bring the photoreceptors into the plane of focus by active thickening and thinning [5]. The choriocapillaris is highly anastomosed and, in contrast to retinal capillaries, fenestrated. The fenestrations are mainly located at the side facing the RPE and enable a high permeability to proteins. This results in a high oncotic pressure in the extravascular stroma enhancing the movement of fluids from the retina to the choroid. The choriocapillaris has a thickness of 10 μm at the fovea and 7 μm in the periphery. Below the capillaries lie the medium and small arteries and arterioles of Sattler's layer over the larger vessels of Haller's layer. The thickness of the whole choroid is about 200 μm in young adult humans, but decreases to about 80 μm by the age of 90 [5].

1.2 Neovascular diseases of the posterior eye

Age-related macular degeneration (AMD), diabetic retinopathy (DR) and retinopathy of prematurity (ROP) all are among the leading causes of blindness worldwide. In all three disorders the so called 'wet' forms coming along with neovascularizations (NV) are ranked among the most severe disease manifestations and bear a substantial risk of vision loss [15–18].

1.2.1 Age-related macular degeneration

Worldwide, AMD is the major cause of irreversible blindness in elderly patients and around 70% of blindness in general are caused by this disease [19,20]. In the early stages of AMD, deposits are formed mostly between the basement membrane of the RPE and the inner collagenous layer of Bruch's membrane. These deposits are called drusen and consist mainly of lipids, proteins, zinc and iron ions. Another type of drusen occurs between the basement membrane of the RPE and its plasma membrane and consists of basement membrane proteins and collagen [21].

Additionally, RPE abnormalities are sometimes already found early in the disease progression, although in the early stage of AMD, only minor visual symptoms are observed. Late AMD can manifest either as a dry or a wet form. The dry form, termed geographic atrophy, is characterized by a massive loss of RPE cells, overlying photoreceptors and underlying choroidal capillaries in a sharply defined area mostly starting in the perifoveal region. Histological studies suggest that RPE atrophy takes place first, followed by the choriocapillaris [21], but it is still a matter of discussion whether the loss of RPE leads to dysfunctional choroidal vasculature or vice versa [5,22,23]. Various important risk factors that have been reported for AMD, like age, smoking, alcohol consumption, diet, and obesity, are linked to oxidative stress, so it seems obvious that oxidative stress might play a key role in AMD pathogenesis. An alternate pathological model postulates that innate immunity and autoimmune components, like complement factors, cytokines, macrophages, and microglia are involved in AMD [24] and that an aggressive inflammatory response to drusen formation in genetically predisposed individuals causes secondary damage to the retinal pigment epithelium [25].

In wet AMD, choriocapillaris degeneration initially occurs in the presence of a viable RPE [5]. It is hypothesized that the RPE responds to oxidative stress by producing vascular endothelial growth factor (VEGF), triggering choroidal neovascularizations (CNV; Figure 3A). Depending on the degree of invasion of the newly formed vessels into the retina, neovascular AMD is classified in three subtypes. In type 1, the CNV are located below the RPE, in type 2, they penetrate the subretinal space and in type 3, they reach into the retina and anastomosis between retinal and choroidal capillaries can occur. The newly formed vessels are typically leaky and can cause edema and hemorrhage [21,26–28]. Neovascular AMD accounts for only 10 – 20% of total AMD cases, but often results in a sudden and severe vision loss. In contrast, the visual impairment in geographic atrophy usually progresses gradually and is less severe [29,17,16].

Today, neovascular AMD is mainly treated by the intravitreal injection of anti-VEGF drugs [30]. Other options are photodynamic therapy, for which the photosensitizing dye verteporfin is administered intravenously prior to treatment with a photo-activating laser applied through the eye [31], or laser photocoagulation (LPC). Although LPC can reduce the risk of CNV progression and vision loss, it causes damage to the overlying retina, bears the risk of iatrogenic scotoma, and is therefore not recommended in current guidelines for the treatment of AMD [32,33]. In photodynamic therapy, the photo-activated verteporfin emits free radicals that seal the blood vessels without affecting the retina, which makes this procedure less destructive. Due to the availability of the more effective anti-VEGF therapies, PDT became less important as monotherapy for AMD but is still used in combination regimens [31].

The discovery of VEGF as key player in neovascularization and vessel hyper-permeability in the 1990s [34–36] paved the way for the development of today's anti-VEGF therapies for proliferative eye diseases. The first anti-VEGF drug to be used for neovascular AMD was pegaptanib (Macugen®), an aptamer that binds VEGF₁₆₅ [37]. Later, the success of ranibizumab (Lucentis®), an antibody fragment binding all VEGF-A isoforms [37], in clinical trials [38] led to its approval and widespread use for the treatment of neovascular AMD. The antibody bevacizumab (Avastin®), which is approved for the treatment of metastatic colon cancer [39], has been shown to be equally effective as ranibizumab [40] and is often used off-label due to its much lower costs. In contrast to ranibizumab and bevacizumab, aflibercept (Eylea®) is not an antibody. The recombinant fusion protein acts as soluble VEGF receptor scavenging all VEGF-A isoforms and VEGF-B. It additionally blocks placental growth factor [37], which is a synergistic amplifier of VEGF-driven angiogenesis [41]. The latest anti-VEGF agent is brolucizumab (Beovu®), a very small single-chain antibody fragment [42]. Its low molecular weight allows a high drug concentration in the solution for injection [32] and brolucizumab has proven noninferiority to aflibercept in two phase 3 studies [43]. The development of anti-VEGF agents allowed for the first time a visual improvement in patients with neovascular AMD, whereas PDT and LPC were only able to reduce the degree of vision loss [32,40].

Corticosteroids, like dexamethasone or triamcinolone acetonide play a minor role in AMD treatment and are only used in conjunction with anti-VEGF agents and PDT in refractory patients. As elderly people, who account for the majority of AMD patients, are more prone to adverse effects of anti-inflammatory agents, safety and toxicity must be taken into consideration [24].

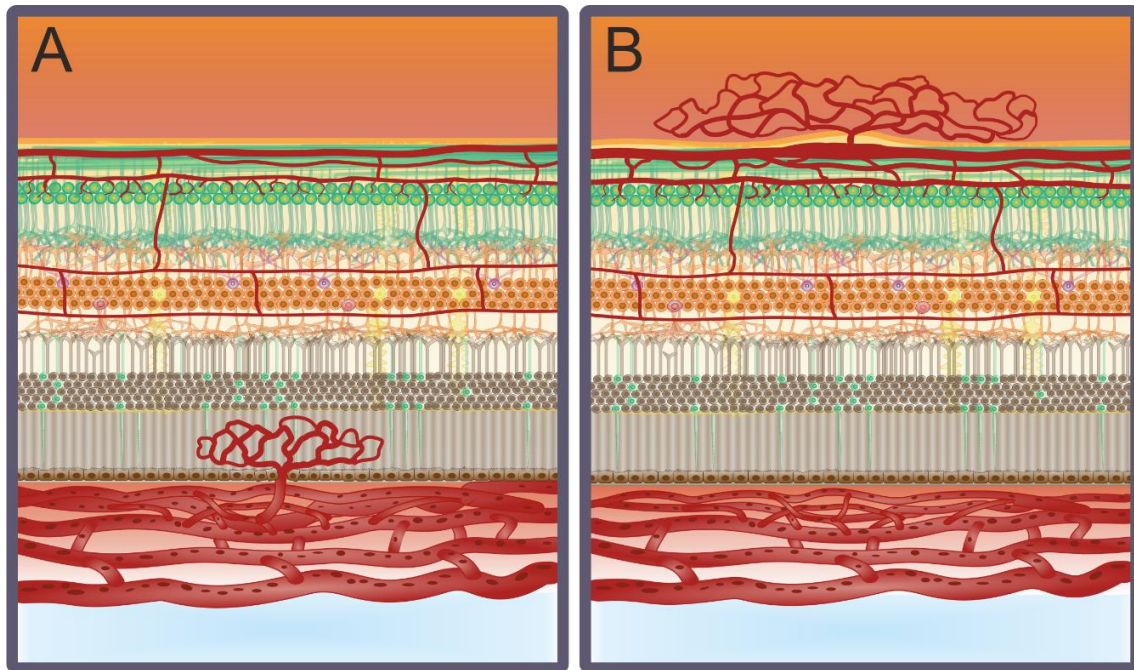


Figure 3: Different origins of pathological neovascularizations in the posterior eye. Choroidal neovascularizations sprouting from the subretinal space through the RPE (A) are characteristic for proliferative AMD, while in diabetic retinopathy and retinopathy of prematurity, neovascularizations typically emanate from intraretinal vessels (B) and may intrude into the vitreous body.

1.2.2 Diabetic retinopathy

It is estimated that about 460 million people worldwide have diabetes [44] and more than 20% of these patients develop some degree of DR [44–46]. Today, DR is the leading cause of vision loss in working-age adults and the number of vision-threatening DR has been estimated to rise further to 56.3 million by 2030 [47,48].

In early stages of DR, high blood glucose levels, an increased formation of advanced glycation end products (AGE) and the production of reactive oxygen species lead to retinal hypoperfusion and a loss of pericytes. Current research suggests that, additional to microvascular changes, also inflammatory processes and neurodegeneration play an important role in the progression of DR [46,49–51]. As a reaction to hypoperfusion, increased levels of VEGF are secreted. VEGF exhibits protective effects on various cells of the retina [52–54], but overshooting VEGF levels impair the barrier function of the endothelium by downregulating tight junctional proteins [14] and can stimulate the pathological vessel growth observed in proliferative DR [10]. In contrast to AMD,

the neovascularizations in DR are usually originating from intraretinal blood vessels, as depicted in Figure 3B. The newly formed vessels are typically leaky, can cause edema, retinal and vitreous hemorrhage, and can lead to tractional retinal detachment [55–57].

The main treatment options are intravitreal injections with VEGF inhibitors and LPC. In the last decades, great developments in laser therapies have emerged. An example are non-photocoagulating subthreshold lasers, which rather act via the stimulation of outer retinal tissues, primarily the RPE, than by the destruction of neovascular areas. But nevertheless, today laser therapy is playing a minor role besides anti-VEGF drugs, mostly in VEGF non-responders, patients with poor visit compliance or during pregnancy. Surgical vitrectomy, in which a part of the vitreous body is removed, is a pivotal treatment option for non-clearing vitreous hemorrhage or in patients with evidence of vitreomacular traction [58]. As inflammation is assumed to be a major driving force behind DR, the use of anti-inflammatory drugs like corticosteroids seems obvious. However, although corticosteroids provide benefits in diabetic macular edema, those advantages are often counterbalanced by side effects including an increased intraocular pressure and the risk of cataract development or progression [58,59].

1.2.3 Retinopathy of prematurity

A similar succession of hypoperfusion, release of growth factors and neovascularization as observed in DR characterizes the pathomechanism of retinopathy of prematurity (ROP). ROP is one of the major reasons for avoidable blindness in children globally, especially in developing countries [60]. In 2010, approximately 170,000 preterm babies worldwide developed some degree of ROP [61].

In humans, the retinal vasculature reaches maturity at 36 – 40 weeks' gestation and is therefore not yet completely developed at birth in preterm babies. A high and variable oxygen exposure after birth, mainly due to incubators, can inhibit normal vessel growth and lead to vaso-obliteration [60,62]. When the infant is transferred from high supplemental oxygen to room air, the avascular retina becomes hypoxic and reacts with the secretion of proangiogenic factors [63] including VEGF [64,65]. The overproduction of VEGF leads to aberrant vasoproliferation, similar to that observed in DR [56]. ROP is categorized in three phases: Phase I is the stage of vaso-obliteration with an insufficient retinal vascularization, phase II is characterized by 'plus disease'

with vasoproliferation, dilatation and hemorrhage, and in phase III, the most severe manifestation, fibrovascular changes with retinal detachment are observed [60].

Until the 1990s, cryotherapy was the only treatment with proven effects for ROP, but today it has been largely replaced by LPC and anti-VEGF therapy due to better outcomes, less inflammatory response and lower rates of myopia [62]. Despite the treatment options are similar in DR and ROP, LPC plays a bigger role in the management of ROP and remains the standard of care for most ROP cases, although anti-VEGF therapy gains importance [62,66,67]. Clinical trials showed no differences in visual and safety outcomes between LPC and intravitreal anti-VEGF injections. Compared to anti-VEGF therapy, LPC had a lower likelihood of requiring additional treatment, while anti-VEGF injections were associated with a longer interval from treatment to retreatment or recurrence, reduced risk of surgical intervention and a lower risk of myopia, so both options have advantages [68]. Analogous to DR, vitrectomy can be considered to remove vitreoretinal tractional components and subsequently prevent retinal detachment [60].

1.2.4 Drawbacks of anti-VEGF therapies

The innovation of VEGF inhibitors revolutionized the therapy of neovascular eye diseases and widely replaced destructive physical treatment options [40,58,67]. For the first time, it was possible to not only delay disease progression but finally improve visual acuity [32,40] and the incidence of disease-related blindness has fallen dramatically [21].

But despite the outstanding success of anti-VEGF treatment, real-world data indicate that undertreatment due to suboptimal injection frequency is very common [21,69]. The unfavorable administration route by intraocular injections is certainly a leading cause for this issue. Apart from the procedure itself being uncomfortable, intravitreal injections often lead to increased intraocular pressure and bear the risk of intraocular injuries, endophthalmitis or uveitis, although these severe side effects are fortunately rare [70].

Systemic side effects of VEGF blockage are mainly of concern in ROP management, where infants at an early stage of life are treated. VEGF antibodies have been shown to leak into systemic circulation and to reduce systemic VEGF concentrations [71,72]. Therefore, potential side effects on organ development have to be considered and need to be further investigated in clinical trials and practice [62]. Systemic side effects after the intravitreal application of VEGF antibodies have also been observed in adults. The RISE/RIDE studies found an increased incidence of stroke in the

group treated with a higher ranibizumab dose [73], although other studies did not show increased non-ocular side effects of intravitreal anti-VEGF therapy [74].

Moreover, a rigorous and continuous VEGF inhibition can also compromise retinal cells and normal ocular vascularization. Although overshooting VEGF production is clearly associated with pathological vessel permeability and growth, the secretion of VEGF is a physiological reaction to hypoxia and oxidative stress to protect the affected tissues. Studies have shown that selective stimulation of VEGFR-1 even prevents oxygen-induced retinal vascular degeneration in retinopathy of prematurity [75] and that VEGF is a survival factor for fenestrated endothelium [76]. But the protective effects of VEGF are not limited to endothelial cells. VEGF receptors are expressed on a number of other cell types in the retina, such as Müller cells, astrocytes, photoreceptors or RPE cells [52,53,77]. *In vitro*, VEGF neutralization increased RPE cell apoptosis and reduced the microvilli by which they interact with photoreceptors [54]. Apoptosis was also detrimentally increased in Müller cells when their autocrine VEGF production was reduced with siRNA [53]. *In vivo*, reduced VEGF-signaling was associated with remarkable damage in the RPE cell layer and the choroid [54] as well as with massive neural cell death [53].

Clinically, a rigorous suppression of VEGF levels has been associated to a decrease in choroid thickness [78], and in epidemiologic studies long-term anti-VEGF therapy was described to enhance the risk of geographic atrophy accompanied by local cell death of RPE cells and photoreceptors [79–81]. A severe vision-threatening complication of anti-VEGF therapy is the development of tractional retinal detachment in patients with proliferative DR and pre-existing tractional membranes. When VEGF signaling is inhibited in these patients, the homeostasis between VEGF-associated neovascularization and connective tissue growth factor (CTGF)-associated fibrosis comes out of equilibrium, promoting cell apoptosis, fibrosis and resulting traction on the retina lying underneath the formed membranes [82–85].

Last but not least it has to be mentioned that despite the great improvement in disease prognosis due to the implementation of anti-VEGF therapy, not all patients have a long-term benefit from this approach. In AMD, 10 - 45% of all patients are non-responders [86–88] and also in DR progression can often not be stopped [45]. In ROP, the recurrence rates after anti-VEGF-treatment remain high with an incidence of up to one third in clinical trials [60,67,89]. One reason for the inadequate response to anti-VEGF may be that other molecular pathways involved in the pathogenesis of these diseases, like inflammatory response, are not targeted [24,58].

Taken together, there is a high demand for more treatment options for patients with poor response to VEGF inhibition and for approaches that do not come along with intravitreal injections or the disadvantages of an unspecific knockdown of physiological VEGF signaling. Although VEGF inhibitors have been an important milestone in the fight against neovascular eye diseases, they should not be the end of the road.

1.3 References

- [1] V.W. Li, I.R. Gabriel, M.M. Li, A.N. Antoszyk, C.W. Baker, P.U. Dugel, R.A. Goldberg, J.S. Heier, A.C. Ho, J.S. Pollack, C.C. Wykoff, D. Vavvas, W.W. Li, Treatment and Management of Neovascular AMD: Impact on Patients, *Invest. Ophthalmol. Vis. Sci.* 60 (2019) 136–136.
- [2] H.J. Kaplan, Anatomy and Function of the Eye, in: J.Y. Niederkorn, H.J. Kaplan (Eds.), *Chemical Immunology and Allergy*, Karger, Basel, 2007: pp. 4–10. <https://doi.org/10.1159/000099236>.
- [3] M.P. Gupta, A.A. Herzlich, T. Sauer, C.-C. Chan, Retinal Anatomy and Pathology, in: Q.D. Nguyen, E.B. Rodrigues, M.E. Farah, W.F. Mieler, D.V. Do (Eds.), *Developments in Ophthalmology*, S. Karger AG, 2015: pp. 7–17. <https://doi.org/10.1159/000431128>.
- [4] R.H. Masland, Cell Populations of the Retina: The Proctor Lecture, *Invest. Ophthalmol. Vis. Sci.* 52 (2011) 4581–4591. <https://doi.org/10.1167/iovs.10-7083>.
- [5] D.L. Nickla, J. Wallman, The multifunctional choroid, *Progress in Retinal and Eye Research*. 29 (2010) 144–168. <https://doi.org/10.1016/j.preteyeres.2009.12.002>.
- [6] A. Reichenbach, A. Bringmann, Glia of the human retina, *Glia*. 68 (2020) 768–796. <https://doi.org/10.1002/glia.23727>.
- [7] M. Fruttiger, Development of the Mouse Retinal Vasculature: Angiogenesis Versus Vasculogenesis, *Invest. Ophthalmol. Vis. Sci.* 43 (2002) 522–527.
- [8] M. Fruttiger, Development of the retinal vasculature, *Angiogenesis*. 10 (2007) 77–88. <https://doi.org/10.1007/s10456-007-9065-1>.
- [9] M. Saint-Geniez, P.A. D’Amore, Development and pathology of the hyaloid, choroidal and retinal vasculature, *Int J Dev Biol.* 48 (2004) 1045–1058. <https://doi.org/10.1387/ijdb.041895ms>.
- [10] J. Kur, E.A. Newman, T. Chan-Ling, Cellular and physiological mechanisms underlying blood flow regulation in the retina and choroid in health and disease, *Progress in Retinal and Eye Research*. 31 (2012) 377–406. <https://doi.org/10.1016/j.preteyeres.2012.04.004>.
- [11] S. Selvam, T. Kumar, M. Fruttiger, Retinal vasculature development in health and disease, *Progress in Retinal and Eye Research*. 63 (2018) 1–19. <https://doi.org/10.1016/j.preteyeres.2017.11.001>.
- [12] C. Lavia, P. Mecê, M. Nassisi, S. Bonnin, J. Marie-Louise, A. Couturier, A. Erginay, R. Tadayoni, A. Gaudric, Retinal Capillary Plexus Pattern and Density from Fovea to Periphery Measured in Healthy Eyes with Swept-Source Optical Coherence Tomography Angiography, *Sci Rep*. 10 (2020) 1474. <https://doi.org/10.1038/s41598-020-58359-y>.

-
- [13] T.T. Hormel, Y. Jia, Y. Jian, T.S. Hwang, S.T. Bailey, M.E. Pennesi, D.J. Wilson, J.C. Morrison, D. Huang, Plexus-specific retinal vascular anatomy and pathologies as seen by projection-resolved optical coherence tomographic angiography, *Progress in Retinal and Eye Research*. 80 (2021) 100878. <https://doi.org/10.1016/j.preteyeres.2020.100878>.
- [14] C.J. Pournaras, E. Rungger-Brändle, C.E. Riva, S.H. Hardarson, E. Stefansson, Regulation of retinal blood flow in health and disease, *Progress in Retinal and Eye Research*. 27 (2008) 284–330. <https://doi.org/10.1016/j.preteyeres.2008.02.002>.
- [15] J.L. Leasher, R.R.A. Bourne, S.R. Flaxman, J.B. Jonas, J. Keeffe, K. Naidoo, K. Pesudovs, H. Price, R.A. White, T.Y. Wong, S. Resnikoff, H.R. Taylor, Global Estimates on the Number of People Blind or Visually Impaired by Diabetic Retinopathy: A Meta-analysis From 1990 to 2010, *Diabetes Care*. 39 (2016) 1643–1649. <https://doi.org/10.2337/dc15-2171>.
- [16] R.R.A. Bourne, J.B. Jonas, A.M. Bron, M.V. Cicinelli, A. Das, S.R. Flaxman, D.S. Friedman, J.E. Keeffe, J.H. Kempen, J. Leasher, H. Limburg, K. Naidoo, K. Pesudovs, T. Peto, J. Saadine, A.J. Silvester, N. Tahhan, H.R. Taylor, R. Varma, T.Y. Wong, S. Resnikoff, Prevalence and causes of vision loss in high-income countries and in Eastern and Central Europe in 2015: magnitude, temporal trends and projections, *British Journal of Ophthalmology*. 102 (2018) 575–585. <https://doi.org/10.1136/bjophthalmol-2017-311258>.
- [17] R.R.A. Bourne, G.A. Stevens, R.A. White, J.L. Smith, S.R. Flaxman, H. Price, J.B. Jonas, J. Keeffe, J. Leasher, K. Naidoo, K. Pesudovs, S. Resnikoff, H.R. Taylor, Vision Loss Expert Group, Causes of vision loss worldwide, 1990–2010: a systematic analysis, *Lancet Glob Health*. 1 (2013) e339–349. [https://doi.org/10.1016/S2214-109X\(13\)70113-X](https://doi.org/10.1016/S2214-109X(13)70113-X).
- [18] W.L. Wong, X. Su, X. Li, C.M.G. Cheung, R. Klein, C.-Y. Cheng, T.Y. Wong, Global prevalence of age-related macular degeneration and disease burden projection for 2020 and 2040: a systematic review and meta-analysis, *The Lancet Global Health*. 2 (2014) e106–e116. [https://doi.org/10.1016/S2214-109X\(13\)70145-1](https://doi.org/10.1016/S2214-109X(13)70145-1).
- [19] M.A. Zarbin, Age-Related Macular Degeneration: Review of Pathogenesis, *European Journal of Ophthalmology*. 8 (1998) 199–206. <https://doi.org/10.1177/112067219800800401>.
- [20] M.A. Zarbin, Current concepts in the pathogenesis of age-related macular degeneration, *Arch Ophthalmol*. 122 (2004) 598–614. <https://doi.org/10.1001/archopht.122.4.598>.
- [21] P. Mitchell, G. Liew, B. Gopinath, T.Y. Wong, Age-related macular degeneration, *The Lancet*. 392 (2018) 1147–1159. [https://doi.org/10.1016/S0140-6736\(18\)31550-2](https://doi.org/10.1016/S0140-6736(18)31550-2).
- [22] A. Biesemeier, T. Taubitz, S. Julien, E. Yoeuruek, U. Schraermeyer, Choriocapillaris breakdown precedes retinal degeneration in age-related macular degeneration, *Neurobiol Aging*. 35 (2014) 2562–2573. <https://doi.org/10.1016/j.neurobiolaging.2014.05.003>.

- [23] K.R. Chirco, E.H. Sohn, E.M. Stone, B.A. Tucker, R.F. Mullins, Structural and molecular changes in the aging choroid: implications for age-related macular degeneration, *Eye (Lond)*. 31 (2017) 10–25. <https://doi.org/10.1038/eye.2016.216>.
- [24] Y. Wang, V.M. Wang, C.-C. Chan, The role of anti-inflammatory agents in age-related macular degeneration (AMD) treatment, *Eye*. 25 (2011) 127–139. <https://doi.org/10.1038/eye.2010.196>.
- [25] D.H. Anderson, M.J. Radeke, N.B. Gallo, E.A. Chapin, P.T. Johnson, C.R. Curletti, L.S. Hancox, J. Hu, J.N. Ebright, G. Malek, M.A. Hauser, C. Bowes Rickman, D. Bok, G.S. Hageman, L.V. Johnson, The pivotal role of the complement system in aging and age-related macular degeneration: Hypothesis re-visited, *Progress in Retinal and Eye Research*. 29 (2010) 95–112. <https://doi.org/10.1016/j.preteyeres.2009.11.003>.
- [26] A.C. Bird, N.M. Bressler, S.B. Bressler, I.H. Chisholm, G. Coscas, M.D. Davis, P.T.V.M. de Jong, C.C.W. Klaver, B.E.K. Klein, R. Klein, P. Mitchell, J.P. Sarks, S.H. Sarks, G. Soubrane, H.R. Taylor, J.R. Vingerling, An international classification and grading system for age-related maculopathy and age-related macular degeneration, *Survey of Ophthalmology*. 39 (1995) 367–374. [https://doi.org/10.1016/S0039-6257\(05\)80092-X](https://doi.org/10.1016/S0039-6257(05)80092-X).
- [27] G.A. Peyman, J. Koziol, Age-related macular degeneration and its management, *Journal of Cataract & Refractive Surgery*. 14 (1988) 421–430. [https://doi.org/10.1016/S0886-3350\(88\)80152-4](https://doi.org/10.1016/S0886-3350(88)80152-4).
- [28] H.E. Grossniklaus, W.R. Green, Choroidal neovascularization, *American Journal of Ophthalmology*. 137 (2004) 496–503. <https://doi.org/10.1016/j.ajo.2003.09.042>.
- [29] F.L. Ferris, S.L. Fine, L. Hyman, Age-related macular degeneration and blindness due to neovascular maculopathy, *Arch Ophthalmol*. 102 (1984) 1640–1642. <https://doi.org/10.1001/archopht.1984.01040031330019>.
- [30] S.G. Schorr, H.-P. Hammes, U.A. Müller, H.-H. Abholz, R. Landgraf, B. Bertram, The prevention and treatment of retinal complications in diabetes, *Deutsches Aerzteblatt Online*. (2016). <https://doi.org/10.3238/arztebl.2016.0816>.
- [31] R. Wormald, J.R. Evans, L.L. Smeeth, K.S. Henshaw, Photodynamic therapy for neovascular age-related macular degeneration, *Cochrane Database of Systematic Reviews*. (2007). <https://doi.org/10.1002/14651858.CD002030.pub3>.
- [32] I. Mantel, Management Strategies for Neovascular AMD, in: J. Chhablani (Ed.), *Choroidal Neovascularization*, Springer, Singapore, 2020: pp. 99–108. https://doi.org/10.1007/978-981-15-2213-0_8.
- [33] G. Virgili, A. Bini, Laser photocoagulation for neovascular age-related macular degeneration, *Cochrane Database of Systematic Reviews*. (2007). <https://doi.org/10.1002/14651858.CD004763.pub2>.

-
- [34] A.P. Adamis, J.W. Miller, M.-T. Bernal, D.J. D'Amico, J. Folkman, T.-K. Yeo, K.-T. Yeo, Increased Vascular Endothelial Growth Factor Levels in the Vitreous of Eyes With Proliferative Diabetic Retinopathy, *American Journal of Ophthalmology*. 118 (1994) 445–450. [https://doi.org/10.1016/S0002-9394\(14\)75794-0](https://doi.org/10.1016/S0002-9394(14)75794-0).
- [35] L.P. Aiello, R.L. Avery, P.G. Arrigg, B.A. Keyt, H.D. Jampel, S.T. Shah, L.R. Pasquale, H. Thieme, M.A. Iwamoto, J.E. Park, Vascular endothelial growth factor in ocular fluid of patients with diabetic retinopathy and other retinal disorders, *N Engl J Med*. 331 (1994) 1480–1487. <https://doi.org/10.1056/NEJM199412013312203>.
- [36] N. Ferrara, T. Davis-Smyth, The biology of vascular endothelial growth factor, *Endocr Rev*. 18 (1997) 4–25. <https://doi.org/10.1210/edrv.18.1.0287>.
- [37] S. Fogli, M. Del Re, E. Rofi, C. Posarelli, M. Figus, R. Danesi, Clinical pharmacology of intravitreal anti-VEGF drugs, *Eye (Lond)*. 32 (2018) 1010–1020. <https://doi.org/10.1038/s41433-018-0021-7>.
- [38] R.D. Patel, R.S. Momi, S.M. Hariprasad, Review of ranibizumab trials for neovascular age-related macular degeneration, *Semin Ophthalmol*. 26 (2011) 372–379. <https://doi.org/10.3109/08820538.2011.570845>.
- [39] L.M. Ellis, Bevacizumab, *Nat Rev Drug Discov. Suppl* (2005) S8-9. <https://doi.org/10.1038/nrd1727>.
- [40] S.D. Solomon, K. Lindsley, S.S. Vedula, M.G. Krzystolik, B.S. Hawkins, Anti-vascular endothelial growth factor for neovascular age-related macular degeneration, *Cochrane Database Syst Rev*. 3 (2019) CD005139. <https://doi.org/10.1002/14651858.CD005139.pub4>.
- [41] M. Autiero, J. Waltenberger, D. Communi, A. Kranz, L. Moons, D. Lambrechts, J. Kroll, S. Plaisance, M. De Mol, F. Bono, S. Kliche, G. Fellbrich, K. Ballmer-Hofer, D. Maglione, U. Mayr-Beyrle, M. Dewerchin, S. Dombrowski, D. Stanimirovic, P. Van Hummelen, C. Dehio, D.J. Hicklin, G. Persico, J.-M. Herbert, D. Communi, M. Shibuya, D. Collen, E.M. Conway, P. Carmeliet, Role of PlGF in the intra- and intermolecular cross talk between the VEGF receptors Flt1 and Flk1, *Nat Med*. 9 (2003) 936–943. <https://doi.org/10.1038/nm884>.
- [42] A. Markham, Brolucizumab: First Approval, *Drugs*. 79 (2019) 1997–2000. <https://doi.org/10.1007/s40265-019-01231-9>.
- [43] P.U. Dugel, A. Koh, Y. Ogura, G.J. Jaffe, U. Schmidt-Erfurth, D.M. Brown, A.V. Gomes, J. Warburton, A. Weichselberger, F.G. Holz, HAWK and HARRIER Study Investigators, HAWK and HARRIER: Phase 3, Multicenter, Randomized, Double-Masked Trials of Brolucizumab for Neovascular Age-Related Macular Degeneration, *Ophthalmology*. 127 (2020) 72–84. <https://doi.org/10.1016/j.ophtha.2019.04.017>.

- [44] Z.L. Teo, Y.-C. Tham, M.C. Yan Yu, M.L. Chee, T.H. Rim, N. Cheung, M.M. Bikbov, Y.X. Wang, Y. Tang, Y. Lu, I.Y. Hin Wong, D.S. Wei Ting, G.S. Wei Tan, J.B. Jonas, C. Sabanayagam, T.Y. Wong, C.-Y. Cheng, Global Prevalence of Diabetic Retinopathy and Projection of Burden through 2045: Systematic Review and Meta-analysis, *Ophthalmology*. (2021). <https://doi.org/10.1016/j.ophtha.2021.04.027>.
- [45] A.W. Stitt, T.M. Curtis, M. Chen, R.J. Medina, G.J. McKay, A. Jenkins, T.A. Gardiner, T.J. Lyons, H.-P. Hammes, R. Simó, N. Lois, The progress in understanding and treatment of diabetic retinopathy, *Progress in Retinal and Eye Research*. 51 (2016) 156–186. <https://doi.org/10.1016/j.preteyeres.2015.08.001>.
- [46] C. Altmann, M.H.H. Schmidt, The Role of Microglia in Diabetic Retinopathy: Inflammation, Microvasculature Defects and Neurodegeneration, *Int J Mol Sci*. 19 (2018). <https://doi.org/10.3390/ijms19010110>.
- [47] D.S.W. Ting, G.C.M. Cheung, T.Y. Wong, Diabetic retinopathy: global prevalence, major risk factors, screening practices and public health challenges: a review, *Clinical & Experimental Ophthalmology*. 44 (2016) 260–277. <https://doi.org/10.1111/ceo.12696>.
- [48] D.R. Whiting, L. Guariguata, C. Weil, J. Shaw, IDF Diabetes Atlas: Global estimates of the prevalence of diabetes for 2011 and 2030, *Diabetes Research and Clinical Practice*. 94 (2011) 311–321. <https://doi.org/10.1016/j.diabres.2011.10.029>.
- [49] W. Wang, A.C.Y. Lo, Diabetic Retinopathy: Pathophysiology and Treatments, *Int J Mol Sci*. 19 (2018). <https://doi.org/10.3390/ijms19061816>.
- [50] R. Simó, A.W. Stitt, T.W. Gardner, Neurodegeneration in diabetic retinopathy: does it really matter?, *Diabetologia*. 61 (2018) 1902–1912. <https://doi.org/10.1007/s00125-018-4692-1>.
- [51] B.A. Coughlin, D.J. Feenstra, S. Mohr, Müller cells and diabetic retinopathy, *Vision Res*. 139 (2017) 93–100. <https://doi.org/10.1016/j.visres.2017.03.013>.
- [52] J.M. Rosenstein, J.M. Krum, New roles for VEGF in nervous tissue - beyond blood vessels, *Experimental Neurology*. 187 (2004) 246–253. <https://doi.org/10.1016/j.expneurol.2004.01.022>.
- [53] M. Saint-Geniez, A.S.R. Maharaj, T.E. Walshe, B.A. Tucker, E. Sekiyama, T. Kurihara, D.C. Darland, M.J. Young, P.A. D’Amore, Endogenous VEGF Is Required for Visual Function: Evidence for a Survival Role on Müller Cells and Photoreceptors, *PLOS ONE*. 3 (2008) e3554. <https://doi.org/10.1371/journal.pone.0003554>.
- [54] K.M. Ford, M. Saint-Geniez, T. Walshe, A. Zahr, P.A. D’Amore, Expression and Role of VEGF in the Adult Retinal Pigment Epithelium, *Invest. Ophthalmol. Vis. Sci*. 52 (2011) 9478. <https://doi.org/10.1167/iovs.11-8353>.
- [55] Q. Mohamed, M.C. Gillies, T.Y. Wong, Management of Diabetic Retinopathy: A Systematic Review, *JAMA*. 298 (2007) 902. <https://doi.org/10.1001/jama.298.8.902>.

-
- [56] P. Sapieha, D. Hamel, Z. Shao, J.C. Rivera, K. Zaniolo, J.S. Joyal, S. Chemtob, Proliferative retinopathies: Angiogenesis that blinds, *The International Journal of Biochemistry & Cell Biology*. 42 (2010) 5–12. <https://doi.org/10.1016/j.biocel.2009.10.006>.
- [57] D.A. Chistiakov, Diabetic retinopathy: Pathogenic mechanisms and current treatments, *Diabetes & Metabolic Syndrome: Clinical Research & Reviews*. 5 (2011) 165–172. <https://doi.org/10.1016/j.dsx.2012.02.025>.
- [58] S.E. Mansour, D.J. Browning, K. Wong, H.W. Flynn, A.R. Bhavsar, The Evolving Treatment of Diabetic Retinopathy, *Clin Ophthalmol*. 14 (2020) 653–678. <https://doi.org/10.2147/OPTH.S236637>.
- [59] J. Chawan-Saad, M. Wu, A. Wu, L. Wu, Corticosteroids for Diabetic Macular Edema, *Taiwan J Ophthalmol*. 9 (2019) 233–242. https://doi.org/10.4103/tjo.tjo_68_19.
- [60] M.E. Hartnett, Advances in understanding and management of retinopathy of prematurity, *Surv Ophthalmol*. 62 (2017) 257–276. <https://doi.org/10.1016/j.survophthal.2016.12.004>.
- [61] A.L. Solebo, L. Teoh, J. Rahi, Epidemiology of blindness in children, *Arch Dis Child*. 102 (2017) 853–857. <https://doi.org/10.1136/archdischild-2016-310532>.
- [62] R. Cayabyab, R. Ramanathan, Retinopathy of Prematurity: Therapeutic Strategies Based on Pathophysiology, *Neonatology*. 109 (2016) 369–376. <https://doi.org/10.1159/000444901>.
- [63] N. Ashton, B. Ward, G. Serpell, Effect of oxygen on developing retinal vessels with particular reference to the problem of retrolental fibroplasia, *Br J Ophthalmol*. 38 (1954) 397–432. <https://doi.org/10.1136/bjo.38.7.397>.
- [64] T. Alon, I. Hemo, A. Itin, J. Pe'er, J. Stone, E. Keshet, Vascular endothelial growth factor acts as a survival factor for newly formed retinal vessels and has implications for retinopathy of prematurity, *Nat Med*. 1 (1995) 1024–1028. <https://doi.org/10.1038/nm1095-1024>.
- [65] J. Stone, A. Itin, T. Alon, J. Pe'er, H. Gnessin, T. Chan-Ling, E. Keshet, Development of retinal vasculature is mediated by hypoxia-induced vascular endothelial growth factor (VEGF) expression by neuroglia, *J. Neurosci*. 15 (1995) 4738–4747. <https://doi.org/10.1523/JNEUROSCI.15-07-04738.1995>.
- [66] F.M. Mutlu, S.U. Sarici, Treatment of retinopathy of prematurity: a review of conventional and promising new therapeutic options, *Int J Ophthalmol*. 6 (2013) 228–236. <https://doi.org/10.3980/j.issn.2222-3959.2013.02.23>.
- [67] M.J. Sankar, J. Sankar, P. Chandra, Anti-vascular endothelial growth factor (VEGF) drugs for treatment of retinopathy of prematurity, *Cochrane Database Syst Rev*. 1 (2018) CD009734. <https://doi.org/10.1002/14651858.CD009734.pub3>.

- [68] M.M. Popovic, P. Nichani, R.H. Muni, K. Mireskandari, N.N. Tehrani, P.J. Kertes, Intravitreal anti-vascular endothelial growth factor injection versus laser photocoagulation for retinopathy of prematurity: A meta-analysis of 3,701 eyes, *Surv Ophthalmol.* (2020). <https://doi.org/10.1016/j.survophthal.2020.12.002>.
- [69] J. Talks, V. Daien, R.P. Finger, B. Eldem, T. Sakamoto, J.A. Cardillo, P. Mitchell, T.Y. Wong, J.-F. Korobelnik, The use of real-world evidence for evaluating anti-vascular endothelial growth factor treatment of neovascular age-related macular degeneration, *Survey of Ophthalmology.* 64 (2019) 707–719. <https://doi.org/10.1016/j.survophthal.2019.02.008>.
- [70] Y. Zhao, R.P. Singh, The role of anti-vascular endothelial growth factor (anti-VEGF) in the management of proliferative diabetic retinopathy, *Drugs Context.* 7 (2018). <https://doi.org/10.7573/dic.212532>.
- [71] T. Sato, K. Wada, H. Arahori, N. Kuno, K. Imoto, C. Iwahashi-Shima, S. Kusaka, Serum concentrations of bevacizumab (avastin) and vascular endothelial growth factor in infants with retinopathy of prematurity, *Am J Ophthalmol.* 153 (2012) 327-333.e1. <https://doi.org/10.1016/j.ajo.2011.07.005>.
- [72] R. Hoerster, P. Muether, C. Dahlke, K. Mehler, A. Oberthür, B. Kirchhof, S. Fauser, Serum concentrations of vascular endothelial growth factor in an infant treated with ranibizumab for retinopathy of prematurity, *Acta Ophthalmol.* 91 (2013) e74-75. <https://doi.org/10.1111/j.1755-3768.2012.02469.x>.
- [73] Q.D. Nguyen, D.M. Brown, D.M. Marcus, D.S. Boyer, S. Patel, L. Feiner, A. Gibson, J. Sy, A.C. Rundle, J.J. Hopkins, R.G. Rubio, J.S. Ehrlich, Ranibizumab for Diabetic Macular Edema: Results from 2 Phase III Randomized Trials: RISE and RIDE, *Ophthalmology.* 119 (2012) 789–801. <https://doi.org/10.1016/j.ophtha.2011.12.039>.
- [74] J.S. Heier, J.-F. Korobelnik, D.M. Brown, U. Schmidt-Erfurth, D.V. Do, E. Midena, D.S. Boyer, H. Terasaki, P.K. Kaiser, D.M. Marcus, Q.D. Nguyen, G.J. Jaffe, J.S. Slakter, C. Simader, Y. Soo, T. Schmelter, R. Vitti, A.J. Berliner, O. Zeitz, C. Metzger, F.G. Holz, Intravitreal Aflibercept for Diabetic Macular Edema: 148-Week Results from the VISTA and VIVID Studies, *Ophthalmology.* 123 (2016) 2376–2385. <https://doi.org/10.1016/j.ophtha.2016.07.032>.
- [75] S.-C. Shih, M. Ju, N. Liu, L.E.H. Smith, Selective stimulation of VEGFR-1 prevents oxygen-induced retinal vascular degeneration in retinopathy of prematurity, *J Clin Invest.* 112 (2003) 50–57. <https://doi.org/10.1172/JCI17808>.
- [76] T. Kamba, B.Y.Y. Tam, H. Hashizume, A. Haskell, B. Sennino, M.R. Mancuso, S.M. Norberg, S.M. O'Brien, R.B. Davis, L.C. Gowen, K.D. Anderson, G. Thurston, S. Joho, M.L. Springer, C.J. Kuo, D.M. McDonald, VEGF-dependent plasticity of fenestrated capillaries in the normal adult microvasculature, *Am J Physiol Heart Circ Physiol.* 290 (2006) H560-576. <https://doi.org/10.1152/ajpheart.00133.2005>.

- [77] A.S.R. Maharaj, T.E. Walshe, M. Saint-Geniez, S. Venkatesha, A.E. Maldonado, N.C. Himes, K.S. Matharu, S.A. Karumanchi, P.A. D'Amore, VEGF and TGF- are required for the maintenance of the choroid plexus and ependyma, *Journal of Experimental Medicine*. 205 (2008) 491–501. <https://doi.org/10.1084/jem.20072041>.
- [78] K. Sayanagi, Y. Jo, Y. Ikuno, Transient Choroidal Thinning after Intravitreal Bevacizumab Injection for Myopic Choroidal Neovascularization, *Journal of Clinical & Experimental Ophthalmology*. 02 (2011). <https://doi.org/10.4172/2155-9570.1000165>.
- [79] J.E. Grunwald, E. Daniel, J. Huang, G. Ying, M.G. Maguire, C.A. Toth, G.J. Jaffe, S.L. Fine, B. Blodi, M.L. Klein, A.A. Martin, S.A. Hagstrom, D.F. Martin, Risk of Geographic Atrophy in the Comparison of Age-related Macular Degeneration Treatments Trials, *Ophthalmology*. 121 (2014) 150–161. <https://doi.org/10.1016/j.ophtha.2013.08.015>.
- [80] M.R. Munk, L. Ceklic, A. Ebnetter, W. Huf, S. Wolf, M.S. Zinkernagel, Macular atrophy in patients with long-term anti-VEGF treatment for neovascular age-related macular degeneration, *Acta Ophthalmologica*. 94 (2016) e757–e764. <https://doi.org/10.1111/aos.13157>.
- [81] J.E. Grunwald, M. Pistilli, G. Ying, M.G. Maguire, E. Daniel, D.F. Martin, Growth of Geographic Atrophy in the Comparison of Age-related Macular Degeneration Treatments Trials, *Ophthalmology*. 122 (2015) 809–816. <https://doi.org/10.1016/j.ophtha.2014.11.007>.
- [82] C. Jiao, D. Elliott, C. Spee, S. He, K. Wang, R.F. Mullins, D.R. Hinton, E.H. Sohn, Apoptosis and angiofibrosis in diabetic tractional membranes after vascular endothelial growth factor inhibition: Results of a Prospective Trial. Report No. 2, *Retina*. 39 (2019) 265–273. <https://doi.org/10.1097/IAE.0000000000001952>.
- [83] E.J. Kuiper, F.A. Van Nieuwenhoven, M.D. de Smet, J.C. van Meurs, M.W. Tanck, N. Oliver, I. Klaassen, C.J.F. Van Noorden, R. Goldschmeding, R.O. Schlingemann, The Angio-Fibrotic Switch of VEGF and CTGF in Proliferative Diabetic Retinopathy, *PLoS ONE*. 3 (2008) e2675. <https://doi.org/10.1371/journal.pone.0002675>.
- [84] J.F. Arevalo, J.G. Sanchez, L. Saldarriaga, M.H. Berrocal, J. Fromow-Guerra, V. Morales-Canton, L. Wu, M. Maia, M.J. Saravia, J. Bareño, Retinal Detachment after Bevacizumab, *Ophthalmology*. 118 (2011) 2304.e3-2304.e7. <https://doi.org/10.1016/j.ophtha.2011.05.015>.
- [85] J.F. Arevalo, M. Maia, H.W. Flynn, M. Saravia, R.L. Avery, L. Wu, M.E. Farah, D.J. Pieramici, M.H. Berrocal, J.G. Sanchez, Tractional retinal detachment following intravitreal bevacizumab (Avastin) in patients with severe proliferative diabetic retinopathy, *British Journal of Ophthalmology*. 92 (2008) 213–216. <https://doi.org/10.1136/bjo.2007.127142>.
- [86] I. Krebs, C. Glittenberg, S. Ansari-Shahrezaei, S. Hagen, I. Steiner, S. Binder, Non-responders to treatment with antagonists of vascular endothelial growth factor in age-related macular degeneration, *British Journal of Ophthalmology*. 97 (2013) 1443–1446. <https://doi.org/10.1136/bjophthalmol-2013-303513>.

- [87] A. Lux, H. Llacer, F.M.A. Heussen, A.M. Joussen, Non-responders to bevacizumab (Avastin) therapy of choroidal neovascular lesions, *British Journal of Ophthalmology*. 91 (2007) 1318–1322. <https://doi.org/10.1136/bjo.2006.113902>.
- [88] T. Otsuji, Y. Nagai, K. Sho, A. Tsumura, N. Koike, M. Tsuda, T. Nishimura, K. Takahashi, Initial non-responders to ranibizumab in the treatment of age-related macular degeneration (AMD), *Clin Ophthalmol*. 7 (2013) 1487–1490. <https://doi.org/10.2147/OPTH.S46317>.
- [89] U. Spandau, S.J. Kim, Recurrence of ROP After Anti-VEGF Treatment, in: U. Spandau, S.J. Kim (Eds.), *Pediatric Retinal Vascular Diseases: From Angiography to Vitrectomy*, Springer International Publishing, Cham, 2019: pp. 149–152. https://doi.org/10.1007/978-3-030-13701-4_19.

Goals of the thesis

Over the last decades, nanoparticles have widely been investigated for their great potential to deliver drugs preferentially to their site of action and thereby avoid side effects on off-target tissues. Especially in cancer therapy, this approach has already successfully found its way into clinical practice [1]. Two major principles lead to an enhanced distribution of nanoparticles into tumor tissues. One is the passive accumulation in tissues with high blood flow, endothelial fenestrations, and leaky vasculature. The other is active targeting with modifications on the particle surface that allow for the recognition of receptors that are overexpressed in pathological conditions. These principles can also be transferred to the nanotherapy of ocular neovascularization.

This thesis was focused on the development of an endothelial-cell specific therapy for neovascular ocular diseases. The goal of this strategy was to effectively block pathological neovascularization while avoiding the severe complications associated with an unspecific inhibition of VEGF signaling (**Chapter 1**). This was realized by the combination of lipid nanocapsules (LNC) as nanoparticulate vehicle, a surface modification for the specific binding to proliferating endothelium and a promising drug combination as cargo to inhibit overshooting angiogenesis.

LNC are nanoparticles with a liquid lipid core and a shell consisting of poly(ethylene glycol) (PEG)-containing surfactants and lecithin [2]. As nanoparticle size and surface charge are crucial factors for the biodistribution and passive accumulation of nanoparticles in tissues, it was first evaluated how the size of LNC can be adjusted by the balance of lipid and surfactant in the particle composition (**Chapter 3**). An aminated PEG₂₀-cetyl/stearyl ether was synthesized and used to shift the surface charge of LNC to positive values, and the influence of this modification on the biocompatibility of LNC was investigated. Cyclosporin A (CsA) and itraconazole (Itra) were used as active cargo in the LNC. The combination of these drugs exerts synergistic antiangiogenic effects *in vitro* [3], and additionally, CsA might inhibit the inflammation that augments angiogenesis, vasopermeability and tissue damage in proliferative eye diseases [4–6]. Therefore, a method to load LNC with this highly promising combination was developed, and the efficiency and extent of drug loading was quantified by high pressure liquid chromatography (HPLC).

The next step was the modification of the nanoparticle surface. Peptides containing the amino acid sequence arginine-glycine-aspartic acid (RGD) bind to the $\alpha_v\beta_3$ -integrin [7,8], which is upregulated by endothelial cells during active angiogenesis [9]. For this reason, RGD-peptides are widely investigated as targeting motifs for nanoparticles. RGD-decorated quantum dots have already been shown to accumulate in capillaries even in the healthy retina [10] and RGD-LNC have been found

in $\alpha_v\beta_3$ -overexpressing tumors after intravenous administration. For the modification of LNC with RGD, the peptide is conjugated to a PEGylated phospholipid which is then post-inserted into the LNC shell at increased temperatures [11]. In **Chapter 4**, the surface modification of LNC with cyclo(arginine-glycine-aspartic-acid-D-phenylalanine-cysteine) (c(RGDfC)) was tested with and without previous chemical reduction of the thiol group and the amount of successfully grafted RGD-peptide on the LNC surface was quantified by a colorimetric assay with phenanthrenequinone. The stability of post-insertion was tested making use of the fluorescence resonance energy transfer between one dye encapsulated inside the particles and a second dye which was tethered to the post-inserted PEGylated phospholipid. The binding of RGD-LNC to endothelial cells and the effect of serum proteins on this interaction was investigated and quantified.

In **Chapter 5**, drug-loading and surface modification were combined. LNC loaded with CsA and Itra were post-inserted with RGD-conjugated PEG-phospholipids. *In vitro* assays covering different steps of angiogenesis, like cell proliferation, angiogenesis-associated signaling, and tube formation, were employed to investigate the effect of this formulation on endothelial cells.

The biodistribution of RGD-grafted LNC was investigated *in vivo* by the means of fluometry and fluorescence microscopy. The mouse model of oxygen-induced retinopathy is widely used to study the pathological mechanisms of proliferative eye diseases as well as new therapeutic options. For this model, newborn mice with immature retinal vascularization are exposed to increased oxygen levels for several days. Afterwards, they are transferred to room air again. These mice develop retinopathies comparable to retinopathy of prematurity (ROP) [12]. In **Chapter 6** the therapeutic potential of integrin-targeted lipid nanocapsules loaded with CsA and Itra was challenged *in vivo* in this animal model.

References

- [1] A.C. Anselmo, S. Mitragotri, Nanoparticles in the clinic: An update, *Bioengineering & Translational Medicine*. 4 (2019) e10143. <https://doi.org/10.1002/btm2.10143>.
- [2] B. Heurtault, P. Saulnier, B. Pech, J. Proust, J. Benoit, A novel phase inversion-based process for the preparation of lipid nanocarriers, *Pharmaceutical Research*. 19 (2002) 875–880. <https://doi.org/10.1023/A:1016121319668>.
- [3] B.A. Nacev, J.O. Liu, Synergistic Inhibition of Endothelial Cell Proliferation, Tube Formation, and Sprouting by Cyclosporin A and Itraconazole, *PLoS ONE*. 6 (2011) e24793. <https://doi.org/10.1371/journal.pone.0024793>.
- [4] M. Capitão, R. Soares, Angiogenesis and Inflammation Crosstalk in Diabetic Retinopathy, *J Cell Biochem*. 117 (2016) 2443–2453. <https://doi.org/10.1002/jcb.25575>.
- [5] O. Dammann, Inflammation and Retinopathy of Prematurity, *Acta Paediatr*. 99 (2010) 975–977. <https://doi.org/10.1111/j.1651-2227.2010.01836.x>.
- [6] C. Altmann, M.H.H. Schmidt, The Role of Microglia in Diabetic Retinopathy: Inflammation, Microvasculature Defects and Neurodegeneration, *Int J Mol Sci*. 19 (2018). <https://doi.org/10.3390/ijms19010110>.
- [7] M. Pfaff, K. Tangemann, B. Müller, M. Gurrath, G. Müller, H. Kessler, R. Timpl, J. Engel, Selective recognition of cyclic RGD peptides of NMR defined conformation by α IIb β 3, α V β 3, and α 5 β 1 integrins, *J. Biol. Chem*. 269 (1994) 20233–20238. [https://doi.org/10.1016/S0021-9258\(17\)31981-6](https://doi.org/10.1016/S0021-9258(17)31981-6).
- [8] M. Aumailley, M. Gurrath, G. Müller, J. Calvete, R. Timpl, H. Kessler, Arg-Gly-Asp constrained within cyclic pentapeptides Strong and selective inhibitors of cell adhesion to vitronectin and laminin fragment P1, *FEBS Letters*. 291 (1991) 50–54. [https://doi.org/10.1016/0014-5793\(91\)81101-D](https://doi.org/10.1016/0014-5793(91)81101-D).
- [9] C. Kumar, Integrin α v β 3 as a Therapeutic Target for Blocking Tumor-Induced Angiogenesis, *CDT*. 4 (2003) 123–131. <https://doi.org/10.2174/1389450033346830>.
- [10] K. Pollinger, R. Hennig, A. Ohlmann, R. Fuchshofer, R. Wenzel, M. Breunig, J. Tessmar, E.R. Tamm, A. Goepferich, Ligand-functionalized nanoparticles target endothelial cells in retinal capillaries after systemic application, *Proceedings of the National Academy of Sciences*. 110 (2013) 6115–6120. <https://doi.org/10.1073/pnas.1220281110>.
- [11] S. Hirsjärvi, C. Belloche, F. Hindré, E. Garcion, J.-P. Benoit, Tumour targeting of lipid nanocapsules grafted with cRGD peptides, *European Journal of Pharmaceutics and Biopharmaceutics*. (2013). <https://doi.org/10.1016/j.ejpb.2013.12.006>.
- [12] K.M. Connor, N.M. Krah, R.J. Dennison, C.M. Aderman, J. Chen, K.I. Guerin, P. Sapieha, A. Stahl, K.L. Willett, L.E.H. Smith, Quantification of oxygen-induced retinopathy in the mouse: a model of vessel loss, vessel regrowth and pathological angiogenesis, *Nat Protoc*. 4 (2009) 1565–1573. <https://doi.org/10.1038/nprot.2009.187>.

New approaches for the fine tuning
of size and surface charge of
lipid nanocapsules

Abstract

Size and surface charge are crucial factors for the pharmacokinetics, cellular interaction and biocompatibility of nanoparticles. Therefore, it is highly desirable to have nanocarriers which can be precisely adjusted regarding these attributes to meet the requirements for different applications and target tissues. Lipid nanocapsules (LNC) are promising candidates as vehicles for lipophilic drugs. They consist of a medium-chain triglyceride core surrounded by a shell of poly(ethylene glycol)-containing surfactants and lecithin. It has already been shown in literature that LNC can be prepared in different sizes and with versatile surface modifications. In this work the precise correlation between LNC composition and size was investigated to enable their pinpointed preparation with a predefined diameter. In addition to dynamic light scattering, nanoparticle tracking analysis and cryo-TEM were used to confirm the diameter, shape and size distribution of the obtained nanoparticles. A new approach to surface charge modification of LNC was evaluated. Therefore, different proportions of PEG-hydroxy stearate, which is typically used for LNC preparation, were replaced by an aminated PEG-cetyl/stearyl alcohol. The effect on the particle surface charge was investigated by electrophoretic light scattering measurements. Last but not least, LNC were loaded with cyclosporin A and itraconazole as promising cargo candidates for an extension of their therapeutic applications by nanotechnology. Their complete encapsulation was confirmed by HPLC.

3.1 Introduction

The rules dictating the pharmacokinetics of nanoparticles are different from those for small molecular drugs [1]. Size and surface properties are main factors which govern the way a nanoparticle takes in the body after oral or parenteral administration [2–7]. For example, particles with a diameter below 10 nm might be eliminated rapidly by the kidneys but on the other hand particles bigger than 150 nm can activate the complement system and accumulate in liver and spleen [7]. The highest uptake rates into nonphagocytic cells are often achieved with particles between 10 and 60 nm [7,8]. Therefore, the precise adjustment of nanoparticle size is pivotal for their therapeutic use.

Lipid nanocapsules (LNC) are colloidal particles with a liquid core consisting of medium-chain triglycerides, and a shell of poly(ethylene glycol) (PEG)-containing surfactants and lecithin. LNC can be produced in a phase-inversion process developed by Heurtault et al. without the use of organic solvents [9,10]. Other publications have already shown that LNC size can be influenced by the proportions of their components [10,11]. In this work it was evaluated how exactly the ratio between PEG-hydroxy stearate and MCT in the formulation affects the particle diameter. The resulting correlation function can be used for the preparation of LNC with exactly predefined sizes. LNC with sizes between 22 and 139 nm could be obtained here. As different analytical methods might lead to different results in the determination of particle size [12–14], LNC were investigated by dynamic light scattering as well as by cryogenic transmission electron microscopy and nanoparticle tracking analysis.

Additionally, different amounts of amine-terminated PEG-cetyl/stearyl ether prepared by a method previously described by Mongondry et al. [15] were incorporated in the LNC shell to influence the particle surface charge. By this approach, zeta-potentials between -5 and +26 mV were achieved. Besides biodistribution, another aspect for which surface charge is crucial is toxicology. Positively charged particles are known to have easier access into cells, but also to have higher toxicological potency [8,16]. Therefore, the ability to adjust the surface charge of nanoparticles can play a key role for their further application.

As LNC with their lipid core are highly attractive as carriers for lipophilic agents, the encapsulation of two drug candidates was investigated. Nanoparticles have the potential to boost the effect of drugs with an otherwise unfavorable distribution profile. The formulation in colloidal systems can

change the pharmacokinetics of therapeutic agents tremendously [17,18]. Besides their established fields of application, cyclosporin A and itraconazole show promising synergistic effects on the VEGF-dependent proliferation of vascular endothelial cells *in vitro* [19–22]. The successful encapsulation in nanoparticles might open the door to new therapeutic applications in diseases with pathological neovascularization for these substances.

3.2 Materials

Miglyol®812 (medium-chain triglycerides (MCT)) was purchased from Caesar&Loretz, Hilden, Germany. Solutol®HS 15 (Poly(ethylene glycol (PEG))₁₅-12-hydroxy-stearate with about 30% free PEG) and Lipoid S75-3 (soy lecithin with 70% phosphatidylcholine) were kindly provided by BASF, Ludwigshafen, Germany and Lipoid, Ludwigshafen, Germany, respectively. Sympatens ACS/200 G (PEG₂₀-cetyl/stearyl ether) was supplied by Kolb, Hedingen, Switzerland. 1,1'-Dioctadecyl-3,3,3',3'-tetramethylindocarbocyanine perchlorate (DiI) and 3,3'-dioctadecyloxacarbocyanine perchlorate (DiO) were purchased from Thermo Fisher Scientific (life technologies), Waltham, USA (MA). Cyclosporin A (CsA) was a kind gift of Pharma Stulln, Stulln, Germany. Itraconazole (Itra) was purchased from Fagron, Barsbüttel, Germany. MeOH and MeCN (both HPLC grade) were purchased from Merck, Darmstadt, Germany. Endothelial Cell Growth Medium MV (growth medium) was purchased from PromoCell, Heidelberg, Germany. Leibovitz's L-15 medium was obtained from Life Technologies, Carlsbad, USA (CA). All other chemicals were purchased from Sigma Aldrich, Taufkirchen, Germany. Ultrapure water was obtained from a Milli-Q water purification system from Millipore, Billerica, USA (MA). Binding buffer contained 20 mM Tris(hydroxymethyl)aminomethane (TRIS), 150 mM NaCl, 2 mM CaCl₂, 1 mM MnCl₂ and MgCl₂ each, and 0.10% bovine serum albumin (BSA), according to Pollinger et al. [29]. The pH was adjusted to 7.4 with hydrochloric acid.

3.3 Methods

3.3.1 Synthesis of Sympatensamine

For the amine-modification of the PEG-chain of Sympatens, a method previously described by Mongondry et al. [15] was applied with slight modifications. Briefly, 4 mmol of the dried surfactant and 6 mmol of phthalimide and triphenylphosphine were dissolved in 25 ml

tetrahydrofuran (THF). 6 mmol diisopropyl azodicarboxylate were dissolved in THF and added dropwisely to the reaction mixture. After stirring for 48 h at room temperature, the solvent was evaporated. The product was dissolved in dichloromethane (DCM), diluted in the 10-fold volume of diethyl ether (DEE) and crystallized at -80°C . The precipitate was collected by filtration and washed with ice cold DEE. Subsequently, the received phthalimido-Sympatens was dried over night. It was dissolved in 50 ml ethanol and 800 μl hydrazine hydrate were added. The mixture was heated to 85°C under reflux for 5 h. The hydrazinolysis of phthalimido-Sympatens to Sympatensamine (SA) and phthalhydrazide is shown in Figure 1. After cooling to room temperature, the formed precipitate was removed by filtration and the pH of the solution was adjusted to 2-3 with hydrochloric acid. The solvent was evaporated, and the residue was dissolved in 25 ml water. The precipitate was again filtered off. The pH of the solution was adjusted to 9 - 10 with sodium hydroxide and the raw product was extracted with DCM. The organic phase was dried over anhydrous sodium sulfate and concentrated to 10 ml under reduced pressure. It was diluted with 100 ml DEE and crystallized at -80°C . The precipitate was collected by filtration and washed with ice cold DEE. The SA yield was calculated from the weight of the dried product and the conversion rate determined by $^1\text{H-NMR}$ in deuterated chloroform.

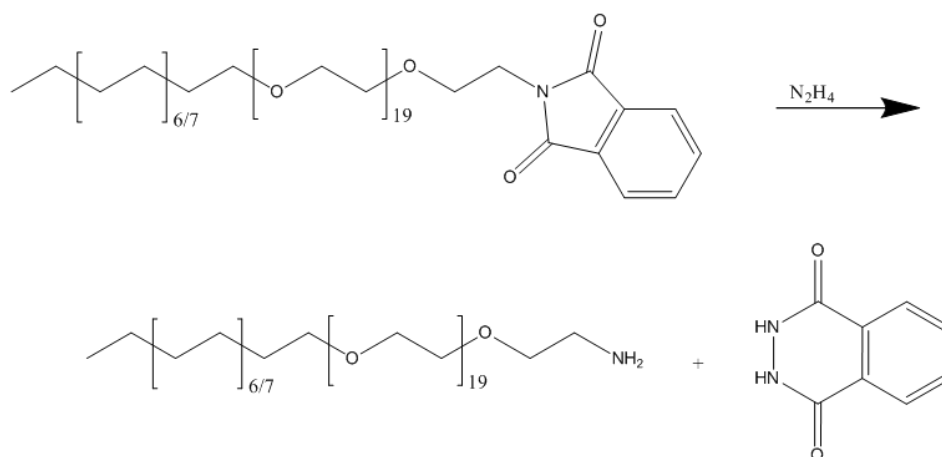


Figure 1: Hydrazinolysis of Sympatens phthalimide to Sympatensamine and phthalhydrazide.

3.1.1 Preparation of LNC

The LNC were prepared in a phase inversion process which was developed by Heurtault et al. [9]. Briefly, 1.5% Lipoid S75-3 and 38.5% of Solutol HS®15 and MCT in eight different ratios between 0.25 and 2.80 (Solutol/MCT) were mixed with 60% NaCl-solution 1% in water. The

mixture was subjected to a heating and cooling cycle in which the phase inversion temperature was passed in each step for three times. In the last cycle the mixture was cooled down in the phase inversion zone with the 2.5-fold amount of water at room temperature to obtain stable LNC. The resulting preparations were filtered through a 0.22 μm poly(ether sulfone) syringe filter prior to further use. The correlation between size and Solutol/MCT ratio was analyzed with SigmaPlot 12.0 using one-phase exponential decay curve fitting. If not stated otherwise, LNC with a Solutol/MCT ratio of 0.82 and a resulting diameter of approximately 50 nm were used for further investigations.

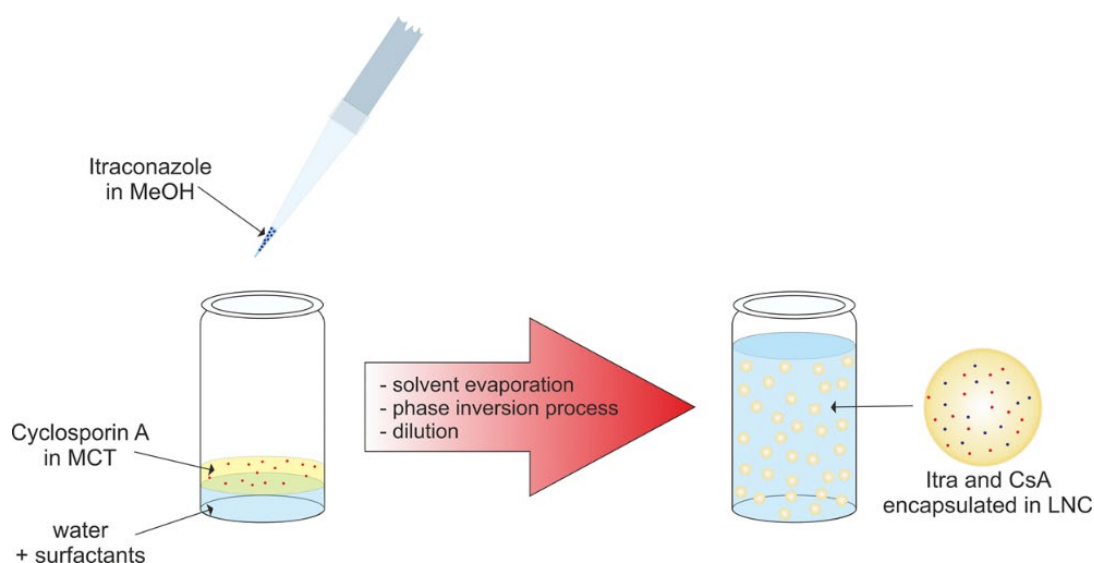


Figure 2: Loading of LNC with cyclosporin A or itraconazole. Cyclosporin was directly dissolved in MCT before LNC preparation. Itraconazole was dissolved in MeOH before it was mixed with the other LNC components. MeOH was evaporated before the phase inversion process.

For the preparation of fluorescently labeled LNC, 3.9 mg DiO per g MCT were added to the mixture prior to the heating and cooling cycles. For DiI-labeled LNC, DiI was dissolved in acetone and mixed with the other LNC ingredients, namely Lipoid, Solutol and MCT (1 - 4 mg DiI per g MCT). Acetone was evaporated before the addition of NaCl-solution for the subsequent heating and cooling cycles.

Positively charged LNC were prepared by replacement of 5 or 10% of the Solutol by SA. As control, unmodified Sympatens was used instead of SA.

CsA-loaded LNC were prepared by dissolving CsA in MCT at a concentration of 4.25 mg CsA per g MCT. LNC preparation was conducted as described above. For itraconazole-loaded LNC,

itraconazole was first dissolved in methanol. The solution together with the LNC ingredients Solutol, MCT and Lipoid was kept at 75°C for 30 min to evaporate the methanol. Subsequently, the NaCl 1% solution was added and LNC were prepared in the phase-inversion process described above (Figure 2).

Non-purified LNC for the determination of drug encapsulation were not filtered after preparation. For purified LNC, potentially remaining free drug was removed by the following steps: The particle stock solutions were filtered through a 0.22 µm syringe filter. They were further purified by size exclusion chromatography using a Sephadex G-25 resin in a PD-10 column (GE Healthcare, Munich, Germany) with Dulbecco's phosphate buffered saline (DPBS) as the eluent followed by three ultrafiltration steps with Amicon Ultra-4 centrifugal filter units (MWCO: 100 kDa; Sigma Aldrich, Taufkirchen, Germany) at 3,000 g for 10 min. The LNC concentration was determined by the UV absorption at 370 nm with an Omega FLUOstar plate reader (BMG Labtech, Ortenberg, Germany) and samples of purified and non-purified LNC were diluted to the same concentration with DPBS before high pressure liquid chromatography (HPLC) analysis.

3.1.2 Calculation of LNC concentration

The mass concentration c_m of LNC was calculated from the mass of the LNC ingredients MCT, Lipoid, Solutol and, if applicable, SA and fluorescence dye, and the volume of the resulting LNC dispersion after preparation. As Solutol contains about 30% free PEG, which was not assumed to be incorporated in the structure of the LNC [23], only 70% of the Solutol mass was included in the calculation. The number of LNC per ml particle dispersion was calculated from the known volume of MCT in the preparation and the volume of an LNC-core. The LNC core volume was estimated from the LNC diameter determined by dynamic light scattering (DLS) under the assumption, that the LNC shell thickness is approximately 4.5 nm [24,25]. The particle concentration c_n was calculated according to equation (1):

$$c_n = \frac{m_{MCT}}{\frac{4}{3}\pi \cdot \left(\frac{d_{LNC} - 2 \times d_{shell}}{2}\right)^3 \cdot \rho_{MCT} \cdot V} \quad (1)$$

where m_{MCT} is the mass of MCT, ρ_{MCT} is the density of MCT with 945 mg/ml, according to the manufacturer, d_{LNC} is the diameter (Z-Av) determined by DLS, d_{shell} is the thickness of one shell layer with 4.5 nm and V is the total volume of the LNC preparation. The molar LNC concentration was calculated by dividing c_n by the Avogadro constant $N_A = 6.022 \times 10^{23} \text{ mol}^{-1}$.

3.1.3 Nanoparticle tracking analysis (NTA)

For further investigations on particle size and concentration, an LNC sample of DiI-labeled LNC with 10% SA was analyzed by NTA with a NanoSight NS300 device (Malvern Instruments, Herrenberg, Germany) with NTA 3.0 software. To this purpose the sample was diluted 1:10⁶ with water. The camera level was set to 11 with a threshold of 2.

3.1.4 Dynamic Light Scattering (DLS)

Z-Average (Z-Av), polydispersity indices (PDIs) and zeta-potentials were determined with a Zetasizer Nano ZS (Malvern Instruments, Herrenberg, Germany), equipped with a He-Ne-Laser at a wavelength of 633 nm and a fixed angle of 173°. If not stated otherwise, the samples were diluted 1:40 with water and the sample temperature was equilibrated to 25°C prior to each measurement.

3.1.5 Cryogenic Transmission Electron Microscopy (cryo-TEM)

LNC were diluted to a concentration of 3 mg/ml. The specimens were prepared by vitrification of a thin liquid film on a 600 mesh copper grid (Science Services, Munich, Germany) in liquid ethane and transferred to a Zeiss EM922 EFTEM (Zeiss NTS GmbH, Oberkochen, Germany). Images were taken with an Ultrascan 1000 CCD digital camera (Gatan, Pleasanton, USA (CA)) and analyzed using a GMS 1.8 software (Gatan, Pleasanton, USA (CA)). On four images showing an area of 9 µm² each, the projected area of all particles was measured with the Image-J software (NIH, Bethesda, USA (MD), <http://imagej.nih.gov/ij>). Particle diameters were calculated from the particle areas.

3.1.6 Stability

The stability of LNC in four different media was tested over 90 min at 37°C. The media tested were DPBS, binding buffer, Leibovitz' medium and growth medium. DiO-labeled LNC were diluted 1:50 with the respective medium. Z-Av and PDI were determined by DLS directly after the dilution and after 90 min of incubation at 37°C. For DLS measurements, samples were equilibrated to 25°C.

3.1.7 High pressure liquid chromatography (HPLC)

For the quantification of encapsulated CsA and Itra, 500 μ l isopropanol and 500 μ l methanol were added to 1 ml of each LNC sample. The mixture was ultrasonicated for 15 min to destroy the LNC structure and dissolve the incorporated drugs. The samples were filtered through a 0.2 μ m-filter before chromatography. External standard solutions of CsA and Itra were prepared in MeOH.

The chromatographic equipment (Shimadzu Deutschland, Duisburg, Germany) consisted of an SCL-10AVP controller, an LC-10ATVP pump operated, an SIL-10ADVP auto injector, a CTO-10ASVP oven and an SPD-10AVP UV detector. A reversed phase octadecyl column Luna 3 μ C18(2) 100A with 100 x 4.6 mm (Phenomenex, Aschaffenburg, Germany) was used as solid phase.

Isocratic elution with MeCN/H₂O with 0.1% trifluoroacetic acid was carried out at a flow rate of 0.75 ml/min. The MeCN/H₂O ratio was 75/25 for CsA and 40/60 for Itra. The oven temperature, detection wavelength and run duration were 75°C, 220 nm and 20 min for CsA and 40°C, 258 nm and 25 min for Itra.

3.1.8 Cytotoxicity assay

Mouse fibroblast L-929 cells were seeded into a 96-well plate at a density of 10,000 cells per well in Eagle's Minimum essential Medium (EMEM) with 10% fetal calf serum (FCS). The cells were allowed to adhere for 24 h. Samples of DiI-labeled standard LNC and LNC in which 10% of the Solutol was replaced by Sympatens (10%S LNC) were prepared in EMEM with 10% FCS in concentrations between 30 and 10⁴ μ g/ml. As control for complete cell death 0.1% sodium dodecyl sulfate in EMEM with 10% FCS was used. Cell culture medium alone served as 100% viability control. All solutions were preheated to 37°C before they were added to cells. After 4 h of incubation at 37°C, samples were aspirated gently from the wells. 200 μ l of a 0.6 mg/ml 3-(4,5-dimethylthiazol-2-yl)-2,5-diphenyl tetrazolium bromide (MTT) solution in serum-containing EMEM were added. Cells were incubated at 37°C for further 4 h. The MTT-solution was discarded carefully and 80 μ l of 10% SDS-solution were added to each well to solubilize the formed formazan crystals over night. The absorbance of each well was measured at 570 nm and 690 nm with a plate reader (Omega FLUOstar, BMG Labtech, Ortenberg, Germany) and the difference (A₅₇₀-A₆₉₀) was used to calculate cell viability related to the 100% viability control. All samples were tested in six replicates. The IC₅₀ value was calculated with SigmaPlot 12.0 using sigmoidal dose-response curve fitting with a variable slope.

3.1.9 Statistical analysis

If not stated otherwise, data are expressed as mean \pm standard deviation. Statistical significance was assessed by two-tailed t-test for comparison of two groups or by One-way ANOVA with post-hoc Tukey test to compare more than two groups. Data were analyzed with SigmaPlot 12.0.

3.4 Results and discussion

3.4.1 Correlation between LNC size and composition

The different Solutol/MCT ratios resulted in particle sizes between 22 nm (ratio 2.80) and 139 nm (ratio 0.25). Very low PDIs, mostly lower than 0.05, were determined in all DLS measurements, which indicated monodispersity for all samples [14]. Heurtault et al. have already shown a strong decrease in particle size with increasing proportions of Solutol, although only sizes up to 95 nm could be obtained in this publication [10]. As the amount of Lipoid in the formulation has only minor effects on LNC size according to literature [10] it was kept constant here. The size of LNC determined by DLS decreased exponentially with higher Solutol/MCT ratios (see Figure 3). A previous publication of Hoarau et al. in contrast observed a linear decrease of LNC size between Solutol/MCT ratios from 0.6 to 1.0. But only ratios between 0.55 and 1.00 were tested by them, what might have led to the impression of a rather linear correlation [11]. The broader range of formulations tested here enabled an exponential curve fitting with an R^2 of 0.995. The obtained fitting equation (2) can be used to calculate the Solutol/MCT ratio (w) needed to get LNC with a predefined target size d_{LNC} :

$$d_{LNC} = 24.5 + 209.8 \cdot e^{-2.5 \cdot w} \quad (2)$$

This knowledge enables the well-directed preparation of LNC with distinct sizes for specific investigations on the influence of particle size in *in-vitro* and *in-vitro* experiments.

Furthermore, not only the mean particle size, but also size distribution is important for the particle characterization. To confirm the results from DLS the size of 10%SA LNC was also determined by NTA. Both methods are based on the Stokes-Einstein equation to calculate the particle diameter from its correlation with Brownian motion, which is indirectly observed via light scattering. But while in DLS fluctuations in the intensity of scattered light over time are used for the correlation, NTA is capturing the scattered light from individual particles to follow their movement [14,26].

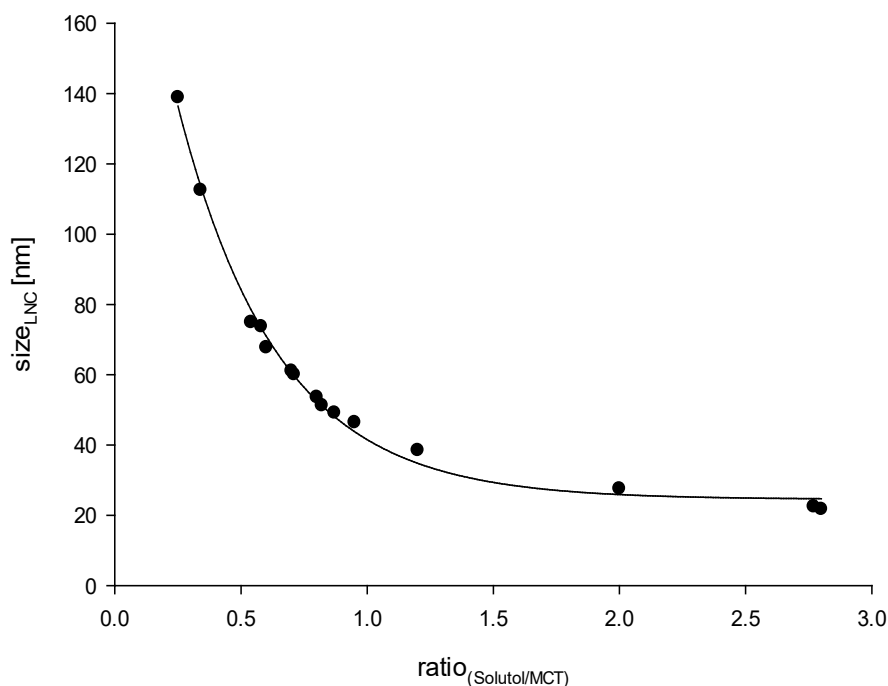


Figure 3: Influence of the Solutol/MCT ratio on particle size. The diameter of LNC decreases exponentially with higher Solutol/MCT ratios.

In DLS, the Z-Average of 10%SA LNC was 51.6 nm with a PDI of 0.05. In NTA the mean particle size was 58.2 ± 2.2 nm with a modal size of 46.2 ± 0.4 nm. It is typical that mean sizes obtained from DLS are smaller than those from NTA as the detection limit in DLS is lower. Therefore, smaller particles, especially below 30 nm, might not be detectable by NTA but decrease the average size in DLS [26].

As both, DLS and NTA, only reveal the hydrodynamic diameter of particles, which can vary with the amount and type of ions in the surrounding media, also cryo-TEM microscopy was performed to confirm the size and shape of LNC. The particle diameter of the sample for cryo-TEM imaging was 55 nm (Z-Av) determined by DLS (PDI = 0.03). Cryo-TEM images confirmed the spherical shape of LNC. The diameter of 277 particles was calculated from their projected area in the images. With a diameter of 42 ± 9 nm in average, the particles seemed about 13 nm smaller than in DLS measurements. This difference can be attributed to the hydration shell according to the literature, where a hydration shell thickness of 10 – 20 nm is stated for soft colloidal particles [27]. The size distribution of LNC seemed broader in cryo-TEM than in DLS with one size population with 45 – 50 nm and a smaller one with 18 - 30 nm (Figure 4). As especially smaller melting ice crystals,

resulting from condensed and frozen air humidity, were hard to distinguish from LNC, it is possible that they also contributed to the smaller peak.

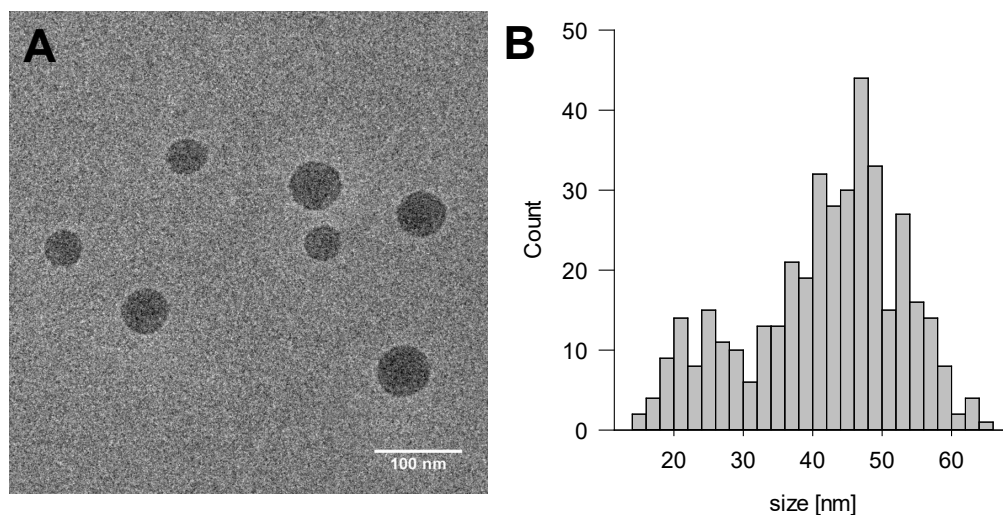


Figure 4: Cryo-TEM images enabled the visualization of LNC in their hydrated state (A). The spherical shape was confirmed. Besides the main particle population with a diameter of 45 to 50 nm a second population with about 18-30 nm was observed. The area of 277 particles in the images was measured to calculate their diameter and obtain size distribution data from the cryo-TEM images (B).

3.1.1 Calculation of LNC concentration

The calculated concentration of 50 nm LNC in the obtained dispersions with a total volume of 6.5 ml was 107 mg/ml with 1.9×10^{15} particles/ml, corresponding to a 3 μ M concentration. The concentration was also determined by NTA. Taking into account the dilution factor of the NTA sample, a concentration of 9.5×10^{14} particles/ml (1.6 μ M) was obtained for the LNC stock solution. This value is in the same order of magnitude as the calculated concentration, confirming these results. The difference might be caused by smaller LNC being below the detection limit of NTA.

As the Solutol content is higher in smaller LNC and only 70% of Solutol is contributing to the actual particle mass, their mass concentration in the initial dispersions is slightly lower than for bigger LNC. Therefore, the calculated concentration is 99 mg/ml for 25 nm LNC, 107 mg/ml for 50 nm LNC, 110 mg/ml for 75 nm LNC and 113 mg/ml for 100 nm LNC. In contrast, the molar concentration of LNC in the initial dispersion decreases for rising particle diameters, as described

in Equation (1). The calculated concentration is 28 μM for 25 nm LNC, 3 μM for 50 nm LNC, 0.9 μM for 75 nm LNC and 0.4 μM for 100 nm LNC.

For this reason it is very important to consider whether the same mass or molar concentrations are compared in experiments, if nanoparticles with different sizes are tested against each other.

3.1.2 Variation of surface charge by the introduction of Sympatensamine

Perrier et al. have already described the modification of the LNC surface with amine groups by post-insertion of a functionalized phospholipid [28]. The modification of Sympatens and the subsequent use in the formulation in contrast enables the functionalization of LNC directly during the preparation process without further post-insertion steps. This functional groups can be used either for the conjugation of targeting molecules to the nanoparticles or to influence the surface charge, which is a crucial factor for the interaction with cells and biodistribution [5,8].

Sympatens was converted to SA with a rate of 91.2% determined by $^1\text{H-NMR}$. The partial replacement of Solutol by SA in the LNC formulation resulted in a positive zeta-potential of the particles, which increased with higher amounts of SA in the LNC composition (Figure 5). The mean particle size ($Z\text{-}Av$) determined by DLS was 52 – 54 nm for all compositions and was not influenced by Sympatens or SA. The zeta-potential was slightly negative for standard LNC with -4.9 ± 1.0 mV and was not changed by the addition of unmodified Sympatens (-5.1 mV for 5%S and 4.9 ± 1.1 mV for 10%S LNC). The addition of SA to the LNC formulation resulted in a positive surface charge 17.6 mV for 5%SA LNC and 24.9 ± 1.7 mV for 10%SA LNC. 5%S and 5%SA LNC were only evaluated in singular determination, so no standard deviations are given for those samples. The PDI stayed below 0.05 for all LNC preparations.

Positive surface charge often leads to a higher cellular uptake of nanoparticles, which is very important if they have an intracellular target. But this advantage often comes along with faster clearance from systemic circulation and higher toxicity [5,8,16]. For that reason, a precise adjustment of zeta-potential is pivotal to optimize nanoparticles for clinical use.

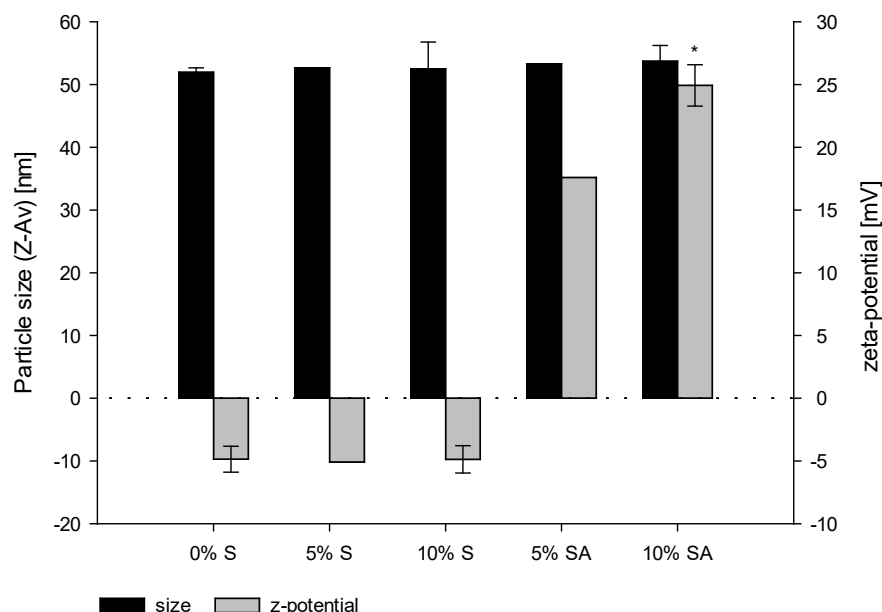


Figure 5: Influence of different proportions of Sympatens (S) and Sympatensamine (SA) in the LNC. The percentage expresses the amount of Solutol replaced by Sympatens. Particle size was not influenced by the amount of Sympatens. LNC without functional groups on their surface (0% and S-LNC) had a slightly negative surface charge. The introduction of amine groups led to a positive zeta-potential. Statistically significant difference compared to 0%S LNC is indicated with (*). Data for 5%S and 5%SA LNC were only evaluated in singular determination.

3.1.3 Stability of LNC in different media

It is crucial for all *in-vitro* investigations and especially for *in-vivo* application that nanoparticles are stable under physiological conditions. To proof that LNC do not aggregate or change their properties at 37°C and in the presence of electrolytes, the nanoparticles were incubated for 90 min in four different media and the effect on size and PDI was assessed by DLS. The media tested were DPBS, Leibovitz' medium, binding buffer and growth medium to cover media with different buffers and protein content. Directly after preparation LNC had a mean particle size (Z-Av) of 52.3 nm and a PDI of 0.03 measured after 1:40 dilution in water. Regardless of the incubation medium, the particle diameter did not change directly after dilution or after 90 min at 37°C (53-54 nm). The PDI stayed ≤ 0.05 , proofing that no aggregation occurred (Figure 6).

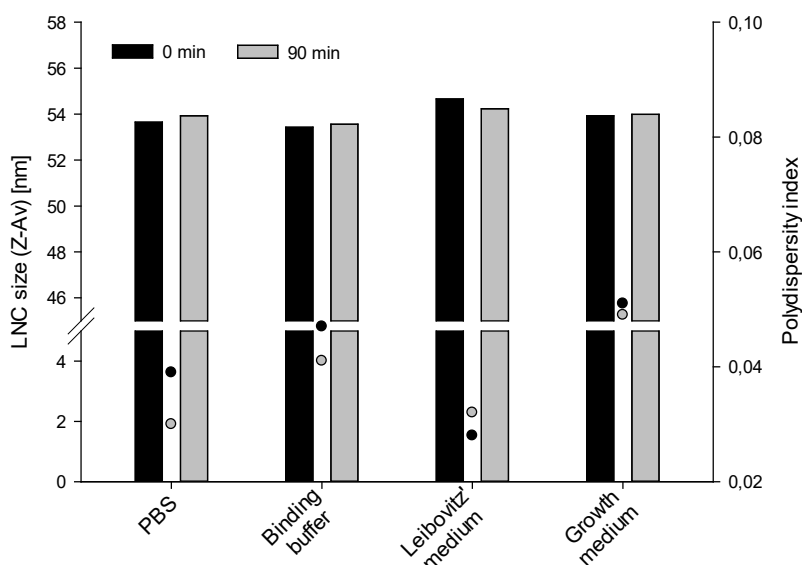


Figure 6: Stability of LNC over 90 min at 37°C in different media. The size (columns) and PDI (dots) of LNC was not changed regardless of the medium.

3.1.4 Encapsulation of CsA and Itra in LNC

If LNC should be used as vehicles to optimize the biodistribution of therapeutics, it is important to make sure that those are actually encapsulated inside the particles and not dissolved in the surrounding media. For the quantification of drug encapsulation different samples were prepared: LNC stock solutions without further purification, where CsA or Itra might still be present in the dispersant and samples of the stock solution which were subjected to various purification steps to remove any CsA and Itra not encapsulated in LNC. The encapsulation efficiency was defined as the proportion of drug actually incorporated into the particles and calculated from drug content in purified LNC in relation to the unpurified stock solution. The results show that CsA as well as Itra were completely encapsulated into LNC with $100 \pm 6\%$ and $102 \pm 6\%$ encapsulation efficiency, respectively (Figure 7). LNC size and PDI were not changed by the purification steps (49 nm for Itra-loaded and 50 nm for CsA-loaded LNC with a $PDI < 0.05$ for both). To be sure that no drug was lost during the filtration for HPLC and the quantification method was valid, the drug recovery was calculated. For this purpose, the absolute drug content in LNC quantified by HPLC was compared to the calculated drug content of LNC according to the amounts used for preparation. The recovery rates were $95 \pm 7\%$ (CsA) and $93 \pm 4\%$ (Itra), showing that no significant drug losses

were caused by the sample preparation and that the quantification method was reliable. The successful encapsulation of Itra and CsA encourages further investigations on the intracellular targeting with these drug candidates for antiangiogenic therapies.

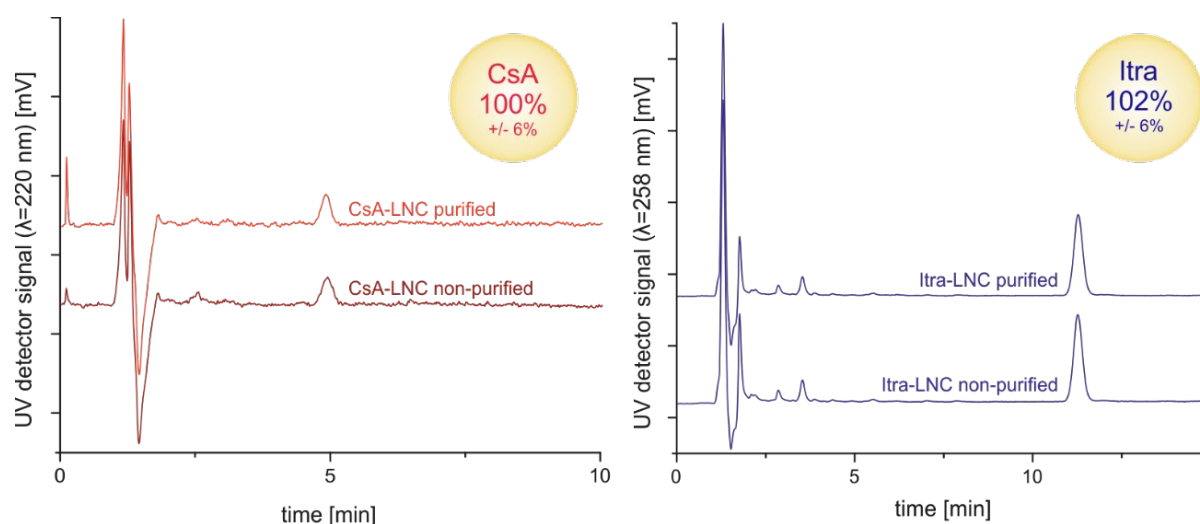


Figure 7: Encapsulation efficiencies determined by HPLC were about 100% for both, Itra and CsA. Drugs were completely encapsulated in LNC. Recoveries were $95 \pm 7\%$ (CsA) and $93 \pm 4\%$ (Itra) of the calculated drug content. The chromatogram baselines were shifted for better visibility.

3.1.5 Cytotoxicity assay

It is already described in literature that LNC toxicity is mainly mediated by the surfactants in the LNC formulation [29]. Therefore, the effects of standard LNC consisting of Solutol, Lipoid and MCT and LNC in which 10% of Solutol was replaced by Sympatens on cell viability were tested against each other.

It was shown that 10%S LNC were significantly more toxic than standard LNC ($p < 0.05$). The IC₅₀ values, specified as the particle concentrations which lead to a 50% reduction of cell viability after the incubation time of 4 h, were 1.30 ± 0.28 mg/ml for LNC and 0.21 ± 0.047 mg/ml for 10%S LNC. The IC₅₀ value determined for LNC is also in accordance with findings of Hirsjärvi et al. who found a reduction of the metabolic activity of U87 MG cells to about 50 – 70% after 1.5 h of incubation with 1.15 mg/ml LNC [30]. The about one order of magnitude higher toxicity of 10%S LNC does not necessarily have to be an exclusion criterion for the application of such particles. On the one hand, due to the high loading capacity for lipophilic substances and the good

possibilities of surface modification, the concentrations needed for therapeutic use might be much lower than the levels for toxicity. On the other hand, further modifications of the particle surface might again change their biocompatibility.

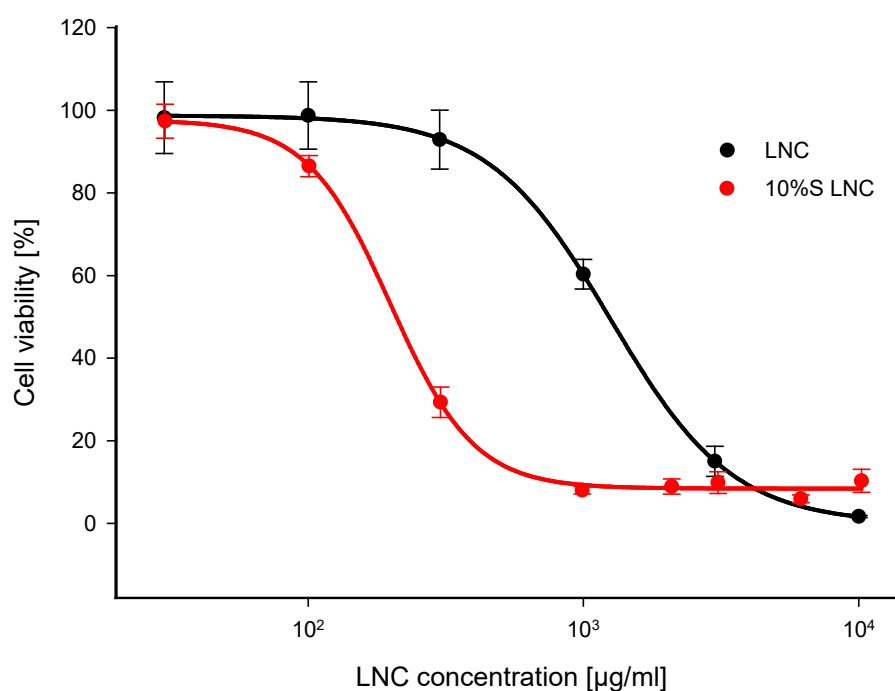


Figure 8: Cell viability after incubation of L-929 cells with different concentrations of LNC formulations with and without Sympatens for 4 h. Viability was determined by the colorimetric MTT-assay. LNC with Sympatens were significantly more toxic than standard LNC with IC₅₀ values of 0.21 ± 0.05 mg/ml and 1.30 ± 0.28 mg/ml, respectively ($p < 0.05$).

3.5 Conclusion

Through the mathematical description of the relationship between particle diameter and the ratio of surfactant to lipid core material it is possible to precisely adjust the LNC size by their composition. The two model drugs itraconazole and cyclosporine A were completely encapsulated inside the particles without any leakage during purification steps. Despite the narrow size distribution of LNC observed in DLS and NTA, cryo-TEM revealed a second size population that was not detectable by the other measurement techniques. That again proved how important it is not to rely only on a single method for nanoparticle size analysis. The LNC were stable in different media even at increased temperatures. With the amine modification of Sympatens and its use in

LNC preparation, a new method for surface functionalization without the need for time-consuming post-insertion processes was established. This can be used either for the adjustment of surface charge as shown by electrophoretic light scattering or for further conjugational steps. Nevertheless, it has to be considered that changes in the surfactant composition of LNC do also affect biocompatibility. With their versatile opportunities for drug loading, size adjustment and surface modification, lipid nanocapsules bare great potential for therapeutic applications in the emerging field of nanomedicines.

3.6 References

- [1] S.-D. Li, L. Huang, Pharmacokinetics and Biodistribution of Nanoparticles, *Mol. Pharmaceutics*. 5 (2008) 496–504. <https://doi.org/10.1021/mp800049w>.
- [2] M.J. Ernsting, M. Murakami, A. Roy, S.-D. Li, Factors controlling the pharmacokinetics, biodistribution and intratumoral penetration of nanoparticles, *Journal of Controlled Release*. 172 (2013) 782–794. <https://doi.org/10.1016/j.jconrel.2013.09.013>.
- [3] S. Dufort, L. Sancey, J.-L. Coll, Physico-chemical parameters that govern nanoparticles fate also dictate rules for their molecular evolution, *Advanced Drug Delivery Reviews*. 64 (2012) 179–189. <https://doi.org/10.1016/j.addr.2011.09.009>.
- [4] S. Zhang, H. Gao, G. Bao, Physical Principles of Nanoparticle Cellular Endocytosis, *ACS Nano*. (2015). <https://doi.org/10.1021/acsnano.5b03184>.
- [5] J.P.M. Almeida, A.L. Chen, A. Foster, R. Drezek, In vivo biodistribution of nanoparticles, *Nanomedicine*. 6 (2011) 815–835. <https://doi.org/10.2217/nmm.11.79>.
- [6] S. Hirsjärvi, L. Sancey, S. Dufort, C. Belloche, C. Vanpouille-Box, E. Garcion, J.-L. Coll, F. Hindré, J.-P. Benoît, Effect of particle size on the biodistribution of lipid nanocapsules: Comparison between nuclear and fluorescence imaging and counting, *International Journal of Pharmaceutics*. 453 (2013) 594–600. <https://doi.org/10.1016/j.ijpharm.2013.05.057>.
- [7] N. Hoshyar, S. Gray, H. Han, G. Bao, The effect of nanoparticle size on in vivo pharmacokinetics and cellular interaction, *Nanomedicine*. 11 (2016) 673–692. <https://doi.org/10.2217/nmm.16.5>.
- [8] E. Fröhlich, The role of surface charge in cellular uptake and cytotoxicity of medical nanoparticles, *Int J Nanomedicine*. 7 (2012) 5577–5591. <https://doi.org/10.2147/IJN.S36111>.
- [9] B. Heurtault, P. Saulnier, B. Pech, J.-E. Proust, J.-P. Benoit, A novel phase inversion-based process for the preparation of lipid nanocarriers, *Pharmaceutical Research*. 19 (2002) 875–880.
- [10] B. Heurtault, P. Saulnier, B. Pech, M.-C. Venier-Julienne, J.-E. Proust, R. Phan-Tan-Luu, J.-P. Benoît, The influence of lipid nanocapsule composition on their size distribution, *European Journal of Pharmaceutical Sciences*. 18 (2003) 55–61. [https://doi.org/10.1016/S0928-0987\(02\)00241-5](https://doi.org/10.1016/S0928-0987(02)00241-5).
- [11] D. Hoarau, P. Delmas, David, Stéphanie, E. Roux, J.-C. Leroux, Novel Long-Circulating Lipid Nanocapsules, *Pharm Res*. 21 (2004) 1783–1789. <https://doi.org/10.1023/B:PHAM.0000045229.87844.21>.

- [12] M. Gaumet, A. Vargas, R. Gurny, F. Delie, Nanoparticles for drug delivery: The need for precision in reporting particle size parameters, *European Journal of Pharmaceutics and Biopharmaceutics*. 69 (2008) 1–9. <https://doi.org/10.1016/j.ejpb.2007.08.001>.
- [13] P.-C. Lin, S. Lin, P.C. Wang, R. Sridhar, Techniques for physicochemical characterization of nanomaterials, *Biotechnology Advances*. 32 (2014) 711–726. <https://doi.org/10.1016/j.biotechadv.2013.11.006>.
- [14] S. Bhattacharjee, DLS and zeta potential – What they are and what they are not?, *Journal of Controlled Release*. 235 (2016) 337–351. <https://doi.org/10.1016/j.jconrel.2016.06.017>.
- [15] P. Mongondry, C. Bonnans-Plaisance, M. Jean, J.F. Tassin, Mild Synthesis of Amino-Poly(ethylene glycol)s. Application to Steric Stabilization of Clays, *Macromolecular Rapid Communications*. 24 (2003) 681–685. <https://doi.org/10.1002/marc.200350012>.
- [16] M.C. Garnett, P. Kallinteri, Nanomedicines and nanotoxicology: some physiological principles, *Occup Med (Lond)*. 56 (2006) 307–311. <https://doi.org/10.1093/occmed/kql052>.
- [17] M.R. Longmire, M. Ogawa, P.L. Choyke, H. Kobayashi, Biologically optimized nanosized molecules and particles: More than just size, *Bioconjugate Chemistry*. 22 (2011) 993–1000. <https://doi.org/10.1021/bc200111p>.
- [18] S. Parveen, R. Misra, S.K. Sahoo, Nanoparticles: a boon to drug delivery, therapeutics, diagnostics and imaging, *Nanomedicine: Nanotechnology, Biology and Medicine*. 8 (2012) 147–166. <https://doi.org/10.1016/j.nano.2011.05.016>.
- [19] P. Rafiee, J. Heidemann, H. Ogawa, N.A. Johnson, P.J. Fisher, M.S. Li, M.F. Otterson, C.P. Johnson, D.G. Binion, Cyclosporin A differentially inhibits multiple steps in VEGF induced angiogenesis in human microvascular endothelial cells through altered intracellular signaling, *Cell Communication and Signaling*. 2 (2004) 3. <https://doi.org/10.1186/1478-811X-2-3>.
- [20] C. Esposito, A. Fornoni, F. Cornacchia, N. Bellotti, G. Fasoli, A. Foschi, I. Mazzucchelli, T. Mazzullo, L. Semeraro, A. Dal Canton, Cyclosporine induces different responses in human epithelial, endothelial and fibroblast cell cultures, *Kidney Int*. 58 (2000) 123–130. <https://doi.org/10.1046/j.1523-1755.2000.00147.x>.
- [21] B.A. Nacev, P. Grassi, A. Dell, S.M. Haslam, J.O. Liu, The Antifungal Drug Itraconazole Inhibits Vascular Endothelial Growth Factor Receptor 2 (VEGFR2) Glycosylation, Trafficking, and Signaling in Endothelial Cells, *Journal of Biological Chemistry*. 286 (2011) 44045–44056. <https://doi.org/10.1074/jbc.M111.278754>.
- [22] B.A. Nacev, J.O. Liu, Synergistic Inhibition of Endothelial Cell Proliferation, Tube Formation, and Sprouting by Cyclosporin A and Itraconazole, *PLoS ONE*. 6 (2011) e24793. <https://doi.org/10.1371/journal.pone.0024793>.

-
- [23] A. Barras, A. Mezzetti, A. Richard, S. Lazzaroni, S. Roux, P. Melnyk, D. Betbeder, N. Monfilliette-Dupont, Formulation and characterization of polyphenol-loaded lipid nanocapsules, *International Journal of Pharmaceutics*. 379 (2009) 270–277. <https://doi.org/10.1016/j.ijpharm.2009.05.054>.
- [24] I. Minkov, Tz. Ivanova, I. Panaiotov, J. Proust, P. Saulnier, Reorganization of lipid nanocapsules at air–water interface: I. Kinetics of surface film formation, *Colloids and Surfaces B: Biointerfaces*. 45 (2005) 14–23. <https://doi.org/10.1016/j.colsurfb.2005.03.009>.
- [25] F. Lacoeyille, F. Hindre, F. Moal, J. Roux, C. Passirani, O. Couturier, P. Cales, J.J. Le Jeune, A. Lamprecht, J.P. Benoit, In vivo evaluation of lipid nanocapsules as a promising colloidal carrier for paclitaxel, *International Journal of Pharmaceutics*. 344 (2007) 143–149. <https://doi.org/10.1016/j.ijpharm.2007.06.014>.
- [26] V. Filipe, A. Hawe, W. Jiskoot, Critical Evaluation of Nanoparticle Tracking Analysis (NTA) by NanoSight for the Measurement of Nanoparticles and Protein Aggregates, *Pharm Res*. 27 (2010) 796–810. <https://doi.org/10.1007/s11095-010-0073-2>.
- [27] Z. Varga, B. Fehér, D. Kitka, A. Wacha, A. Bóta, S. Berényi, V. Pipich, J.-L. Fraikin, Size Measurement of Extracellular Vesicles and Synthetic Liposomes: The Impact of the Hydration Shell and the Protein Corona, *Colloids and Surfaces B: Biointerfaces*. 192 (2020) 111053. <https://doi.org/10.1016/j.colsurfb.2020.111053>.
- [28] T. Perrier, F. Fouchet, G. Bastiat, P. Saulnier, J.-P. Benoit, OPA quantification of amino groups at the surface of Lipidic NanoCapsules (LNCs) for ligand coupling improvement, *International Journal of Pharmaceutics*. 419 (2011) 266–270. <https://doi.org/10.1016/j.ijpharm.2011.07.028>.
- [29] C. Maupas, B. Moulari, A. Béduneau, A. Lamprecht, Y. Pellequer, Surfactant dependent toxicity of lipid nanocapsules in HaCaT cells, *International Journal of Pharmaceutics*. 411 (2011) 136–141. <https://doi.org/10.1016/j.ijpharm.2011.03.056>.
- [30] S. Hirsjärvi, C. Belloche, F. Hindré, E. Garcion, J.-P. Benoit, Tumour targeting of lipid nanocapsules grafted with cRGD peptides, *European Journal of Pharmaceutics and Biopharmaceutics*. (2013). <https://doi.org/10.1016/j.ejpb.2013.12.006>.

Modification of LNC with an
integrin-binding peptide for
endothelial cell targeting

Abstract

Targeted therapy with nanoparticles with the ability to transport therapeutic agents specifically to a selected tissue is a highly promising vision. Therefore, particles are grafted with recognition motifs guiding them to their destination. The peptide sequence RGD is such a targeting moiety. Especially cyclic RGD-peptides bind specifically to integrin receptors which are overexpressed in newly formed blood vessels. Nanocarriers modified with integrin ligands have already been demonstrated to accumulate in tumor tissues with proliferative vasculature. This rises hope that such particles might also be a therapeutic option for other proliferative diseases like the wet forms of diabetic retinopathy and age-related macular degeneration. In this work the peptide was conjugated to lipid nanocapsules (LNC), as these nanoparticles are potential carriers, especially for lipophilic drugs. In order to attach the targeting peptide to their surface, it was conjugated to a PEGylated phospholipid via maleimide-thiol reaction. Subsequently the phospholipid was incubated with LNC at increased temperatures to enable its incorporation into the shell of the nanoparticles. The integrity of nanoparticles and the increase in size due to the longer PEG-chains was confirmed by DLS. The successfully bound peptide was quantified photometrically after a reaction with phenanthrenequinone. Proof of concept for the receptor-mediated binding of RGD-conjugated LNC was provided by uptake experiments with microvascular endothelial cells. RGD-modification resulted in significantly elevated cellular uptake, while the tolerability of the modified particles for cells was even higher than for blank LNC.

3.1 Introduction

When it comes to pharmacotherapy, even the most potent drug has no effect, if it is not able to reach its target. One option to influence the pharmacokinetics of drugs with an unfavorable biodistribution profile is to use nanocarriers as a vehicle. PEG-coronas are often used to shield these nanocarriers from protein adsorption and subsequent clearance by the mononuclear phagocyte system (MPS) [1,2]. Such shielding can prolong the half-life time of nanoparticles in the blood tremendously and therefore increases the chance for accumulation in the target tissue by specific interactions. This opens the way for cellular targeting, where specific recognition motifs are bound to the nanoparticle surface to guide them to tissues or cells of interest. RGD-peptides are such molecules. They are used to target the $\alpha_v\beta_3$ -integrin [3,4], which plays a pivotal role in cell migration and angiogenesis [5,6]. The expression of the $\alpha_v\beta_3$ -receptor is upregulated by endothelial cells in proliferating vasculature for example during tumor growth [7]. Cyclic RGD-pentapeptides show a 20-100 fold higher affinity compared to linear peptides while being much more specific for the $\alpha_v\beta_3$ -receptor [4,8]. Therefore, the use of cyclic RGD-peptides as targeting molecules for tumor therapy seems obvious and has been investigated extensively [1,7,9]. But there are also other pathological conditions, where proliferation of blood vessels plays a key role. In the wet forms of diabetic retinopathy and age-related macular degeneration [10–12], newly formed leaky vessels can damage the surrounding tissue and can lead to retinal detachment due to tensile forces. Today these diseases of the posterior eye are mostly treated by laser coagulation and intravitreal injection of anti-VEGF therapeutics [13,14]. Pollinger et al. have already shown that even in the healthy retina, RGD-modified nanoparticles are able to accumulate [15]. The nanoparticles used in this work were quantum dots, which are perfect model particles due to their strong fluorescence, uniformity and commercial availability. Despite these positive attributes, quantum dots are not suitable for therapeutic applications, as they cannot be loaded with therapeutic agents and contain toxic heavy metals [16]. In contrast, lipid nanocapsules consist exclusively of non-toxic materials and are suitable as carriers especially for lipophilic drugs [17–21]. The surface of LNC can be modified by incorporation of amphiphilic molecules into their shell either during the process of LNC preparation [22] or afterwards by a method named post-insertion [23–25]. For post-insertion the nanocapsules are incubated with PEGylated phospholipids at increased temperatures, typically for 1.5 to 4 hours [23]. In this work, we obtained integrin-targeted nanoparticles by coupling cyclo(-Arg-Gly-Asp-D-Phe-Cys) (c(RGDfC)) to PEGylated distearoyl-*sn*-glycero-

phosphoethanolamine via maleimide-thiol reaction and subsequent post-insertion in LNC. After purification, the RGD-peptide on the particle surface was quantified by a colorimetric assay with phenanthrenequinone. Particle integrity and size increase after post-insertion were confirmed by dynamic light scattering (DLS). The stability of post-inserted LNC was investigated by FRET-measurements for which the LNC were loaded with an acceptor dye and the PEGylated phospholipid was coupled to a donor dye instead of an RGD-peptide. As model cells to show the integrin-mediated uptake of RGD-LNC human dermal microvascular endothelial cells (HDMEC) were used. The availability of the $\alpha_v\beta_3$ -integrin on the cell surface was confirmed by immunostaining with Alexa Fluor 488 anti-human CD51/61. The binding of LNC with and without RGD-modification to HDMEC was quantified by flow cytometry. Further investigation by confocal laser scanning microscopy (CLSM) showed that the nanoparticles are distributed in clusters inside the cell, indicating that they are taken up into cellular vesicles. To make sure that the enhanced cellular interaction of RGD-modified LNC does not go along with toxic effects, HDMEC were incubated with the nanoparticles for 24 hours and their viability was measured by an MTT assay.

3.2 Materials

Miglyol®812 (medium-chain triglycerides (MCT)) was purchased from Caesar&Loretz, Hilden, Germany. Solutol®HS 15 (Poly(ethylene glycol (PEG))₁₅-12-hydroxy-stearate with about 30 % free PEG) and Lipoid S75-3 (soy lecithin with 70% phosphatidylcholine) were kindly provided by BASF, Ludwigshafen, Germany and Lipoid, Ludwigshafen, Germany, respectively. Sympatens (PEG₂₀-cetyl/stearyl ether) was supplied by Kolb, Hedingen, Switzerland. 1,1'-Di-octadecyl-3,3',3'-tetramethylindocarbocyanine perchlorate (DiI), 3,3'-di-octadecyl-oxacarbocyanine perchlorate (DiO), 1,1'-di-octadecyl-3,3',3'-tetramethylindocarbocyanine perchlorate (DiD oil) and 5-((2-(and-3)-S-(acetylmercapto) succinoyl) amino) Fluorescein (SAMSA-fluorescein) were purchased from Thermo Fisher Scientific Inc. (Life Technologies), Waltham, USA (MA). 1,2-distearoyl-*sn*-glycero-3-phosphoethanolamine-N-[methoxy-PEG-2000] (DSPE-mPEG) ammonium salt and DSPE-N-[maleimide(polyethylene glycol)-2000] (DSPE-PEG-Mal) ammonium salt were purchased from Avanti Polar Lipids, Alabaster, USA (AL). Cyclo-(Arg-Gly-Asp-D-Phe-Cys) acetate salt c(RGDfC) was purchased from Bachem Distribution Service, Weil a. Rhein, Germany. All other chemicals were purchased from Sigma Aldrich, Taufkirchen, Germany.

Ultrapure water was obtained from a Milli-Q water purification system from Millipore, Billerica, USA (MA).

3.3 Methods

3.3.1 Preparation of LNC

The LNC were prepared in a phase inversion process which was developed by Heurtault et al. [26]. Briefly, a mixture of 60% NaCl-solution 1% in water, 1.5% Lipoid S75-3 and 17.8% Solutol HS®15 and 20.7% Miglyol®812 was subjected to a heating and cooling cycle in which the phase inversion temperature was passed in each step for three times. In the last cycle the mixture was cooled down in the phase inversion zone with the 2.5-fold amount of water at room temperature to obtain stable LNC. The resulting preparations were filtered through a 0.22 µm poly(ether sulfone) syringe filter prior to further use. For the preparation of fluorescently labeled LNC 3.9 mg DiO or 3.6 mg DiD per g MCT were added to the mixture prior to the heating and cooling cycles. For DiI-labeled LNC, DiI was dissolved in acetone and mixed with the other LNC ingredients, namely Lipoid, Solutol and MCT (4 mg DiI per g MCT). Acetone was evaporated before the addition of NaCl-solution for the subsequent heating and cooling cycles. The calculated concentration of LNCs in the obtained dispersions was 107 mg/ml.

4.1.1 Dynamic Light Scattering (DLS)

Z-Average, polydispersity indices (PDIs) and zeta potentials were determined with a Zetasizer Nano ZS (Malvern Instruments, Herrenberg, Germany), equipped with a He-Ne-Laser at a wavelength of 633 nm and a fixed angle of 173°. The samples were diluted 1:40 with water and the sample temperature was equilibrated to 25°C prior to each measurement.

4.1.2 Coupling of DSPE-PEG-Mal with c(RGDfC) and post-insertion into LNC

The modification of LNC with c(RGDfC) was conducted with and without the addition of tris(2-carboxyethyl)phosphine hydrochloride (TCEP) as reducing agent. In order to reduce disulfide bonds in c(RGDfC), TCEP (15 mg/ml in Dulbecco's phosphate buffered saline (DPBS)) was added to 0.3 mg/ml c(RGDfC) in 30 mM borate buffer (pH 8.5) at a resulting concentration of 15 mM and shaken for 30 min. Reduced or untreated c(RGDfC) was mixed with DSPE-PEG-Mal

(12 mg/ml in DPBS) in a molar ratio of 2:1 and shaken for 2 h protected from light. Fluorescently labeled LNC were incubated with the mixture in a mass ratio of 1:40 (c(RGDfC):LNC) for 3 h at 37°C and subsequently cooled down in an ice water bath for 5 min. For the preparation of control-LNC without RGD-peptide, DSPE-mPEG was incubated with LNC instead of RGD-conjugated DSPE-PEG-Mal (Figure 1).

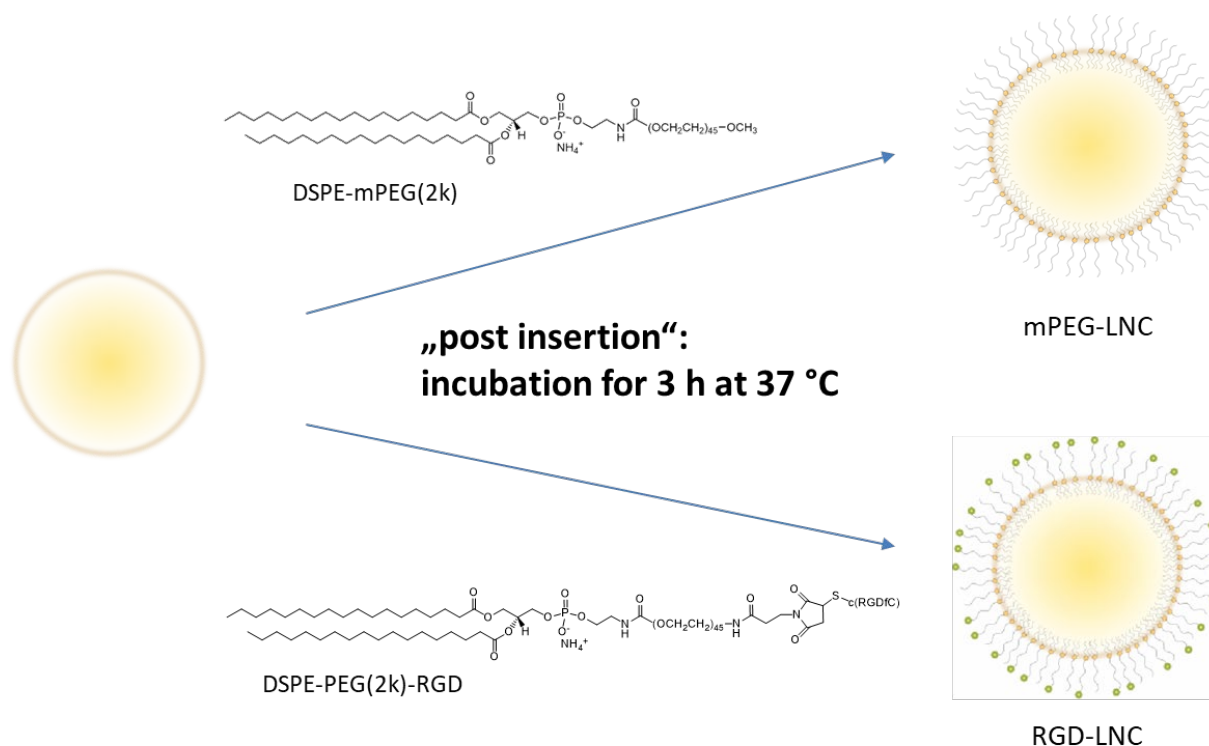


Figure 1: Schematic representation of the surface modification of LNC by post-insertion with DSPE-mPEG or DSPE-PEG-RGD.

Modified LNC were purified two times by ultrafiltration with Amicon Ultra-4 centrifugal filter units (MWCO: 100 kDa; Sigma Aldrich, Taufkirchen, Germany) at 4000 g for 15 min and dialysed against water in Float-A-Lyzer dialysis cassettes (MWCO: 300 kDa; Spectrum Europe BV, Breda, Netherlands) over night. The dialysis medium was changed to DPBS the next day for another 1 h of dialysis. LNC were concentrated by ultrafiltration with Amicon filter units (as specified above).

For cell culture experiments, the particles were sterile-filtered under aseptic conditions. The particle concentration was determined by fluorescence measurement with an Omega FLUOstar plate reader (BMG Labtech, Ortenberg, Germany).

4.1.3 Quantification of c(RGDfC)-modification with phenanthrenequinone

The c(RGDfC)-peptide on the particle surface was quantified by a colorimetric assay with 9,10-phenanthrenequinone as described previously [27,28]. For this assay, the dispersion medium for LNC was changed to water in the last ultrafiltration step after post-insertion. Cyclo(RGDfN(Me)V) (Merck, Darmstadt, Germany) was used as standard for the calibration. The phenanthrenequinone solution (150 μ M in EtOH) was mixed in a ratio of 6:1 with 2 M NaOH. 175 μ l of the resulting reagent solution were pipetted into each vial. 50 μ l LNC-sample or standard solution were added and vortexed. All samples were incubated for 3 h at 50°C. 125 μ l from each vial and 125 μ l 1 M HCl were pipetted into the wells of a 96-well plate and incubated for 1 h at room temperature protected from light. Fluorescence at 395 nm was measured with an LS 55 fluorimeter (Perkin Elmer LAS, Rodgau-Jügesheim, Germany) with an excitation wavelength of 312 nm. To take the potentially higher background fluorescence of LNC samples into account, mPEG-LNC were treated analogously to the other LNC samples and their fluorescence at 395 nm was subtracted as blank value.

4.1.4 Stability testing with fluorescence resonance energy transfer (FRET)

In order to investigate the stability of post-inserted LNC via the FRET-effect, DSPE-PEG-Mal was coupled to SAMSA-fluorescein before the insertion into DiI-labeled LNC. Therefore, SAMSA-fluorescein was dissolved in 0.1 M NaOH (1 mg/ml) and incubated for 15 min at ambient temperature to remove the acetyl protecting group. Afterwards the solution was neutralized with 3 M HCl and mixed with 400 mM phosphate buffer (pH 7.2). The resulting solution had a concentration of 6.8 mg thiol-containing SAMSA-fluorescein per ml and was buffered with 90 mM phosphate. Activated SAMSA-fluorescein was diluted with DPBS, mixed with DSPE-PEG-Mal in a molar ratio of 2:1 (0.5 mM SAMSA-fluorescein in DPBS) and shaken for 2 h protected from light.

The post-insertion of DiI-LNC with DSPE-PEG-SAMSA-fluorescein and the following purification steps were conducted analogously to the post-insertion of LNC with DSPE-PEG-RGD.

For FRET-measurements the LNC were diluted 1:30 with DPBS in a well-plate and fluorescence emission spectra were recorded from 495 – 665 nm with an excitation wavelength of 440 nm and an emission cut-off at 480 nm. Fluorescence measurements with an LS 55 fluorimeter were

conducted daily starting directly after post-insertion (d0) until d13. The samples were stored at 2 - 8°C protected from light.

Additionally, samples of SAMSA-fluorescein modified LNC (FRET-LNC) were subjected to different stress tests before the fluorescence measurement. One sample was heated until boiling for 5 min, one sample was diluted with isopropanol (two parts LNC and one part isopropanol) and one was subjected to five cycles of freezing and thawing. As a control (noPI control) LNC were mixed with free SAMSA-fluorescein in the same ratio that was assumed in the FRET-samples when calculated with complete DSPE-PEG-Mal coupling and post-insertion.

4.1.5 Cell culture

Human dermal microvascular endothelial cells (HDMEC) and Endothelial Cell Growth Medium MV (growth medium), Endothelial Cell Basal Medium MV (basal medium) and phenol red-free basal medium were purchased from PromoCell, Heidelberg, Germany. Cells were cultured in growth medium and used in passages below p6 for all experiments. RGD-binding buffer contained 20 mM Tris(hydroxymethyl)aminomethane (TRIS), 150 mM NaCl, 2 mM CaCl₂, 1 mM MnCl₂ and MgCl₂ each, and 0.10% bovine serum albumin (BSA), according to Pollinger et al. [29]. The pH was adjusted to 7.4 with hydrochloric acid.

4.1.6 Immunostaining of $\alpha_v\beta_3$ - integrin on the cell surface

HDMEC were grown in a cell culture flask to 80-90% confluency. After trypsinization, cells were aliquoted to 500T cells, washed with DPBS and resuspended in 100 μ l ice cold FACS-buffer (0.1% NaN₃ and 1% BSA in DPBS). The cells were kept on ice for all further steps. Alexa Fluor 488 anti-human CD51/61 (400 μ g/ml) and Alexa Fluor 488 Mouse IgG1, K Isotype Ctrl (200 μ g/ml), both purchased from BioLegend, San Diego, USA (CA), were diluted with FACS buffer to 50 μ g/ml. Cells were incubated for 20 min with three different antibody or isotype control concentrations, respectively: 250, 500 and 1000 ng/Mio cells. After the staining, cells were washed two times and resuspended in FACS-buffer. The cell-bound antibody and isotype control were quantified with a FACSCalibur flow cytometer (Becton Dickinson, Franklin Lakes, USA (NJ)). Fluorescence was excited at 488 nm and the emission was detected using a 530/30 nm bandpass filter and 10,000 events per sample were recorded. FACS data were analyzed using the Flowing Software 2 developed by the Turku Centre for Biotechnology, Turku, Finland.

4.1.7 Quantification of nanoparticle binding by flow cytometry

24 h before nanoparticle treatment, HDMEC were seeded at a density of 120,000 cells per well into a 24-well plate. Cells were washed with DPBS. LNC-samples were diluted with RGD-binding buffer to 600 µg/ml. The cells were incubated with 300 µl of the respective LNC-samples for 45 min at 37°C. For the confirmation of receptor mediated binding, free c(RGDfC)-peptide was added at a concentration of 200 µM. To investigate the influence of serum on the nanoparticle uptake 0, 5 or 10% FCS were added to the LNC-samples or LNC were diluted with basal medium instead of RGD-binding buffer prior to incubation with cells. After the incubation, cells were washed with DPBS to remove excess nanoparticles. Afterwards the cells were trypsinized, placed on ice, and washed twice with cold DPBS. After suspending in 100 µl DPBS, dead cells were stained by adding 0.25 µl propidium iodide to each sample. The cell-associated nanoparticle fluorescence was quantified at an excitation wavelength of 488 nm and an emission filter with 530/30 nm using a FACSCalibur flow cytometer. Propidium iodide fluorescence was detected with a 670 nm longpass filter. 10,000 events per sample were recorded and FACS data were analyzed using the Flowing Software 2.

4.1.8 Investigation of LNC uptake by confocal laser scanning microscopy

For the microscopic evaluation of nanoparticle uptake into cells, 20,000 cells per well were seeded into an ibidi chamber µ-slide and let adhere for 24 h. Cells were incubated with DiD-labeled LNC-samples at a concentration of 600 µg/ml in basal medium at 37°C for 45 min. After the incubation, cells were washed twice with phenol red-free basal medium to remove excess nanoparticles. Then they were covered with this medium and examined by confocal laser scanning microscopy (CLSM) with a Zeiss Axiovert 200 microscope combined with an LSM 510 laser-scanning device using a 40x Plan-Neofluar (NA 1.3) oil immersion objective (Zeiss, Jena, Germany). Nanoparticle fluorescence was excited at 633 nm and recorded using a long-pass emission filter at 650 nm. The focal plane was adjusted to 1.1 µm. For image acquisition and processing AIM 4.2. (Zeiss, Jena, Germany) was used.

4.1.9 Cell toxicity assay

DiI-LNC were modified with c(RGDfC) by post-insertion with the addition of TCEP for disulfide bond reduction as described above. HDMEC were seeded into a 96-well plate at a density of

8,000 cells per well. The cells were allowed to adhere for 24 h. RGD-LNC samples with concentrations between 400 and 800 $\mu\text{g/ml}$, as well as samples of mPEG-LNC and blank LNC with 800 $\mu\text{g/ml}$ were prepared in a mixture of DPBS and growth medium. As control, 0.1% sodium dodecyl sulfate in DPBS/growth medium and DPBS/growth medium alone were used. The proportion of growth medium was 46% for all LNC samples as well as for the controls. All solutions were preheated to 37°C before they were added to the cells. After 24 h of incubation at 37°C, all samples were aspirated gently from the wells. 100 μl 3-(4,5-dimethylthiazol-2-yl)-2,5-diphenyl tetrazolium bromide (MTT) solution, prepared by dissolving 6.3 mg MTT in 2.5 ml DPBS and subsequent addition of 7.5 ml growth medium, were added. Cells were incubated for further 2.5 h at 37°C. The MTT-solution was discarded carefully, and cells were lysed with 120 μl 10% SDS-solution per well over night. The absorption of each well was measured at 570 nm and 690 nm with a plate reader (Omega FLUOstar, BMG Labtech, Ortenberg, Germany) and the difference ($A_{570} - A_{690}$) was used to calculate cell viability. All samples were tested in six replicates.

4.1.10 Statistical analysis

If not stated otherwise, experiments were performed in triplicate and data are expressed as mean \pm standard deviation. Statistical significance was assessed by two-tailed t-test for comparison of two groups or by One-way ANOVA with post-hoc Tukey test to compare more than two groups. Data were analyzed with SigmaPlot 12.0.

4.2 Results and discussion

4.2.1 Surface modification of LNC with c(RGDfC)

A variety of approaches for the surface modification of nanoparticles can be found in literature. The maleimide-sulphydryl reaction is widely used, as it is highly efficient and the formed thioether bond is stable under physiological conditions [30,31].

For preparation of endothelial-cell targeting LNC, the thiol group of c(RGDfC) was used as reaction partner for the maleimide-functionalized phospholipid DSPE-PEG(2k)-Mal. The resulting product was post-inserted into the LNC by incubation at 37°C for 3 hours in accordance with Hirsjärvi et al. [24].

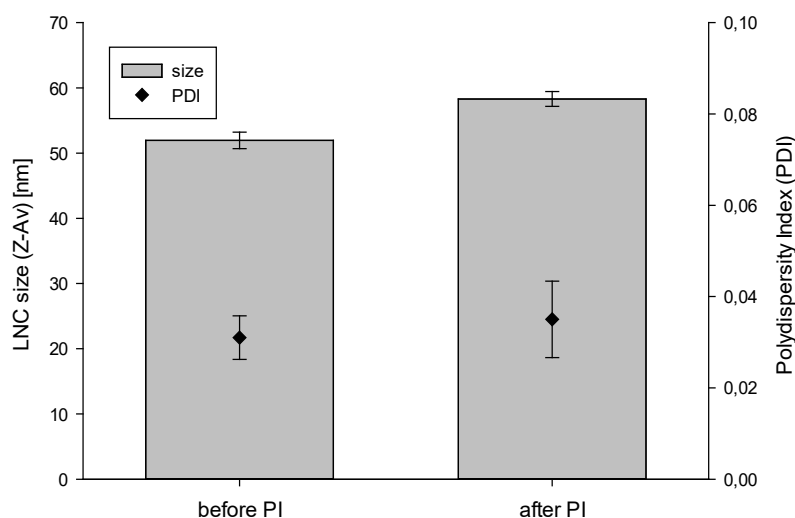


Figure 2: Size and polydispersity indices of LNC before and after post-insertion with DSPE-PEG(2k)-RGD. The change in size is statistically significant ($n=4$; $p < 0.05$). PDI does not change significantly and indicates monodispersity.

The PDI of LNC measured by DLS was below 0.05 for all samples, indicating monodispersity [32]. As no significant change in PDI was observed after particle functionalization, no aggregation was detectable. It is assumed, that during the post-insertion process the phospholipids are integrated into the shell of the LNC with the lipid part protruding into the core and the PEG-chain oriented to the aqueous medium by which the particles are surrounded [23]. Therefore, the longer PEG-chains on the surface lead to an increase in particle size, which was also confirmed by DLS. The mean particle size increased significantly by approximately 6 nm (Figure 2). According to the literature [33,34], the thickness of a polymer layer of PEG₄₅ in brush confirmation is 5.6 nm. As the surface of LNC is already covered with PEG₁₅-chains from Solutol, for which the polymer layer thickness is about 1.1 nm, the maximum increase in size would have been $2 \times (5.6 - 1.1) \text{ nm} = 9 \text{ nm}$. The size of c(RGDfC) is neglected. As the increase in size determined by DLS is lower than expected from these calculations, the protruding ends of the PEG(2k)-chains are likely to be not completely extended. By DLS only the hydrodynamic diameter can be measured and therefore also changes in the hydration shell, which are likely to occur with the RGD-peptide present on the surface, might have an influence on the results.

TCEP is widely used to reduce disulfide bonds which form during storage of thiol-containing molecules over time and therefore to enable an efficient coupling for example with maleimide

groups [24]. As TCEP is not particularly stable in phosphate buffers [35], the TCEP-solution was freshly prepared before use and the reduction step was performed in borate buffer instead of DPBS. It is assumed that TCEP, in contrast to dithiothreitol (DTT), does not impair the reaction of the thiol and the maleimide group and therefore does not have to be removed before the coupling [36]. In a user manual for TCEP•HCl of Thermo Scientific a concentration of 5-50 mM is recommended for the working solution and it is stated that concentrations below 10-20 mM are usually compatible with maleimide conjugation chemistry [37]. Nevertheless, other publications showed a significant decrease in the reaction efficiency in the presence of TCEP [38]. To investigate whether the coupling reaction is more effective with or without the addition of TCEP, both approaches were followed and the quantity of RGD on the LNC surface after the particle modification was determined. Therefore, a quantification method according to Graf et al. [27] was used. In this colorimetric assay 9,10-phenanthrenequinone reacts with arginine residues to a strongly fluorescent product ($\lambda_{\text{ex}} = 312 \text{ nm}/\lambda_{\text{em}} = 395 \text{ nm}$).

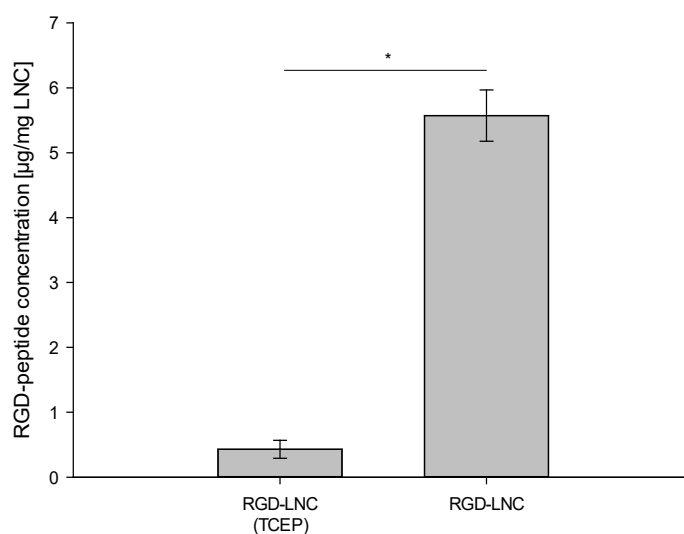


Figure 3: RGD-concentration on lipid nanocapsules determined by phenanthrenequinone assay. The addition of TCEP as reducing agent for c(RGDfC) prior to maleimide coupling led to a tremendous decrease of grafting efficiency. Statistical significance is indicated as (*) $p < 0.05$.

When TCEP was used for c(RGDfC)-reduction before the coupling to DSPE-PEG-Mal, only a marginal amount of RGD was quantified on the LNC ($0.4 \pm 0.1 \text{ µg/mg LNC}$). This peptide-grafting corresponds to approx. 25 ligands per particle. When the LNC modification was conducted without TCEP, $5.6 \pm 0.4 \text{ µg c(RGDfC) per mg LNC}$ were bound to the particle surface (Figure 3),

corresponding to approx. 350 ligands per nanoparticle. The surface area of a spherical particle with 50 nm diameter is approx. 7850 nm². Therefore, the calculated ligand density is 0.04 ligands/nm². Montet et al. have shown strong multivalent nanoparticle-cell interactions even for much lower RGD-grafting densities [39] although Li et al. observed an increase in the uptake of 40 nm nanoparticles with 250 - 5000 RGD-ligands with rising RGD-density [40].

The labelling efficiency was 28% based on a calculated maximum c(RGDfC)-modification of 19.8 µg/mg LNC where c(RGDfC) is completely coupled to DSPE-PEG-Mal and post-inserted into the LNC shell. As the influence of TCEP on the maleimide labelling efficiency is depending on the concentration used, lower TCEP-concentrations might lead to better results. For example, Gretz et al. described a twofold reduction in labelling efficiency with 1 mM TCEP compared to a 0.1 mM concentration [38].

4.1.1 Stability of post-inserted LNC observed by FRET-measurements

Fluorescence resonance energy transfer is the nonradiative transfer of energy from one chromophore to another. This effect is only observable, if the two chromophores are in close proximity to each other, namely about 1-10 nm. In this work LNC which contained an acceptor chromophore (DiI) were post-inserted with a PEGylated phospholipid which was labeled with the donator chromophore (fluorescein) on the end of the PEG-chain. For the quantification of the FRET-effect, fluorescein (495/520) was excited with 440 nm and the emission spectrum was recorded between 495 and 655 nm to record the emission maxima of SAMS-Fluorescein (approx. 520 nm) and DiI (approx. 575 nm). The excitation wavelength was lower than the excitation maximum of fluorescein to avoid recording the excitation light in the emission spectra. When fluorescein and DiI are in close proximity, the FRET-effect is higher and the ratio between the second and the first emission maximum (em_{max2}/em_{max1}) increases (Figure 4A). Therefore, a high em_{max2}/em_{max1} -ratio indicates that the fluorescein is bound to the nanoparticles whereas the ratio decreases if free fluorescein is in the surrounding media.

The em_{max2}/em_{max1} -ratio was 0.70 (± 0.037) in the noPI control and 1.13 (± 0.018) on d0, directly after the post-insertion and subsequent purification (Figure 4B). The ratio remained stable over the following 13 days indicating that the labeled DSPE-PEG-chains were still anchored in the LNC shell (Figure 4C). Also boiling for 5 min had no effect on the em_{max2}/em_{max1} -ratio.

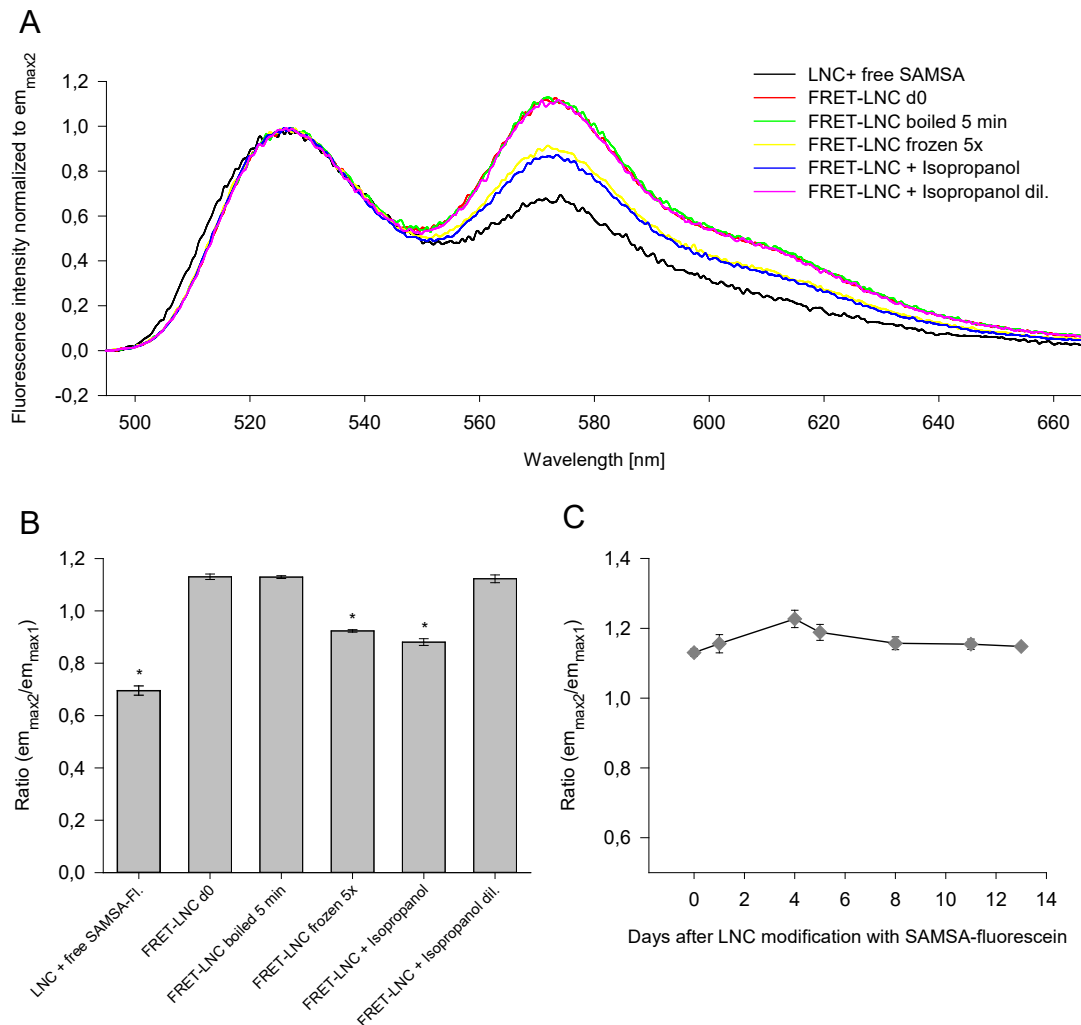


Figure 4: Fluorescence spectra of DiI-LNC with added free SAMSA-fluorescein (noPI control), FRET-LNC directly after preparation and after different stress tests (A) and corresponding FRET-ratios (B). The FRET-ratio em_{max2}/em_{max1} did not decrease over two weeks after LNC preparation, indicating a stable surface modification (C). Statistically significant decrease ($p < 0.05$) compared to FRET-LNC on d0 is indicated by (*).

On the contrary, dilution with isopropanol as well as several cycles of freezing and thawing decreased the ratio to $0.88 (\pm 0.016)$ and $0.92 (\pm 0.006)$, respectively. That indicated, that fluorescein molecules were detached from the LNC surface. Isopropanol in the concentration which was finally present after the 1:30 dilution with DPBS had no effect on the fluorescence or the corresponding FRET-ratio, as the ratio was still at 1.12 ± 0.012 , when isopropanol was added in the respective concentration to DPBS before the addition of LNC (Figure 4B). This proofed that the reduced

FRET-ratio was not resulting from isopropanol interfering with fluorescence measurements but was an effect of the destruction of nanoparticles by isopropanol before further dilution.

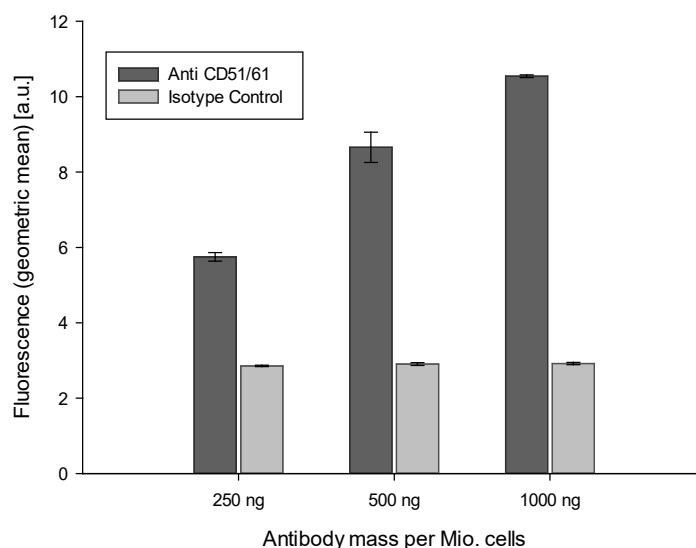


Figure 5: Fluorescence intensity of HDMEC after immunostaining with different antibody concentrations determined by flow cytometry. The cell-associated fluorescence increases with rising concentrations of Alexa Fluor 488-labelled CD51/61-antibody indicating that the receptor was available on the cell surface. In contrast, the concentration of the isotype control-antibody had no influence. This proves that the unspecific antibody binding to cells does not increase with higher concentrations.

4.1.2 Proof for receptor availability on cell surface

The expression of integrins and their availability on the cell surface is depending on several factors like cell proliferation, passage and mechanical stress [5,41–43]. In this work HDMEC in passage ≤ 5 were used as model cells. To confirm that the $\alpha_v\beta_3$ -receptor (CD51/61) is available for targeting on the surface of these cells, immunostaining with a fluorescently labeled anti-CD51/61 antibody was performed with HDMEC in p5. Figure 5 shows the geometric mean of cell fluorescence after immunostaining determined by flow cytometry. While the fluorescence of cells incubated with different concentrations of the control antibody is constantly low, the cell fluorescence increases with rising concentrations of Alexa Fluor 488 anti-CD51/61 antibody. There was no saturation observed with the antibody concentration recommended by the manufacturer. This indicates that the antibody can bind to the integrin and, therefore, the receptor is available on the cell surface.

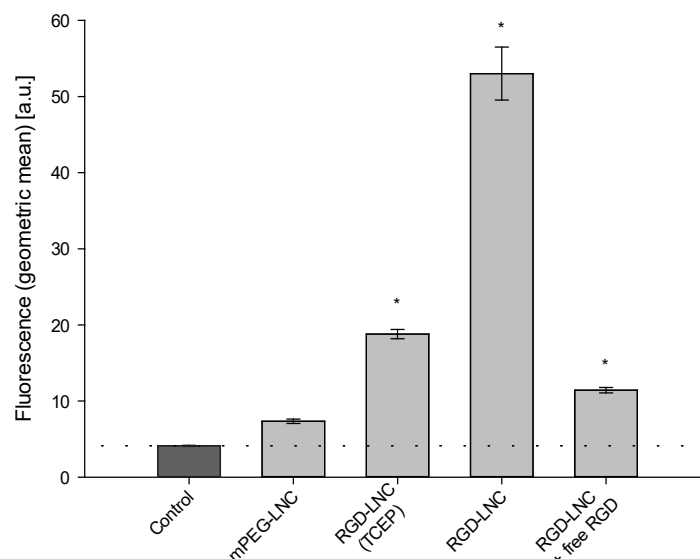


Figure 6: Nanoparticle binding to HDMEC quantified by flow cytometry after 45 min of incubation. RGD-modified LNC show a high interaction with cells which can be inhibited by the addition of free RGD-peptide. If DSPE-PEG-RGD for LNC-functionalization is prepared in the presence of TCEP, the resulting nanoparticles show a lower binding to HDMEC: Statistical significance compared to the fluorescence of untreated control cells is indicated as * ($p < 0.05$).

4.1.3 Quantification of RGD-LNC uptake into endothelial cells by flow cytometry

For the assessment of LNC-uptake into HDMEC the cell-associated particle fluorescence was quantified by FACS (Figure 6). After incubation with LNC which were post-inserted with DSPE-mPEG (mPEG-LNC) the fluorescence of cells was only slightly higher than the fluorescence of untreated cells (control). The presence of RGD on the particle surface (RGD-LNC) led to a 6-fold increase of the cellular binding compared to mPEG-LNC. This is comparable to the binding improvement Hirsjärvi et al. observed for RGD-LNC after incubation with U87MG cells [24]. The interaction was inhibited by the addition of free RGD-peptide, proofing that the binding of RGD-LNC to cells was in fact receptor-mediated. The inhibition was not complete though, which could be explained either by an insufficient amount of free RGD-peptide or by additional non-receptor-mediated interaction of the RGD-decorated particles with the cellular surface. In accordance with the results from the RGD-quantification on the particle surface with phenanthrenequinone, LNC which were modified with RGD-peptide under addition of TCEP (RGD-LNC (TCEP)) showed only slightly increased cellular binding compared to mPEG-LNC.

In this experiment, nanoparticles were incubated with cells in the absence of serum. Under physiological conditions nanoparticles are in contact with serum and therefore, formation of a protein corona might affect the particle-cell interaction [44]. To take that into account, the influence of BSA and FCS on cellular binding was tested (Figure 7). It could be shown that the uptake in binding buffer (0.1% BSA) was higher than in basal medium (no serum protein). Binding of RGD-LNC was further increased in the presence of 5% FCS and was even higher with 10% FCS. This contradicts a publication of Su et al. in which a significantly decreased targeting efficiency of RGD-functionalized gold nanoparticles was observed in the presence of serum [45].

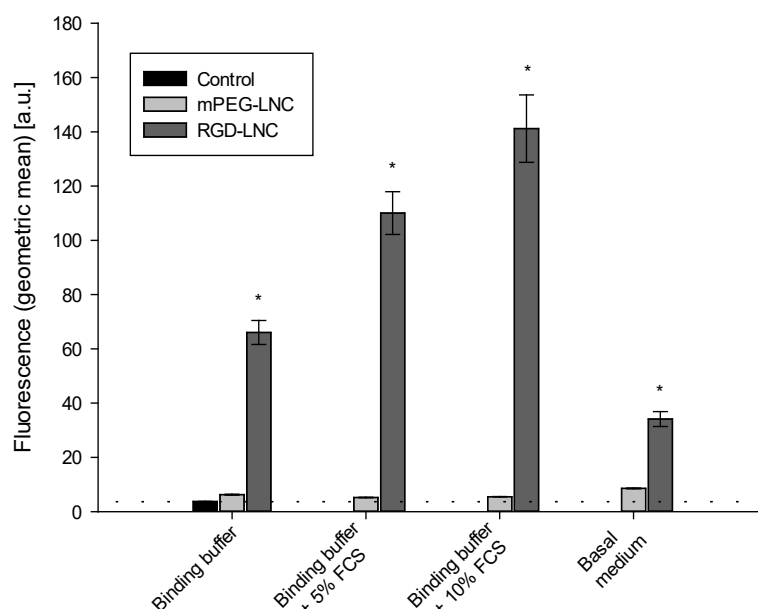


Figure 7: Binding of LNC to HDMEC in different media quantified by FACS. The interaction of RGD-LNC significantly increased in the presence of serum proteins. The influence of the medium on the uptake of mPEG-LNC was not significant. Statistical significance compared to control is indicated as (*) $p < 0.05$.

For the interaction of mPEG-LNC with cells no influence of BSA or FCS was found (Figure 7). Serum concentration and components, like growth factors, influence the expression of different receptors on the cell surface [7,46,47]. Therefore, it might be possible that serum proteins enhance the uptake of nanoparticles due to an increased $\alpha_v\beta_3$ -integrin expression or activity. HDMEC were cultured in medium with a low serum content before the experiments. The higher concentration of serum proteins during the incubation with LNC are therefore likely to change cellular properties.

Another explanation for the increased uptake might be found in the protein corona building up on LNC. Caracciolo et al. showed that nanoparticles can acquire a capability of selective targeting through adsorption of the glycoprotein vitronectin to their surface [48]. Also some bacteria use this mechanism for their internalization into cells [49]. Vitronectin also contains the RGD-motif and binds to the $\alpha_v\beta_3$ -integrin [50]. One explanation for the increased uptake of RGD-LNC at higher FCS-concentrations compared to mPEG-LNC might be a different adsorption-profile for serum proteins. As mentioned before, the RGD-labelling efficiency was about 28%. Therefore, unreacted maleimide residues might have been present as potential reaction partners for serum proteins. In the publication of Su et al. the RGD-density on the nanoparticle surface was comparably high (0.22 - 0.94 ligands/nm²) and no maleimide was used for the conjugation [45], possibly explaining the conflicting results.

Further experiments like the analysis of the protein corona on RGD-LNC versus mPEG-LNC and the quantification of the $\alpha_v\beta_3$ -integrin expression on HDMEC at different FCS-concentrations are necessary to fully understand the influence of FCS on the LNC-cell-interaction. Nevertheless, it is promising for the in-vivo application of RGD-LNC that the presence of serum is even enhancing their interaction with cells instead of blocking it.

4.1.4 Investigation of RGD-mediated nanoparticle uptake by CLSM

Although FACS enables the quantification of the interaction of nanoparticles with cells, it does not allow the differentiation between binding to the cell surface and uptake into the cells. Therefore, the nanoparticle-cell interaction was also investigated by CLSM.

Nanoparticle fluorescence could only be observed, if cells were incubated with RGD-LNC, not with mPEG-LNC. The RGD-LNC were accumulated in vesicle-like structures. The nucleus was free from particle fluorescence, indicating an uptake of the RGD-LNC into vesicles in the cytoplasm of endothelial cells (Figure 8). In general, $\alpha_v\beta_3$ -integrins can be internalized cholesterol- and caveolin 1-dependent as well as in clathrin-coated pits [43]. The uptake of RGD-decorated nanoparticles has been shown to be mostly clathrin-mediated in other publications [51].

Because cells reacted with detachment and clustering to medium changes during the experiments, the incubation with nanoparticles was conducted in basal medium instead of RGD-binding buffer for CLSM. As shown by flowcytometry, the uptake in basal medium is relatively low compared

RGD-binding buffer. Nevertheless, the uptake of RGD-LNC and the difference to mPEG-LNC could be clearly observed.

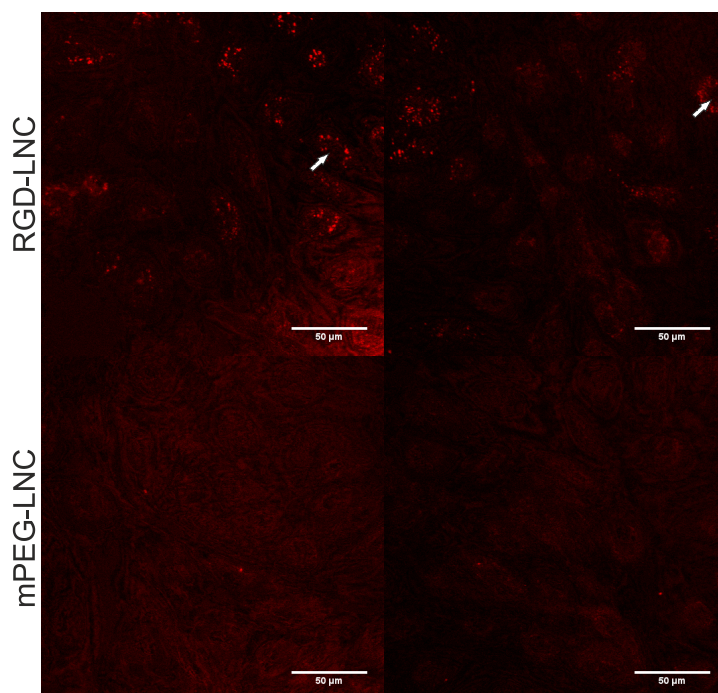


Figure 8: LNC binding to cells observed by confocal microscopy. Nanoparticle fluorescence is displayed in red. RGD-LNC accumulate in the cells in vesicle-like structures. The nucleus is free of nanoparticle fluorescence (white arrows), indicating that the nanoparticle-containing vesicles are located in the cytoplasm. There was no nanoparticle fluorescence observed in cells after incubation with mPEG-LNC.

4.1.5 Tolerability of RGD-functionalized LNC

Because a higher interaction between cells and nanoparticles might probably come along with increased toxicity, the effects of RGD-functionalization of LNC on cell viability was investigated. The MTT-assay was used for the quantification of the metabolic activity of cells. In this assay MTT is converted to an insoluble purple formazan by living cells which can be quantified by its absorbance at 570 nm after solubilization with sodium dodecyl sulfate.

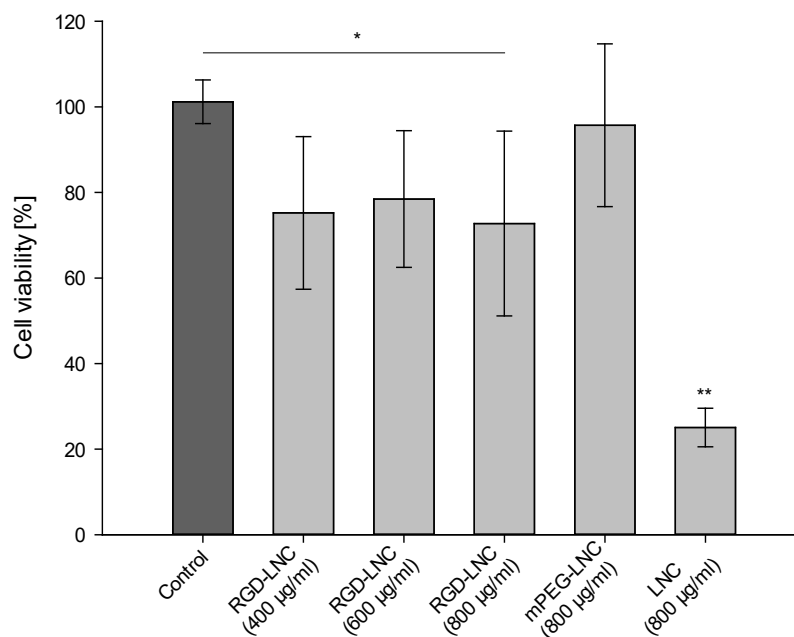


Figure 9: HDMEC viability after 24 h of incubation with different LNC samples quantified by MTT-assay. Treatment with blank LNC was significantly more toxic than every other treatment. RGD-LNC in a concentration of 800 µg/ml decreased cell viability significantly, although the difference to lower concentrations and mPEG-LNC was not significant. Statistical significance is indicated as follows: (**) indicates significant difference to all other groups, (*) indicates significant difference between two groups ($p < 0.05$).

The survival of HDMEC was quantified after 24 h of exposure to LNC (Figure 9). Blank LNC reduced the viability of cells to $25 \pm 5\%$. Paillard et al. also showed a strongly reduced cell viability of less than 10% after 24 h of incubation with LNC with 20 nm, but no such effect for 100 nm LNC (1 mg/ml, F98-cells) [52]. The blank LNC in this experiment were about 50 nm in size and, therefore, the results are consistent with those of Paillard. In contrast, mPEG-LNC had no toxic effects on cells ($96 \pm 19\%$ viability). This difference can be explained by the shielding effect of the longer PEG-chains and the resulting reduced cellular interaction [2]. RGD-LNC slightly reduced the mean viability of cells in all concentrations, although only the effect of the highest concentration tested was significant compared to control cells. The calculated viabilities were $75 \pm 18\%$ for 400 µg/ml, $78 \pm 16\%$ for 600 µg/ml and $73 \pm 22\%$ for 800 µg/ml RGD-LNC.

It is possible that RGD-LNC have a higher toxicity due to the enhanced cellular uptake. But also the targeting motif itself might show inhibitory effects. RGD-peptides have been reported to induce

apoptosis in proliferative endothelial cells due to their $\alpha_v\beta_3$ -antagonism [53,54]. In the treatment of pathological angiogenesis, this “side effect” of RGD as targeting motif might even be useful. For example, Chavakis et al. were able to inhibit the formation of new vessels in a mouse model of hypoxia-induced retinopathy by the injection of a cyclic RGD-pentapeptide [12].

4.2 Conclusion

The successful functionalization of lipid nanocapsules was proven by the direct quantification of RGD on the LNC surface. No reducing agent was needed for RGD-grafting and the addition of TCEP even impaired maleimide-thiol reaction. Stability tests demonstrated that PEG-chains were firmly anchored in the LNC shell and do not detach from the particle core over two weeks. RGD-LNC displayed strongly enhanced uptake into HDMEC which was further increased in the presence of serum protein. The nanoparticles were well tolerated by cells over 24 h of incubation. These results confirm the high potential of RGD-grafted LNC as vehicles for the targeted treatment of pathological angiogenesis, which rises hope for future tumor therapies as well as for proliferative diseases of the eye.

4.3 References

- [1] M.J. Ernsting, M. Murakami, A. Roy, S.-D. Li, Factors controlling the pharmacokinetics, biodistribution and intratumoral penetration of nanoparticles, *Journal of Controlled Release*. 172 (2013) 782–794. <https://doi.org/10.1016/j.jconrel.2013.09.013>.
- [2] S. Dufort, L. Sancey, J.-L. Coll, Physico-chemical parameters that govern nanoparticles fate also dictate rules for their molecular evolution, *Advanced Drug Delivery Reviews*. 64 (2012) 179–189. <https://doi.org/10.1016/j.addr.2011.09.009>.
- [3] M. Pfaff, K. Tangemann, B. Müller, M. Gurrath, G. Müller, H. Kessler, R. Timpl, J. Engel, Selective recognition of cyclic RGD peptides of NMR defined conformation by α IIb β 3, α V β 3, and α 5 β 1 integrins, *J. Biol. Chem*. 269 (1994) 20233–20238. [https://doi.org/10.1016/S0021-9258\(17\)31981-6](https://doi.org/10.1016/S0021-9258(17)31981-6).
- [4] M. Aumailley, M. Gurrath, G. Müller, J. Calvete, R. Timpl, H. Kessler, Arg-Gly-Asp constrained within cyclic pentapeptides Strong and selective inhibitors of cell adhesion to vitronectin and laminin fragment P1, *FEBS Letters*. 291 (1991) 50–54. [https://doi.org/10.1016/0014-5793\(91\)81101-D](https://doi.org/10.1016/0014-5793(91)81101-D).
- [5] B.P. Eliceiri, D.A. Cheresh, The role of α v integrins during angiogenesis., *Mol Med*. 4 (1998) 741–750. <https://doi.org/10.1007/BF03401768>.
- [6] C.R. Cooper, C.H. Chay, K.J. Pienta, The Role of α v β 3 in Prostate Cancer Progression, *Neoplasia*. 4 (2002) 191–194. <https://doi.org/10.1038/sj/neo/7900224>.
- [7] C. Kumar, Integrin α v β 3 as a Therapeutic Target for Blocking Tumor-Induced Angiogenesis, *CDT*. 4 (2003) 123–131. <https://doi.org/10.2174/1389450033346830>.
- [8] R. Haubner, R. Gratias, B. Diefenbach, S.L. Goodman, A. Jonczyk, H. Kessler, Structural and Functional Aspects of RGD-Containing Cyclic Pentapeptides as Highly Potent and Selective Integrin α V/ β 3 Antagonists, *J. Am. Chem. Soc*. 118 (1996) 7461–7472. <https://doi.org/10.1021/ja9603721>.
- [9] T. Lammers, F. Kiessling, W.E. Hennink, G. Storm, Drug targeting to tumors: Principles, pitfalls and (pre-) clinical progress, *Journal of Controlled Release*. 161 (2012) 175–187. <https://doi.org/10.1016/j.jconrel.2011.09.063>.
- [10] S.R. Singh, H.E. Grossniklaus, S.J. Kang, H.F. Edelhauser, B.K. Ambati, U.B. Kompella, Intravenous transferrin, RGD peptide and dual-targeted nanoparticles enhance anti-VEGF intraceptor gene delivery to laser-induced CNV, *Gene Ther*. 16 (2009) 645–659. <https://doi.org/10.1038/gt.2008.185>.
- [11] H. Salehi-Had, M.I. Roh, A. Giani, T. Hisatomi, S. Nakao, I.K. Kim, E.S. Gragoudas, D. Vavvas, S. Guccione, J.W. Miller, Utilizing Targeted Gene Therapy with Nanoparticles Binding α v β 3 for Imaging and Treating Choroidal Neovascularization, *PLOS ONE*. 6 (2011) e18864. <https://doi.org/10.1371/journal.pone.0018864>.

-
- [12] E. Chavakis, B. Riecke, J. Lin, T. Linn, R.G. Bretzel, K.T. Preissner, M. Brownlee, H.-P. Hammes, Kinetics of integrin expression in the mouse model of proliferative retinopathy and success of secondary intervention with cyclic RGD peptides, *Diabetologia*. 45 (2002) 262–267. <https://doi.org/10.1007/s00125-001-0727-z>.
- [13] S.G. Schorr, H.-P. Hammes, U.A. Müller, H.-H. Abholz, R. Landgraf, B. Bertram, The prevention and treatment of retinal complications in diabetes, *Deutsches Ärzteblatt Online*. (2016). <https://doi.org/10.3238/arztebl.2016.0816>.
- [14] Deutsche Ophthalmologische Gesellschaft, Die Anti-VEGF-Therapie bei der neovaskulären altersabhängigen Makuladegeneration – therapeutische Strategien: Stellungnahme der Deutschen Ophthalmologischen Gesellschaft, der Retinologischen Gesellschaft und des Berufsverbandes der Augenärzte Deutschlands – November 2014, *Ophthalmologe*. 112 (2015) 237–245. <https://doi.org/10.1007/s00347-014-3222-x>.
- [15] K. Pollinger, R. Hennig, A. Ohlmann, R. Fuchshofer, R. Wenzel, M. Breunig, J. Tessmar, E.R. Tamm, A. Goepferich, Ligand-functionalized nanoparticles target endothelial cells in retinal capillaries after systemic application, *Proceedings of the National Academy of Sciences*. 110 (2013) 6115–6120. <https://doi.org/10.1073/pnas.1220281110>.
- [16] M.A. Walling, J.A. Novak, J.R.E. Shepard, Quantum Dots for Live Cell and In Vivo Imaging, *International Journal of Molecular Sciences*. 10 (2009) 441–491. <https://doi.org/10.3390/ijms10020441>.
- [17] B. Saliou, O. Thomas, N. Lautram, A. Clavreul, J. Hureauux, T. Urban, J.-P. Benoit, F. Lagarce, Development and in vitro evaluation of a novel lipid nanocapsule formulation of etoposide, *European Journal of Pharmaceutical Sciences*. 50 (2013) 172–180. <https://doi.org/10.1016/j.ejps.2013.06.013>.
- [18] F. Lacoëuille, F. Hindre, F. Moal, J. Roux, C. Passirani, O. Couturier, P. Cales, J.J. Le Jeune, A. Lamprecht, J.P. Benoit, In vivo evaluation of lipid nanocapsules as a promising colloidal carrier for paclitaxel, *International Journal of Pharmaceutics*. 344 (2007) 143–149. <https://doi.org/10.1016/j.ijpharm.2007.06.014>.
- [19] A. Lamprecht, Y. Bouligand, J.-P. Benoit, New lipid nanocapsules exhibit sustained release properties for amiodarone, *Journal of Controlled Release*. 84 (2002) 59–68. [https://doi.org/10.1016/S0168-3659\(02\)00258-4](https://doi.org/10.1016/S0168-3659(02)00258-4).
- [20] A. Babu Dhanikula, N. Mohamed Khalid, S.D. Lee, R. Yeung, V. Risovic, K.M. Wasan, J.-C. Leroux, Long circulating lipid nanocapsules for drug detoxification, *Biomaterials*. 28 (2007) 1248–1257. <https://doi.org/10.1016/j.biomaterials.2006.10.036>.
- [21] M.M.A. Abdel-Mottaleb, D. Neumann, A. Lamprecht, In vitro drug release mechanism from lipid nanocapsules (LNC), *International Journal of Pharmaceutics*. 390 (2010) 208–213. <https://doi.org/10.1016/j.ijpharm.2010.02.001>.

- [22] D. Hoarau, P. Delmas, David, Stéphanie , E. Roux, J.-C. Leroux, Novel Long-Circulating Lipid Nanocapsules, *Pharm Res.* 21 (2004) 1783–1789. <https://doi.org/10.1023/B:PHAM.0000045229.87844.21>.
- [23] T. Perrier, P. Saulnier, F. Fouchet, N. Lautram, J.-P. Benoît, Post-insertion into Lipid NanoCapsules (LNCs): From experimental aspects to mechanisms, *International Journal of Pharmaceutics*. 396 (2010) 204–209. <https://doi.org/10.1016/j.ijpharm.2010.06.019>.
- [24] S. Hirsjärvi, C. Belloche, F. Hindré, E. Garcion, J.-P. Benoit, Tumour targeting of lipid nanocapsules grafted with cRGD peptides, *European Journal of Pharmaceutics and Biopharmaceutics*. (2013). <https://doi.org/10.1016/j.ejpb.2013.12.006>.
- [25] S. Hirsjärvi, S. Dufort, G. Bastiat, P. Saulnier, C. Passirani, J.-L. Coll, J.-P. Benoît, Surface modification of lipid nanocapsules with polysaccharides: From physicochemical characteristics to in vivo aspects, *Acta Biomaterialia*. 9 (2013) 6686–6693. <https://doi.org/10.1016/j.actbio.2013.01.038>.
- [26] B. Heurtault, P. Saulnier, B. Pech, J. Proust, J. Benoit, A novel phase inversion-based process for the preparation of lipid nanocarriers, *Pharmaceutical Research*. 19 (2002) 875–880. <https://doi.org/10.1023/A:1016121319668>.
- [27] N. Graf, D.R. Bielenberg, N. Kolishetti, C. Muus, J. Banyard, O.C. Farokhzad, S.J. Lippard, $\alpha v/\beta 3$ Integrin-Targeted PLGA-PEG Nanoparticles for Enhanced Anti-tumor Efficacy of a Pt(IV) Prodrug, *ACS Nano*. 6 (2012) 4530–4539. <https://doi.org/10.1021/nn301148e>.
- [28] K. Abstiens, M. Gregoritz, A.M. Goepferich, Ligand Density and Linker Length are Critical Factors for Multivalent Nanoparticle–Receptor Interactions, *ACS Appl. Mater. Interfaces*. 11 (2019) 1311–1320. <https://doi.org/10.1021/acsami.8b18843>.
- [29] K. Pollinger, R. Hennig, M. Breunig, J. Tessmar, A. Ohlmann, E.R. Tamm, R. Witzgall, A. Goepferich, Kidney Podocytes as Specific Targets for cyclo(RGDfC)-Modified Nanoparticles, *Small*. 8 (2012) 3368–3375. <https://doi.org/10.1002/smll.201200733>.
- [30] A. Friedman, S. Claypool, R. Liu, The Smart Targeting of Nanoparticles, *CPD*. 19 (2013) 6315–6329. <https://doi.org/10.2174/13816128113199990375>.
- [31] L. Nobs, F. Buchegger, R. Gurny, E. Allémann, Current methods for attaching targeting ligands to liposomes and nanoparticles, *Journal of Pharmaceutical Sciences*. 93 (2004) 1980–1992. <https://doi.org/10.1002/jps.20098>.
- [32] S. Bhattacharjee, DLS and zeta potential – What they are and what they are not?, *Journal of Controlled Release*. 235 (2016) 337–351. <https://doi.org/10.1016/j.jconrel.2016.06.017>.
- [33] A.K. Kenworthy, K. Hristova, D. Needham, T.J. McIntosh, Range and magnitude of the steric pressure between bilayers containing phospholipids with covalently attached poly(ethylene glycol), *Biophysical Journal*. 68 (1995) 1921–1936. [https://doi.org/10.1016/S0006-3495\(95\)80369-3](https://doi.org/10.1016/S0006-3495(95)80369-3).

-
- [34] D. Marsh, R. Bartucci, L. Sportelli, Lipid membranes with grafted polymers: physicochemical aspects, *Biochimica et Biophysica Acta (BBA) - Biomembranes*. 1615 (2003) 33–59. [https://doi.org/10.1016/S0005-2736\(03\)00197-4](https://doi.org/10.1016/S0005-2736(03)00197-4).
- [35] J.C. Han, G.Y. Han, A Procedure for Quantitative Determination of Tris(2-Carboxyethyl)phosphine, an Odorless Reducing Agent More Stable and Effective Than Dithiothreitol, *Analytical Biochemistry*. 220 (1994) 5–10. <https://doi.org/10.1006/abio.1994.1290>.
- [36] C.C. Visser, L. Heleen Voorwinden, L.R. Harders, M. Eloualid, L. van Bloois, D.J.A. Crommelin, M. Danhof, A.G. de Boer, Coupling of Metal Containing Homing Devices to Liposomes via a Maleimide Linker: Use of TCEP to Stabilize Thiol-groups without Scavenging Metals, *Journal of Drug Targeting*. 12 (2004) 569–573. <https://doi.org/10.1080/10611860400010689>.
- [37] Thermo Scientific Inc., Instructions TCEP•HCl, (2013).
- [38] E.B. Getz, M. Xiao, T. Chakrabarty, R. Cooke, P.R. Selvin, A Comparison between the Sulfhydryl Reductants Tris(2-carboxyethyl)phosphine and Dithiothreitol for Use in Protein Biochemistry, *Analytical Biochemistry*. 273 (1999) 73–80. <https://doi.org/10.1006/abio.1999.4203>.
- [39] X. Montet, M. Funovics, K. Montet-Abou, R. Weissleder, L. Josephson, Multivalent Effects of RGD Peptides Obtained by Nanoparticle Display, *J. Med. Chem.* 49 (2006) 6087–6093. <https://doi.org/10.1021/jm060515m>.
- [40] J. Li, Y. Chen, N. Kawazoe, G. Chen, Ligand density-dependent influence of arginine–glycine–aspartate functionalized gold nanoparticles on osteogenic and adipogenic differentiation of mesenchymal stem cells, *Nano Res.* 11 (2018) 1247–1261. <https://doi.org/10.1007/s12274-017-1738-5>.
- [41] L.T. Kim, K.M. Yamada, The Regulation of Expression of Integrin Receptors, *Experimental Biology and Medicine*. 214 (1997) 123–131. <https://doi.org/10.3181/00379727-214-44078>.
- [42] S.-J. Leu, S.C.-T. Lam, L.F. Lau, Pro-angiogenic Activities of CYR61 (CCN1) Mediated through Integrins $\alpha v \beta 3$ and $\alpha 6 \beta 1$ in Human Umbilical Vein Endothelial Cells, *J. Biol. Chem.* 277 (2002) 46248–46255. <https://doi.org/10.1074/jbc.M209288200>.
- [43] P.T. Caswell, S. Vadrevu, J.C. Norman, Integrins: masters and slaves of endocytic transport, *Nat Rev Mol Cell Biol.* 10 (2009) 843–853. <https://doi.org/10.1038/nrm2799>.
- [44] W. Xiao, J. Xiong, S. Zhang, Y. Xiong, H. Zhang, H. Gao, Influence of ligands property and particle size of gold nanoparticles on the protein adsorption and corresponding targeting ability, *International Journal of Pharmaceutics*. 538 (2018) 105–111. <https://doi.org/10.1016/j.ijpharm.2018.01.011>.

- [45] G. Su, H. Jiang, B. Xu, Y. Yu, X. Chen, Effects of Protein Corona on Active and Passive Targeting of Cyclic RGD Peptide-Functionalized PEGylation Nanoparticles, *Mol. Pharmaceutics*. 15 (2018) 5019–5030. <https://doi.org/10.1021/acs.molpharmaceut.8b00612>.
- [46] Y.-X. Sun, M. Fang, J. Wang, C.R. Cooper, K.J. Pienta, R.S. Taichman, Expression and activation of $\alpha v\beta 3$ integrins by SDF-1/CXC12 increases the aggressiveness of prostate cancer cells, *Prostate*. 67 (2007) 61–73. <https://doi.org/10.1002/pros.20500>.
- [47] N. Bryan, K.D. Andrews, M.J. Loughran, N.P. Rhodes, J.A. Hunt, Elucidating the contribution of the elemental composition of fetal calf serum to antigenic expression of primary human umbilical-vein endothelial cells in vitro, *Bioscience Reports*. 31 (2011) 199–210. <https://doi.org/10.1042/BSR20100064>.
- [48] G. Caracciolo, F. Cardarelli, D. Pozzi, F. Salomone, G. Maccari, G. Bardi, A.L. Capriotti, C. Cavaliere, M. Papi, A. Laganà, Selective Targeting Capability Acquired with a Protein Corona Adsorbed on the Surface of 1,2-Dioleoyl-3-trimethylammonium Propane/DNA Nanoparticles, *ACS Appl. Mater. Interfaces*. 5 (2013) 13171–13179. <https://doi.org/10.1021/am404171h>.
- [49] T.D. Duensing, J.P. van Putten, Vitronectin mediates internalization of *Neisseria gonorrhoeae* by Chinese hamster ovary cells., *Infection and Immunity*. 65 (1997) 964–970. <https://doi.org/10.1128/IAI.65.3.964-970.1997>.
- [50] I. Schwartz, D. Seger, S. Shaltiel, Vitronectin, *The International Journal of Biochemistry & Cell Biology*. 31 (1999) 539–544. [https://doi.org/10.1016/S1357-2725\(99\)00005-9](https://doi.org/10.1016/S1357-2725(99)00005-9).
- [51] Z. Guo, B. He, H. Jin, H. Zhang, W. Dai, L. Zhang, H. Zhang, X. Wang, J. Wang, X. Zhang, Q. Zhang, Targeting efficiency of RGD-modified nanocarriers with different ligand intervals in response to integrin $\alpha v\beta 3$ clustering, *Biomaterials*. 35 (2014) 6106–6117. <https://doi.org/10.1016/j.biomaterials.2014.04.031>.
- [52] A. Paillard, F. Hindré, C. Vignes-Colombeix, J.-P. Benoit, E. Garcion, The importance of endo-lysosomal escape with lipid nanocapsules for drug subcellular bioavailability, *Biomaterials*. 31 (2010) 7542–7554. <https://doi.org/10.1016/j.biomaterials.2010.06.024>.
- [53] P.C. Brooks, A.M.P. Montgomery, M. Rosenfeld, R.A. Reisfeld, T. Hu, G. Klier, D.A. Cheresh, Integrin $\alpha v\beta 3$ antagonists promote tumor regression by inducing apoptosis of angiogenic blood vessels, *Cell*. 79 (1994) 1157–1164. [https://doi.org/10.1016/0092-8674\(94\)90007-8](https://doi.org/10.1016/0092-8674(94)90007-8).
- [54] K. Meerovitch, F. Bergeron, L. Leblond, B. Grouix, C. Poirier, M. Bubenik, L. Chan, H. Gourdeau, T. Bowlin, G. Attardo, A novel RGD antagonist that targets both $\alpha v\beta 3$ and $\alpha 5\beta 1$ induces apoptosis of angiogenic endothelial cells on type I collagen, *Vascular Pharmacology*. 40 (2003) 77–89. [https://doi.org/10.1016/S1537-1891\(02\)00339-7](https://doi.org/10.1016/S1537-1891(02)00339-7).

Antiproliferative effect of cyclosporin A
and itraconazole loaded LNC on
microvascular endothelial cells

Abstract

Today's anti-VEGF therapy for the proliferative forms of age-related macular degeneration and diabetic retinopathy comes along with periodic intraocular injections and might lead to an increased risk of geographic atrophy due to side effects on off-target cell types. As a new approach, lipid nanocapsules were designed for an endothelial-cell specific antiangiogenic therapy. A cyclic RGD-peptide was anchored in the nanocapsule surface to enhance the accumulation in proliferative cells by targeting the $\alpha_v\beta_3$ -integrin. The nanoparticles were loaded with cyclosporin A and itraconazole. These two drugs have already been shown to exhibit a synergistic antiproliferative and antiangiogenic effect by interfering with intracellular VEGF-signaling, VEGF-receptor 2 trafficking and by the anti-inflammatory effect of cyclosporin A. The antiangiogenic effect of this new nanoparticle formulation was assessed in human dermal microvascular cells. The inhibition of VEGF-stimulated cell proliferation was quantified, and tube formation assays were performed to assess the influence of nanoparticles on VEGF-induced angiogenesis. The expression of pro- and antiangiogenic markers was quantified by reverse transcription qPCR. Drug-loaded RGD-LNC showed promising therapeutic potential, but there is still need for improvement in the nanoparticle formulation as well as in the assays used for the assessment of their antiangiogenic potential.

5.1 Introduction

Age-related macular degeneration (AMD) and diabetic retinopathy (DR) are among the leading causes of blindness and visual impairment, especially in high-income countries [1–4]. Approximately 30 - 50 million and more than 90 million people worldwide, respectively, are affected by AMD and DR and these numbers are still expected to increase [4,5]. There are proliferative or ‘wet’ forms of both diseases, which are characterized by pathological neovascularizations. In AMD, the newly formed vessels are typically originating from the choroid and can sprout across the retinal pigment epithelium (RPE) into the subretinal or intraretinal space [6–8]. In DR, the neovascularizations are usually originating from the intraretinal blood vessels and can lead to tractional retinal detachment [9–11]. In both diseases, the new vasculature is generally leaky and can cause edema and hemorrhage [11,12].

The discovery of increased levels of vascular endothelial growth factor (VEGF) as a key player in the development of pathological neovascularization [13,14] provided the rationale for today’s therapy by intravitreal injections with the anti-VEGF antibodies ranibizumab or bevacizumab [15–18] or the fusion protein aflibercept [19]. This therapeutic approach was extremely successful [15,17] and is currently standard of care for neovascular AMD [16]. Nevertheless, real-world data suggest a lower effect of anti-VEGF treatment than in the setting of controlled clinical trials, mostly because the injection frequencies tend to be lower in every-day clinical practice [20]. Besides the unfavorable administration route by intraocular injections, a continuous and unspecific inhibition of VEGF-signaling is by far not free of adverse effects. VEGF also exhibits physiological effects on the endothelium [21,21,22], as well as on other cell types like Müller cells, astrocytes, photoreceptors or RPE cells [23–25]. In cell culture, VEGF deprivation reduced the microvilli in RPE cells by which they interact with photoreceptors [26]. A rigorous suppression of VEGF levels has been associated to a decrease in choroid thickness [27], and long-term anti-VEGF therapy was described to enhance the risk of geographic atrophy, which is accompanied by a massive local cell death of RPE cells and photoreceptors [28–30].

Therefore, more selective therapeutic concepts are needed. A promising way to achieve a more targeted therapy are intravenously administered nanoparticles. As they are coming from the blood side, they can bring their cargo directly to endothelial cells without affecting other cell types of the eye. Because endothelial cells are lining the vascular system in the whole body, surface modification of the nanoparticles is needed to enhance accumulation selectively in proliferating

vessels. To this purpose, a cyclic peptide with an arginine-glycine-aspartic acid (RGD)-motif was anchored in the particle corona. Such peptides bind to the $\alpha_v\beta_3$ -integrin [31,32], which is overexpressed in endothelial cells with active proliferation [33]. RGD-modified nanoparticles have already been shown to accumulate in tumors [34,35] and retinal and choroidal capillaries [36,37]. The nanoparticles used in this work are lipid nanocapsules (LNC), which are composed of non-toxic ingredients only, and can be used as vehicle to transport therapeutic substances to intracellular targets [38,39].

Cyclosporin A (CsA) and itraconazole (Itra) were chosen as therapeutic cargo for the nanoparticles, as both drugs show highly promising antiangiogenic effects according to the literature. CsA is capable of interfering with intracellular VEGF-signaling [40] and was shown to inhibit endothelial cell sprouting and proliferation *in vitro* [41,42]. The antiangiogenic effect of CsA is linked to an up-regulation of the transcription factor HEY-1, also referred to as hairy/enhancer of split-related protein 1 (HESR-1) [43]. Additionally, the anti-inflammatory effect of CsA was found to restore the blood-retina-barrier in rats with streptozotocin-induced diabetes [44]. Itra inhibits glycosylation and intracellular trafficking of VEGF-receptor type 2 (VEGFR-2) [45] and, like CsA, endothelial cell proliferation [46]. Expression of the angiogenesis associated migratory cell protein (AAMP), which is increased during angiogenesis, can be reduced by over 50% with Itra treatment [47]. Both drugs exert synergistic effects [42] and their intracellular targets make them ideal candidates for the delivery by RGD-modified LNC.

In this work the potential of RGD-LNC loaded with CsA and Itra was investigated *in vitro* in human dermal microvascular endothelial cells (HDMEC). These cells mimic the behavior of the microvascular cells in the eye better than macrovascular cells [48], which are most commonly used for angiogenesis assays [49–52]. The expression levels of HEY-1 and AAMP in HDMEC were quantified after VEGF stimulation with or without preincubation with LNC to examine the role of these markers in the antiangiogenic effect of the particles. The influence of the nanoparticles on cell proliferation was quantified in a straight-forward colorimetric assay for a first assessment of the treatment effect. Angiogenesis is a complex process which not only includes proliferation, but also several other steps like cell migration and arrangement to new vessels. Therefore, a tube formation assay on a basement membrane extract was conducted to cover a range of angiogenesis steps for further drug effect assessment.

Not least due to an insufficient stimulating effect of VEGF in the conducted assays, the impact of the tested nanoparticles was not completely convincing. Nevertheless, RGD-LNC with and without drug-loading showed promising antiproliferative effects. The test systems as well as the nanoparticles should be optimized and investigated further in the future.

5.2 Materials

Miglyol®812 (medium-chain triglycerides (MCT)) was purchased from Caesar&Loretz, Hilden, Germany. Solutol®HS 15 (Poly(ethylene glycol (PEG))₁₅-12-hydroxy-stearate with about 30 % free PEG) and Lipoid S75-3 (soy lecithin with 70% phosphatidylcholine) were kindly provided by BASF, Ludwigshafen, Germany, and Lipoid, Ludwigshafen, Germany, respectively. 1,1'-Dioctadecyl-3,3,3',3'-tetramethylindocarbocyanine perchlorate (DiI) and 1,1'-dioctadecyl-3,3,3',3'-tetramethylindodicarbocyanine perchlorate (DiD oil) were purchased from Thermo Fisher Scientific Inc. (life technologies), Waltham, USA (MA). 1,2-distearoyl-*sn*-glycero-3-phosphoethanolamine-N-[methoxy(PEG)-2000] (DSPE-mPEG) ammonium salt and DSPE-N-[maleimide(polyethylene glycol)-2000] (DSPE-PEG-Mal) ammonium salt were purchased from Avanti Polar Lipids, Alabaster, USA (AL). Cyclo-(Arg-Gly-Asp-D-Phe-Cys) acetate salt c(RGDfC) was purchased from Bachem Distribution Service, Weil a. Rhein, Germany. Cyclosporin A (CsA) was a kind gift of Pharma Stulln, Stulln, Germany. Itraconazole (Itra) was purchased from Fagron, Barsbüttel, Germany. All other chemicals were purchased from Sigma Aldrich, Taufkirchen, Germany. Ultrapure water was obtained from a Milli-Q water purification system from Millipore, Billerica, USA (MA). TE-buffer contained 10 mM tris(hydroxymethyl)aminomethane (TRIS) and 0.1 mM ethylenediaminetetraacetic acid (EDTA) disodium salt dihydrate and was adjusted to pH 8.0 with NaOH.

5.3 Methods

5.3.1 Preparation of LNC

LNC were prepared in a phase inversion process developed by Heurtault et al. [38] with slight modifications. Therefore, DiI was dissolved in acetone and mixed with 30 mg Lipoid, 1420 mg Solutol and 415 mg MCT (ca. 4 mg DiI per g MCT). Acetone was evaporated and a solution of 1% NaCl in water was added to obtain a mixture of 60% NaCl solution, 1.5% Lipoid,

17.8% Solutol and 20.7% MCT. The mixture was subjected to three heating and cooling cycles in which the phase inversion temperature was passed in each step. In the last cycle the mixture was cooled down in the phase inversion zone with the 2.5-fold amount of water at room temperature to obtain stable LNC. For tube formation experiments, DiD was used for LNC labelling instead of DiI. To this purpose, 1 mg DiD was added to the LNC mixture before the heating and cooling cycles. The resulting particle preparations were filtered through a 0.22 μm poly(ether sulfone) syringe filter prior to further use. The calculated concentration of LNC in the obtained dispersions was 106 - 107 mg/ml.

5.1.1 Loading of LNC with cyclosporin A and itraconazole

CsA-loaded LNC were obtained by dissolving CsA in MCT at a concentration of 4.25 mg CsA per gram MCT. The preparation process was conducted as described above. For Itra-loaded LNC, Itra was first dissolved in methanol. The solution together with the LNC ingredients, Solutol, MCT and Lipoid, and fluorescence dye, was held at 75°C for 30 min to evaporate the methanol. In a second step, NaCl 1% solution was added and the LNC were prepared in the phase-inversion process described above. LNC were filtered through a 0.22 μm syringe filter before further use.

5.1.2 Coupling of DSPE-PEG-Mal with c(RGDfC) and post-insertion into LNC

The modification of LNC with c(RGDfC) was conducted with or without the addition of tris(2-carboxyethyl)phosphine hydrochloride (TCEP) as reducing agent, as specified in the corresponding sections. TCEP was dissolved in Dulbecco's phosphate buffered saline (DPBS), added to 0.3 mg/ml c(RGDfC) in 30 mM borate buffer (pH 8.5) in a resulting concentration of 15 mM and shaken for 30 min. Reduced or untreated c(RGDfC) was mixed with DSPE-PEG-Mal (12 mg/ml in DPBS) in a molar ratio of 2:1 and shaken for 2 h protected from light. Fluorescently labeled LNC were incubated with the mixture in a mass ratio of 1:40 (c(RGDfC):LNC) for 3 h at 37°C and subsequently cooled down in an ice water bath for 5 min. For the preparation of control-LNC without RGD-peptide, DSPE-mPEG was incubated with LNC instead of RGD-conjugated DSPE-PEG-Mal.

The LNC used for the experiments had a diameter of about 50 to 55 nm (Z-Average) before surface modification, measured by dynamic light scattering with a Zetasizer Nano ZS (Malvern Instruments, Herrenberg, Germany). Their size increased in the single digit nanometer range due

to post-insertion. Their poly dispersity index stayed below 0.05, indicating that no aggregation occurred.

5.1.3 Cell culture

HDMEC and Endothelial Cell Growth Medium MV (growth medium), Endothelial Cell Basal Medium MV (basal medium) and phenol red-free basal medium were purchased from PromoCell, Heidelberg, Germany. Cells were cultured in growth medium and used in passages below p6, if not stated otherwise. Recombinant Human VEGF-165 was purchased from BioLegend, San Diego, USA (CA).

5.1.4 Immunostaining of VEGFR-2 on the cell surface

HDMEC (p5 and p6) were grown in a cell culture flask to 80 - 90% confluency. After trypsinization, cells were aliquoted to 500,000 cells, washed with DPBS and resuspended in 100 μ l ice cold FACS-buffer (0.1% NaN₃ and 1% BSA in DPBS). The cells were kept on ice for all further steps. APC anti-human CD309 (VEGFR-2; 200 μ g/ml) and APC Mouse IgG1, K Isotype Ctrl (200 μ g/ml), purchased from BioLegend, San Diego, USA (CA), were diluted with FACS-buffer to 50 μ g/ml. Cells in p5 were incubated for 20 min with three different antibody or isotype control concentrations (250, 500 and 1000 ng/million cells), respectively. Cells in p6 were only treated with the highest concentration. After staining, cells were washed two times and resuspended in FACS-buffer. The cell-bound antibody and isotype control were quantified with a FACSCalibur flow cytometer (Becton Dickinson, Franklin Lakes, USA (NJ)). Fluorescence was excited at 635 nm and the emission was detected using a 661/8 nm bandpass filter. 10,000 events per sample were recorded. Data were analyzed using the Flowing Software 2 developed by the Turku Centre for Biotechnology, Turku, Finland.

5.1.5 Polymerase chain reaction (PCR)

Cells were lysed and RNA was isolated with the peqGOLD total RNA Kit (Peqlab, Erlangen, Germany), including a DNA removal step with a peqGOLD DNase I Digest Kit (Peqlab, Erlangen, Germany). The concentration and quality of RNA was determined with a NanoDrop ND-1000 spectrophotometer (Peqlab, Erlangen, Germany) with the ND-1000 V3.8.1 software. Single-strand DNA was obtained by reverse transcription with the cDNA-Synthesis Kit H Minus (Peqlab,

Erlangen, Germany) and a LifeEco thermocycler (Biozym, Hessisch Oldendorf, Germany). A mixture of 85% oligo(dT) primer and 15% random hexamer primer was used for the reaction.

Primers, according to Table 1, were purchased from Eurofins Genomics, Ebersberg, Germany, in high purity salt free quality. The primers were dissolved to a concentration of 100 pmol/μl in RNase-free 10 mM tris(hydroxymethyl)aminomethane (TRIS-)buffer (pH 8.0) containing 0.1 mM ethylenediamine-tetraacetate (EDTA) disodium salt dihydrate and diluted 1:10 with RNase-free water.

Qualitative PCR was conducted to test the suitability of the primers and to confirm the expression of VEGFR-2 in HDMEC. Therefore, RNA was isolated from HDMEC cultured in a T-75 flask to about 80% confluency and reverse transcription was performed with 0.7 μg isolated RNA as described above. PCR was conducted with a peqGOLD Taq-DNA-Polymerase all inclusive kit (PqLab, Erlangen, Germany) according to manufacturer's instructions with 10 pmol of forward and reverse primer and an equivalent of 3.5 ng reversely transcribed RNA. After 2 min of enzyme activation at 94°C, a three-step cycling protocol was applied with 35 amplification cycles including denaturation at 94°C, annealing at 50°C and extension at 72°C for 30 s each. At the end, 72°C were held for 5 min. The PCR products were analyzed by gel electrophoresis in a 2% agarose gel (Life Technologies, Carlsbad, USA (CA)) containing 0.2 μg/ml ethidium bromide. The electrophoresis was run in TRIS-Acetate-EDTA buffer with 80 V for 70 minutes. The peqGold 50 bp DNA ladder and ultra-low range DNA ladder I (PqLab, Erlangen, Germany) were used as size standards. The bands on the gel were visualized with a Fisherbrand FT-20/312 UV transilluminator 312 (Fisher Scientific, Schwerte, Germany) and pictures were taken with a Kodak DC290 camera and Kodak 1D Image Analysis Software (Kodak, Stuttgart, Germany).

For the assessment of the effect of drug-loaded LNC on the expression of cellular angiogenesis markers, HDMEC were grown in 6-well plates with 60,000 cells per well in growth medium. 900 μl LNC samples (surface modification with TCEP) in a concentration of 0.6 mg/ml or corresponding concentrations of free CsA and Itra were added to the cells. After 24 h, the samples were removed, and cells were stimulated with 50 ng/ml VEGF in basal medium for further 24 h. RNA was isolated and reverse transcription was performed with 0.3 μg RNA each as described above. For the quantitative determination of HEY-1 and AAMP expression, real-time reverse transcription (RT-)PCR was performed using a LightCycler Instrument (Roche Diagnostics, Rotkreuz, Switzerland) and a KAPA SYBR Fast Universal Kit (PqLab, Erlangen, Germany). A three-step

cycling protocol was applied with 3 min of enzyme activation at 95°C and 50 amplification cycles with 15 s of denaturation at 95°C, 20 s at 60°C for annealing and further 20 s at 72°C for extension and data collection. At the end, the samples were heated to 95°C for 5 s, cooled down to 55°C and then heated continuously to 95°C over 1 min for melting curve recording. The LightCycler 480 Software Version 1.5 was used for data acquisition and analysis. The expression of HEY-1 and AAMP was related to the housekeeping gene glyceraldehyde 3-phosphate dehydrogenase (GAPDH).

Table 1: Primers for qualitative and quantitative PCR.

Target	Sequence (F = forward, R = reverse; 5' to 3')	Melting point	Product length	Reference
HEY-1	F: GTCTCATTTGGAGTGTGGT	55.2°C	112 bp	[43]
	R: GAATTTGAGATCCGTGTGAT	57.3°C		
AAMP	F: CTTTGCATTGCACTCAGCAT	55.2°C	366 bp	[47]
	R: CAGTCACCATTCGGGACTTT	57.3°C		
VEGFR-2	F: GTGACCAACATGGAGTCGTG	59.4°C	660 bp	[53]
	R: CCAGAGATTCCATGCCACTT	57.3°C		
GAPDH	F: GAAGGTGAAGGTCGGAGTC	57.2°C	226 bp	[37]
	R: GAAGATGGTGATGGGATTTC	53.7°C		

5.1.6 Cell proliferation assay

HDMEC were seeded into a 96-well plate at a density of 4,000 cells per well. The cells were allowed to adhere for 24 h. Two different experimental approaches were tested in a cell proliferation assay.

In the first approach, LNC were modified with RGD reduced with TCEP. Stock solutions of CsA (304 µg/ml) and Itra (18 µg/ml) were prepared in DMSO. The samples were diluted in a mixture of DPBS and basal medium to a final concentration of 0.6 mg/ml LNC or corresponding concentrations of CsA and Itra (CsIt). The proportion of basal medium was 51% for all samples. All solutions were preheated to 37°C before they were added to the cells. The cells were preincubated with LNC or free CsIt at 37°C for 24 h, then all samples were aspirated gently from the wells. Cells were stimulated with 50 ng/ml VEGF in basal medium with 2% FCS for further 24 h.

For the second approach, LNC were modified with RGD without the addition of TCEP and cells were incubated with LNC or corresponding controls simultaneously to stimulation with VEGF for 24 h. In this experiment, all samples contained 50% basal medium, 2% FCS and 10 ng/ml VEGF.

For both protocols, cell proliferation was quantified by a colorimetric assay in which 3-(4,5-dimethylthiazol-2-yl)-2,5-diphenyl tetrazolium bromide (MTT) is converted to an insoluble purple formazan by living cells. Therefore, the VEGF-containing solutions were aspirated from cells and 100 μ l MTT solution, prepared by dissolving 6.3 mg MTT in 2.5 ml DPBS and subsequent addition of 7.5 ml growth medium, were added. Cells were incubated for further 2.5 h at 37°C. The MTT-solution was discarded carefully, and cells were lysed with 120 μ l 10% SDS-solution per well over night. The absorption of each well was measured at 570 nm and 690 nm with an Omega FLUOstar plate reader (BMG Labtech, Ortenberg, Germany) and the difference (A570-A690) was used to calculate the metabolic activity of cells. All samples were tested in six replicates.

5.1.7 Tube formation assay

For the evaluation of the optimal experimental parameters for the tube formation assay, different seeding densities and incubation times were tested. A 96-well plate was coated with growth-factor reduced, phenol-red free Matrigel (VWR international, Ismaning, Germany) and preheated to 37°C overnight. Cells were stained with 2.0 μ g/ml Calcein AM in phenol-red free basal medium for 30 min and seeded in densities between 5,000 and 40,000 cells per well with and without supplementation of 50 or 100 ng/ml VEGF. The cells were incubated at 37°C and tube formation was observed after different incubation times between 4 and 26 h with a Zeiss Axiovert 200 microscope combined with an LSM 510 laser-scanning device using a Plan-Neofluar 5x/0.15 Ph1 objective (Zeiss, Jena, Germany). Calcein fluorescence was excited at 488 nm and recorded using a long-pass emission filter at 505 nm. AIM 4.2. (Zeiss, Jena, Germany) was used for image acquisition and processing. Different tube formation parameters, like tube length, number of meshes and nodes and the area covered by cells, were quantified with the Angiogenesis Analyzer tool for ImageJ (available online at <https://imagej.nih.gov/ij/macros/toolsets/>) [54].

For the investigation of the effect of LNC on tube formation, cells were seeded in a 6-well plate with 60,000 cells per well and allowed to adhere for 24 h. They were pre-incubated with different samples of LNC (modification without TCEP; 0.6 mg/ml) or controls in basal medium for 24 h before the tube formation assay. Cells were stained with 2.0 μ g/ml Calcein AM in basal medium

for 30 min. They were trypsinized carefully and resuspended in phenol-red free basal medium to 80,000 cells per milliliter. VEGF was added to the cell suspensions in a concentration of 190 ng/ml and 8,000 cells per well were seeded into a Matrigel-coated 96-well plate. Tube formation was investigated by laser scanning microscopy as described above.

5.1.8 Statistical analysis

If not stated otherwise, experiments were performed in triplicate and data are expressed as mean \pm standard deviation. Statistical significance was assessed by two-tailed t-test for comparison of two groups or by One-way ANOVA with post-hoc Tukey test to compare more than two groups. Data were analyzed with SigmaPlot 12.0.

5.2 Results and discussion

5.2.1 Expression and availability of VEGFR-2 in HDMEC

Because VEGF stimulation was an important part of the conducted tests for cell proliferation, tube formation and expression of angiogenesis markers, the expression and availability of the VEGFR-2 was examined before HDMEC were used for these experiments.

The expression of VEGFR-2 on mRNA-level was investigated by qualitative PCR and subsequent gel electrophoresis. The band with the PCR product (660 bp) was clearly visible (Figure 1A), so the receptor expression in HDMEC was confirmed.

Because the expression alone does not proof the availability of a receptor on the cellular surface, immunostaining of VEGFR-2 was conducted in addition to PCR. Figure 1 shows the mean fluorescence of HDMEC quantified by flow cytometry after incubation with fluorescently labelled anti-human CD309 (VEGFR-2) antibody and the corresponding isotype control. While the fluorescence stayed at a low level at all three concentrations of the isotype control, it was about eight times higher after incubation with anti-CD309 antibody. This proves that the receptor is accessible on the cells. With 250 ng antibody per million cells no complete staining was achieved (21.6 ± 0.5 a.u.), whereas there was no difference in fluorescence between 500 and 1000 ng/million cells (23.4 ± 0.9 and 23.6 ± 0.8 a.u.), indicating a saturation of the receptor with antibody.

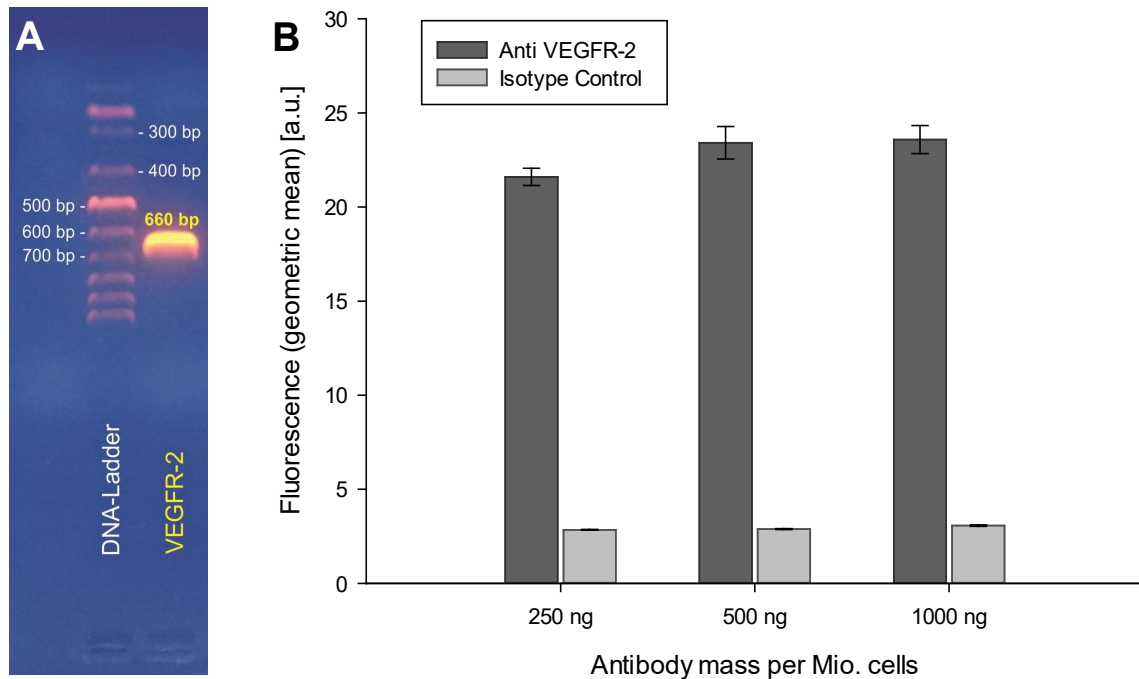


Figure 1: Confirmation of the VEGFR-2 expression in HDMEC on RNA-level by qualitative PCR and subsequent gel electrophoresis (A) and on the cellular surface by immunostaining of HDMEC (p5) with an APC-labelled VEGFR-2 antibody in different concentrations (B). Fluorescence is expressed in arbitrary units (a.u.).

Cryoconservation of cells in higher passages allows to obtain more cells from one batch, what can be useful, especially as the batch to batch variability might be high in primary cells. Nevertheless, the expression of cell-line specific markers might be reduced during cultivation [55–57]. Therefore, it was tested, whether cryoconservation in p5 (staining in p6) was disadvantageous regarding the availability of the VEGFR-2 on the cellular surface compared to cryoconservation in p3 (staining in p5). As maximum staining was achieved with 1,000 ng antibody per million cells, cells in p6 were stained with this concentration as well to see if the extent of receptor availability was lower when cells were frozen and used in higher passages. No significant difference was observed between the two cell batches. The geometric means of fluorescence after deduction of the corresponding isotype control fluorescence were 20.5 ± 0.7 (p5) a.u. and 19.1 ± 0.4 a.u. (p6).

5.1.1 Expression of angiogenesis markers

The primers for AAMP and HEY-1 were first tested in a qualitative reverse transcription PCR with subsequent gel electrophoresis to confirm their suitability. Both bands (AAMP with 366 bp and

HEY-1 with 112 bp) were clearly visible (Figure 2A), so both markers were expressed and the primers and conditions for PCR led to sufficient product amplification.

For the analysis of quantitative RT-PCR, the expression levels of the target genes were correlated to the respective GAPDH expression to correct for different template DNA amounts or variations in the PCR efficiency between runs. The corrected values were then correlated to the gene expression in control cells which were incubated with 50 ng/ml VEGF in basal medium (dd Cp-method). According to the literature, CsA induces a highly elevated HEY-1 expression, which is attributed to the drug's inhibition of angiogenesis. Shah et al. observed a 44-fold increase in HEY-1 expression after treatment with 2 μ g/ml CsA [43]. Upregulation of HEY-1 is associated with reduced VEGFR-2 expression [43,58] and the transcription factor has been described to play an important role in vascular development [59]. As shown in Figure 2B, only treatment with free CsIt led to a significant increase ($2.4\text{-fold} \pm 0.3$) of HEY-1 expression. After treatment with RGD-CsIt-LNC, the HEY-1 RNA-levels were 1.6 ± 0.5 times higher than for control cells, but this difference was not significant. The CsA concentration in the free CsIt control as well as in the RGD-CsIt-LNC sample was 1.5 μ g/ml and, therefore, in a similar range as in the experiments of Shah et al.. The elevation of HEY-1 they observed was partially attributed to Cremophor, which was used as solubilizer for CsA (8.8-fold increase in HEY-1 expression with Cremophor alone). No such effect was observed for DMSO [43].

The fluctuation of the PCR results for AAMP expression was very high in all samples, even for control cells. The results are presented in Figure 2B as individual data points instead of columns, as the data were not normally distributed and this presentation allows a deeper insight into the actual values. The crossing points at which fluorescence was detectable in the real-time PCR occurred at high cycle numbers (>20 cycles). This indicates that too small amounts of isolated template RNA or insufficient PCR efficiency might be responsible for the poor reproducibility. Due to the high scattering of the results, no significant changes in AAMP expression were observable after treatment with LNC or free CsIt. According to Del Carratore et al., expression of AAMP, which is increased during angiogenesis, can be reduced by over 50% with 1.4 or 2.8 μ g/ml Itra [47]. The concentration of Itra in the LNC samples was 90 ng/ml and, therefore, about 16 to 31-fold lower than the concentration used by Del Carratore et al. [47]. In another publication, 0.56 μ g/ml Itra in combination with 10 μ g/ml CsA were used to synergistically and significantly inhibit proliferation, sprouting and tube formation of endothelial cells [42]. The CsA-Itra-ratio used

in LNC was similar, but due to the poor solubility of Itra in the formulation, lower concentrations had to be used to obtain stable LNC without precipitation. Another reason for lower efficacies compared to free drugs might be an insufficient release from LNC after internalization into cells [60].

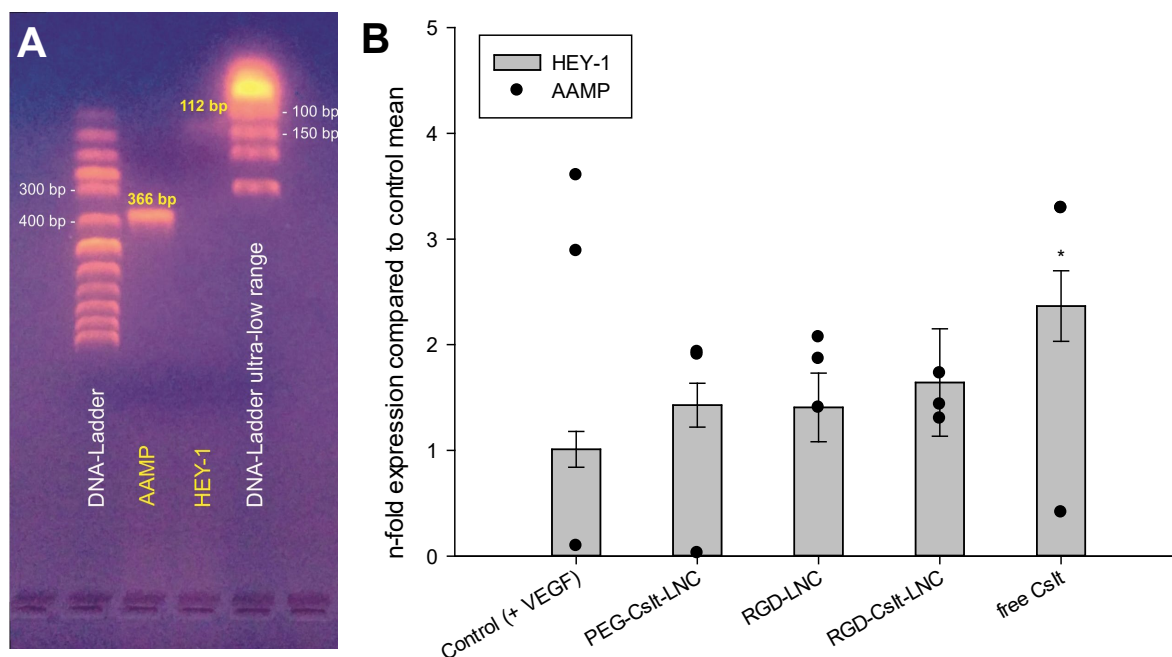


Figure 2: Test of AAMP and HEY-1 primers by qualitative PCR and subsequent gel electrophoresis (A) and change of HEY-1 (grey bars) and AAMP (black dots) expression after treatment with different LNC formulations or corresponding concentrations of free CsA and Itra (CsIt) (B). Statistically significant ($p < 0.05$) difference in HEY-1 expression compared to the control is indicated with (*).

Nevertheless, it is important to say that HEY-1 and AAMP are not the only factors responsible for the antiangiogenic and antiproliferative properties of CsA and Itra, respectively. Both drugs are described to inhibit angiogenesis via multiple mechanisms [40,41,47]. For example, CsA blocks the VEGF-induced translocation of the nuclear factor of activated T-cells (NFAT) and activates the p44/42 MAPK [40], and Itra is an inhibitor of cholesterol biosynthesis [46] and mTOR and ERK 1/2 phosphorylation [47]. Therefore, low effects on HEY-1 and AAMP might not necessarily come along with insufficient antiangiogenic potential.

5.1.1 Inhibition of VEGF-induced cell proliferation by RGD-LNC and RGD-CsIt-LNC

Angiogenesis as formation of new blood vessels from existing ones is a multi-step process. During this process, the endothelial cells have to disrupt the basement membrane, migrate in the direction of a pro-angiogenic stimulus, proliferate and form new tubular structures. There are multiple *in-vitro* tests mimicking these steps [49]. The MTT proliferation assay is a fast and straight-forward method to get a first impression of the inhibitory effect of drug-loading and surface modification of LNC and for the evaluation of different experimental conditions and cell stimulation protocols. In this work, cell proliferation was quantified after pretreatment of cells with the LNC formulations before incubation with 50 ng/ml VEGF (successive treatment) as well as after co-incubation with LNC and 10 ng/ml VEGF. Kruskal-Wallis one-way analysis of variance (ANOVA) on ranks was used to compare the results for different treatments, as the data were not normally distributed. The results are shown in Figure 3. The successive stimulation with 50 ng/ml VEGF led to a $25 \pm 7\%$ increased proliferation compared to unstimulated cells. Nevertheless, this increase was not statistically significant. In the simultaneous stimulation, only 10 ng/ml VEGF were added to the cells. Although the increase in proliferation was lower in this setting than with 50 ng/ml VEGF ($19 \pm 3\%$), the difference was significant here due to lower scattering. A setting, where the effect on cell proliferation of VEGF itself is not significant, is not suitable to find a significant inhibition of VEGF stimulation by other treatments. In general, the standard deviations in the measured absorption were higher after successive treatment, which might be a result of the additional medium change in this protocol. Especially the high standard deviations in cells which were treated with RGD-modified LNC might be caused by cell detachment and loss during the change to the VEGF-containing medium, due to the $\alpha_v\beta_3$ -antagonism of RGD peptides [61,62].

Additionally, surface modification of RGD-LNC and RGD-CsIt-LNC was conducted with TCEP as reducing agent. As described in chapter 4, the use of TCEP leads to significantly reduced RGD coupling to the particle surface and might, therefore, lead to lower particle internalization into the target cells.

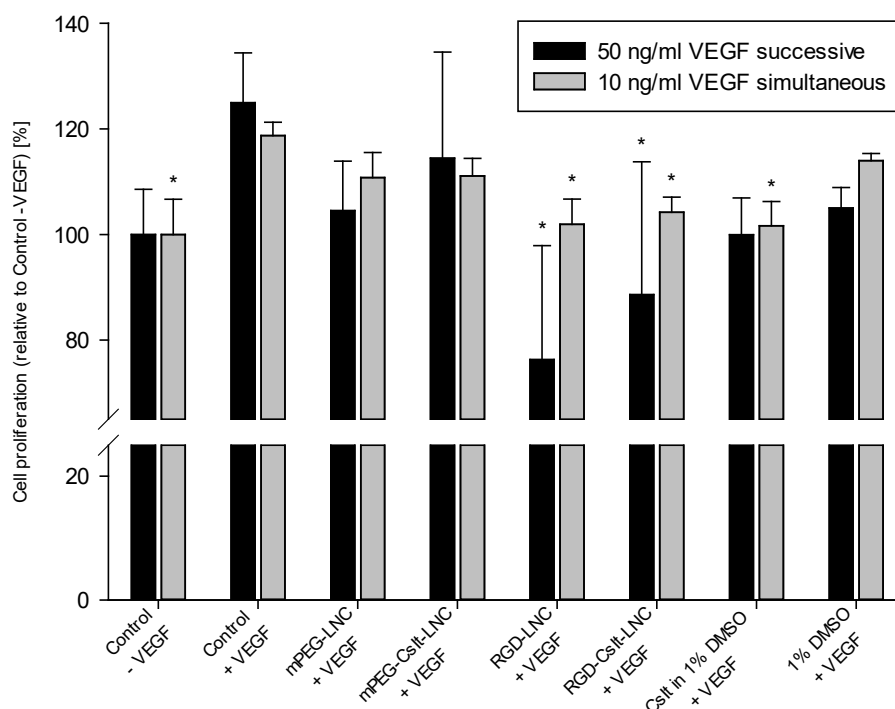


Figure 3: Cell proliferation assay with MTT. For successive stimulation (black bars), cells were incubated with different nanoparticle formulations, free CsA and Itra (CsIt) or the respective DMSO-concentration for 24 h and subsequently stimulated with 50 ng/ml VEGF for further 24 h. For simultaneous stimulation (grey bars), cells were co-incubated with the nanoparticle, CsIt or DMSO samples and 10 ng/ml VEGF for 24 h. In both cases, the metabolic activity of cells was then quantified with the colorimetric MTT-assay. The cell density was normalized to unstimulated cells (Control -VEGF). Statistically significant ($p < 0.05$) difference compared to the respective stimulated control cells (+ VEGF), determined by Kruskal-Wallis ANOVA on ranks, is indicated with (*).

For the above-mentioned reasons, the data from the simultaneous treatment with LNC and VEGF led to more reliable results, which are also presented in Figure 3 (light grey columns). In this experiment the presence of RGD-LNC, CsIt-loaded RGD-LNC as well as free CsIt led to a complete inhibition of the VEGF-induced cell proliferation. LNC without RGD-grafting did not show a significant effect, regardless of their drug loading. It was also excluded that DMSO itself, which was used for drug solubilization for free CsIt, had an inhibitory effect on cell proliferation. Due to the small difference in cell growth with and without VEGF, it was not possible to detect any differences between the effects of drug-loaded and unloaded RGD-LNC or free CsIt in this assay. Nevertheless, the complete inhibition of the VEGF-induced cell proliferation to levels

without VEGF stimulation in this setting suggests great therapeutic potential of RGD-CsIt-LNC without any signs for toxic effects.

5.1.1 Tube formation assay with LNC-treated cells

The MTT-assay can detect an increase or decrease in the number of metabolically active cells and, therefore, allows conclusions on the extent of cell proliferation, when cells were seeded in the same density before the treatments. As already mentioned above, this is a fast and easy method, but the results are very unspecific. Another test which is widely used in the investigation of angiogenesis is the tube formation assay on a basement membrane extract. This assay covers multiple steps of angiogenesis like the interaction with the surrounding matrix, migration, alignment and the formation of tubular structures [49,50,63]. For this reason, the tube formation assay perfectly complements the MTT-assay in the screening of antiangiogenic treatments.

For the assay, the wells were coated with Matrigel, a basement membrane extract derived from the Engelbreth-Holm-Swarm tumor [52]. Pretests were performed to find the right seeding density and incubation time, as these factors are crucial for successful tube formation [52,63]. The pretests (results in the supporting information) revealed poor reproducibility of tube formation in the assay, especially for different cell batches. The batches had highly different proliferation rates and effects of VEGF were only seen at distinct time points, when cells were not too dense to form defined tubes but close enough to interact with each other (see supporting information, Figure 5).

For the assessment of the antiangiogenic effect of LNC, cells were pretreated with different LNC samples or free CsIt before they were seeded on Matrigel. As the proliferation experiments described above showed a stronger stimulating effect for increased VEGF levels, and addition of 100 ng/ml VEGF had no significant effect on the used cell batch in the pretests (supporting information, Figure 6), the VEGF concentration was raised further to 190 ng/ml for this assay. Images taken after 10 and 26 hours of incubation (Figure 4) show that cells did not adhere well to the Matrigel surface. Only few tube-like structures were visible after 26 h of incubation for control cells (with and without VEGF) and no tube formation at all was observable for cells treated with LNC or drugs. A possible explanation is that the VEGF concentration might have been too high. In the literature, concentrations between 10 and 100 ng/ml are typically used to stimulate cell proliferation and tube formation [42,43,45]. Concentrations up to 200 ng/ml are used less frequently [64,65].

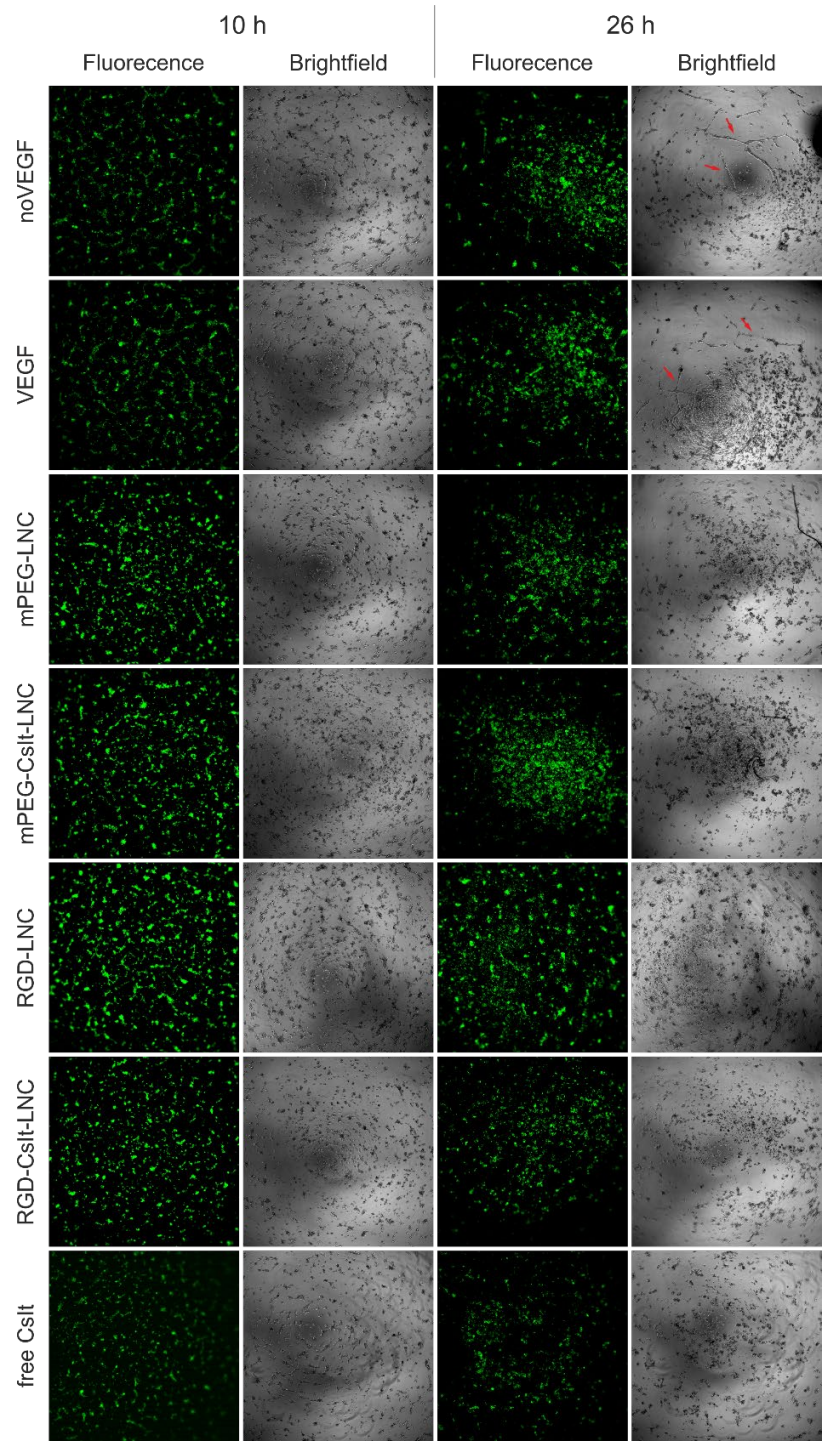


Figure 4: Tube formation assay after 10 and 26 h of incubation with different samples of LNC or free cyclosporin A and itraconazole. The images are showing an area of 2.5 x 2.5 mm each. Cells did not adhere well to the Matrigel surface and minimal tube formation, indicated with red arrows, was only observable for control cells (VEGF and noVEGF) which were not treated with LNC or drugs.

Shah et al. observed a lower stimulation of endothelial cell migration and stress fiber assembly with 50 ng/ml VEGF than with 1 - 10 ng/ml [43]. Due to the limited availability of cells from one batch, dose-response experiments for the evaluation of the optimal VEGF concentrations were not part of the pretests. For future experiments, more cell batches should be pooled and VEGF-concentration should be included in the optimization of the experimental conditions. Another aspect which might be a reason for the reduced tube formation compared to the pretests might be the increased stress on cells due to the treatment with LNC or corresponding controls. The pre-incubation comes along with additional cell detachment and seeding before and after the treatment with the samples of interest, as well as with the involved media changes. This stress might hamper the capability of cells to interact with the Matrigel matrix and form tubes.

5.2 Conclusion

LNC loaded with CsA and Itra have great potential for an endothelial-cell specific antiangiogenic therapy. The surface decoration with c(RGDfC) enables the internalization into cells and might itself exert antiproliferative effects [61,62,66]. The nanoparticles used in the assays for the quantification of angiogenic markers on RNA level and the proliferation assay with successive treatment were conjugated to c(RGDfC) after the addition of TCEP as reducing agent for disulfide bonds in the peptide. As the surface modification without TCEP has been shown to lead to better grafting efficiencies (see chapter 4), internalization and therapeutic effects are expected to be higher when no TCEP is used.

Nevertheless, data from both proliferation assays showed that RGD-LNC were able to completely inhibit VEGF-induced endothelial cell proliferation. Treatment with LNC before VEGF stimulation seemed to have a bigger impact, although the standard deviations were high due to the experimental setting. This implicates that an early therapeutic intervention might be favorable. Still, drug-loading of LNC did not lead to a further enhancement of antiproliferative effects. On the one hand, it is possible that the encapsulated drugs are not able to leave the LNC after internalization and, therefore, cannot bind to their intracellular targets [60]. On the other hand, the experimental conditions might just not have been suitable to show smaller differences in the antiproliferative potential due to an insufficient VEGF effect.

The upregulation of HEY-1 expression was also smaller with RGD-CsIt-LNC than with free CsIt, possibly due to poor drug release from the carriers. A significant alteration of AAMP expression could not be detected with any treatment. As HEY-1 and AAMP are only two of multiple targets influenced by CsA and Itra, and they do not reflect the additional pharmacological effects of the RGD-decoration, these findings do not necessarily exclude the therapeutic potential of RGD-CsIt-LNC.

Also, the results from the tube formation assay are not indicative for the antiangiogenic potential of RGD-CsIt-LNC. Despite tubes were formed under similar conditions in the pretests, almost no tube-like structures were observed in the actual experiment, even for untreated control cells. Therefore, the experimental conditions need to be optimized to obtain more valuable results. Especially, dose-response relations for the VEGF concentration and the corresponding stimulation of cell proliferation and tube formation need to be evaluated, as the VEGF effect was limiting for the significance of most experiments. Generally, *in-vitro* tests are certainly an important tool for the screening for new antiangiogenic therapeutics, but they hardly reflect the complex pathophysiology of ocular neovascularization.

5.3 References

- [1] J.L. Leasher, R.R.A. Bourne, S.R. Flaxman, J.B. Jonas, J. Keeffe, K. Naidoo, K. Pesudovs, H. Price, R.A. White, T.Y. Wong, S. Resnikoff, H.R. Taylor, Global Estimates on the Number of People Blind or Visually Impaired by Diabetic Retinopathy: A Meta-analysis From 1990 to 2010, *Diabetes Care*. 39 (2016) 1643–1649. <https://doi.org/10.2337/dc15-2171>.
- [2] R.R.A. Bourne, J.B. Jonas, A.M. Bron, M.V. Cicinelli, A. Das, S.R. Flaxman, D.S. Friedman, J.E. Keeffe, J.H. Kempen, J. Leasher, H. Limburg, K. Naidoo, K. Pesudovs, T. Peto, J. Saadine, A.J. Silvester, N. Tahhan, H.R. Taylor, R. Varma, T.Y. Wong, S. Resnikoff, Prevalence and causes of vision loss in high-income countries and in Eastern and Central Europe in 2015: magnitude, temporal trends and projections, *British Journal of Ophthalmology*. 102 (2018) 575–585. <https://doi.org/10.1136/bjophthalmol-2017-311258>.
- [3] R.R.A. Bourne, G.A. Stevens, R.A. White, J.L. Smith, S.R. Flaxman, H. Price, J.B. Jonas, J. Keeffe, J. Leasher, K. Naidoo, K. Pesudovs, S. Resnikoff, H.R. Taylor, Vision Loss Expert Group, Causes of vision loss worldwide, 1990-2010: a systematic analysis, *Lancet Glob Health*. 1 (2013) e339-349. [https://doi.org/10.1016/S2214-109X\(13\)70113-X](https://doi.org/10.1016/S2214-109X(13)70113-X).
- [4] W.L. Wong, X. Su, X. Li, C.M.G. Cheung, R. Klein, C.-Y. Cheng, T.Y. Wong, Global prevalence of age-related macular degeneration and disease burden projection for 2020 and 2040: a systematic review and meta-analysis, *The Lancet Global Health*. 2 (2014) e106–e116. [https://doi.org/10.1016/S2214-109X\(13\)70145-1](https://doi.org/10.1016/S2214-109X(13)70145-1).
- [5] E. Ozaki, M. Campbell, A.-S. Kiang, M. Humphries, S.L. Doyle, P. Humphries, Inflammation in Age-Related Macular Degeneration, in: J.D. Ash, C. Grimm, J.G. Hollyfield, R.E. Anderson, M.M. LaVail, C. Bowes Rickman (Eds.), *Retinal Degenerative Diseases*, Springer, New York, NY, 2014: pp. 229–235. https://doi.org/10.1007/978-1-4614-3209-8_30.
- [6] A.C. Bird, N.M. Bressler, S.B. Bressler, I.H. Chisholm, G. Coscas, M.D. Davis, P.T.V.M. de Jong, C.C.W. Klaver, B.E.K. Klein, R. Klein, P. Mitchell, J.P. Sarks, S.H. Sarks, G. Soubrane, H.R. Taylor, J.R. Vingerling, An international classification and grading system for age-related maculopathy and age-related macular degeneration, *Survey of Ophthalmology*. 39 (1995) 367–374. [https://doi.org/10.1016/S0039-6257\(05\)80092-X](https://doi.org/10.1016/S0039-6257(05)80092-X).
- [7] G.A. Peyman, J. Koziol, Age-related macular degeneration and its management, *Journal of Cataract & Refractive Surgery*. 14 (1988) 421–430. [https://doi.org/10.1016/S0886-3350\(88\)80152-4](https://doi.org/10.1016/S0886-3350(88)80152-4).
- [8] H.E. Grossniklaus, W.R. Green, Choroidal neovascularization, *American Journal of Ophthalmology*. 137 (2004) 496–503. <https://doi.org/10.1016/j.ajo.2003.09.042>.

- [9] Q. Mohamed, M.C. Gillies, T.Y. Wong, Management of diabetic retinopathy: a systematic review, *Jama*. 298 (2007) 902–916. <https://doi.org/10.1001/jama.298.8.902>.
- [10] P. Sapicha, D. Hamel, Z. Shao, J.C. Rivera, K. Zaniolo, J.S. Joyal, S. Chemtob, Proliferative retinopathies: Angiogenesis that blinds, *The International Journal of Biochemistry & Cell Biology*. 42 (2010) 5–12. <https://doi.org/10.1016/j.biocel.2009.10.006>.
- [11] D.A. Chistiakov, Diabetic retinopathy: Pathogenic mechanisms and current treatments, *Diabetes & Metabolic Syndrome: Clinical Research & Reviews*. 5 (2011) 165–172. <https://doi.org/10.1016/j.dsx.2012.02.025>.
- [12] P. Mitchell, G. Liew, B. Gopinath, T.Y. Wong, Age-related macular degeneration, *The Lancet*. 392 (2018) 1147–1159. [https://doi.org/10.1016/S0140-6736\(18\)31550-2](https://doi.org/10.1016/S0140-6736(18)31550-2).
- [13] L.P. Aiello, R.L. Avery, P.G. Arrigg, B.A. Keyt, H.D. Jampel, S.T. Shah, L.R. Pasquale, H. Thieme, M.A. Iwamoto, J.E. Park, Vascular endothelial growth factor in ocular fluid of patients with diabetic retinopathy and other retinal disorders, *N Engl J Med*. 331 (1994) 1480–1487. <https://doi.org/10.1056/NEJM199412013312203>.
- [14] A.P. Adamis, J.W. Miller, M.-T. Bernal, D.J. D’Amico, J. Folkman, T.-K. Yeo, K.-T. Yeo, Increased Vascular Endothelial Growth Factor Levels in the Vitreous of Eyes With Proliferative Diabetic Retinopathy, *American Journal of Ophthalmology*. 118 (1994) 445–450. [https://doi.org/10.1016/S0002-9394\(14\)75794-0](https://doi.org/10.1016/S0002-9394(14)75794-0).
- [15] R.L. Avery, D.J. Pieramici, M.D. Rabena, A.A. Castellarin, M.A. Nasir, M.J. Giust, Intravitreal Bevacizumab (Avastin) for Neovascular Age-Related Macular Degeneration, *Ophthalmology*. 113 (2006) 363–372.e5. <https://doi.org/10.1016/j.opthta.2005.11.019>.
- [16] Deutsche Ophthalmologische Gesellschaft, Die Anti-VEGF-Therapie bei der neovaskulären altersabhängigen Makuladegeneration – therapeutische Strategien: Stellungnahme der Deutschen Ophthalmologischen Gesellschaft, der Retinologischen Gesellschaft und des Berufsverbandes der Augenärzte Deutschlands – November 2014, *Ophthalmologie*. 112 (2015) 237–245. <https://doi.org/10.1007/s00347-014-3222-x>.
- [17] D.J. Pieramici, R.L. Avery, Ranibizumab: treatment in patients with neovascular age-related macular degeneration, *Expert Opinion on Biological Therapy*. 6 (2006) 1237–1245. <https://doi.org/10.1517/14712598.6.11.1237>.
- [18] J.W. Miller, The Harvard angiogenesis story, *Survey of Ophthalmology*. 59 (2014) 361–364. <https://doi.org/10.1016/j.survophthal.2013.07.003>.
- [19] M. Ohr, P.K. Kaiser, Aflibercept in wet age-related macular degeneration: a perspective review, *Therapeutic Advances in Chronic Disease*. 3 (2012) 153–161. <https://doi.org/10.1177/2040622312446007>.

- [20] J. Talks, V. Daien, R.P. Finger, B. Eldem, T. Sakamoto, J.A. Cardillo, P. Mitchell, T.Y. Wong, J.-F. Korobelnik, The use of real-world evidence for evaluating anti-vascular endothelial growth factor treatment of neovascular age-related macular degeneration, *Survey of Ophthalmology*. 64 (2019) 707–719. <https://doi.org/10.1016/j.survophthal.2019.02.008>.
- [21] T. Kamba, B.Y.Y. Tam, H. Hashizume, A. Haskell, B. Sennino, M.R. Mancuso, S.M. Norberg, S.M. O'Brien, R.B. Davis, L.C. Gowen, K.D. Anderson, G. Thurston, S. Joho, M.L. Springer, C.J. Kuo, D.M. McDonald, VEGF-dependent plasticity of fenestrated capillaries in the normal adult microvasculature, *Am J Physiol Heart Circ Physiol*. 290 (2006) H560–576. <https://doi.org/10.1152/ajpheart.00133.2005>.
- [22] S. Lee, T.T. Chen, C.L. Barber, M.C. Jordan, J. Murdock, S. Desai, N. Ferrara, A. Nagy, K.P. Roos, M.L. Iruela-Arispe, Autocrine VEGF Signaling Is Required for Vascular Homeostasis, *Cell*. 130 (2007) 691–703. <https://doi.org/10.1016/j.cell.2007.06.054>.
- [23] J.M. Rosenstein, J.M. Krum, New roles for VEGF in nervous tissue—beyond blood vessels, *Experimental Neurology*. 187 (2004) 246–253. <https://doi.org/10.1016/j.expneurol.2004.01.022>.
- [24] A.S.R. Maharaj, T.E. Walshe, M. Saint-Geniez, S. Venkatesha, A.E. Maldonado, N.C. Himes, K.S. Matharu, S.A. Karumanchi, P.A. D'Amore, VEGF and TGF- are required for the maintenance of the choroid plexus and ependyma, *Journal of Experimental Medicine*. 205 (2008) 491–501. <https://doi.org/10.1084/jem.20072041>.
- [25] M. Saint-Geniez, A.S.R. Maharaj, T.E. Walshe, B.A. Tucker, E. Sekiyama, T. Kurihara, D.C. Darland, M.J. Young, P.A. D'Amore, Endogenous VEGF Is Required for Visual Function: Evidence for a Survival Role on Müller Cells and Photoreceptors, *PLOS ONE*. 3 (2008) e3554. <https://doi.org/10.1371/journal.pone.0003554>.
- [26] K.M. Ford, M. Saint-Geniez, T. Walshe, A. Zahr, P.A. D'Amore, Expression and Role of VEGF in the Retinal Pigment Epithelium, *Invest. Ophthalmol. Vis. Sci*. 52 (2011) 3358–3358.
- [27] K. Sayanagi, Y. Jo, Y. Ikuno, Transient Choroidal Thinning after Intravitreal Bevacizumab Injection for Myopic Choroidal Neovascularization, *Journal of Clinical & Experimental Ophthalmology*. 02 (2011). <https://doi.org/10.4172/2155-9570.1000165>.
- [28] J.E. Grunwald, E. Daniel, J. Huang, G. Ying, M.G. Maguire, C.A. Toth, G.J. Jaffe, S.L. Fine, B. Blodi, M.L. Klein, A.A. Martin, S.A. Hagstrom, D.F. Martin, Risk of Geographic Atrophy in the Comparison of Age-related Macular Degeneration Treatments Trials, *Ophthalmology*. 121 (2014) 150–161. <https://doi.org/10.1016/j.ophtha.2013.08.015>.

- [29] M.R. Munk, L. Ceklic, A. Ebnetter, W. Huf, S. Wolf, M.S. Zinkernagel, Macular atrophy in patients with long-term anti-VEGF treatment for neovascular age-related macular degeneration, *Acta Ophthalmologica*. 94 (2016) e757–e764. <https://doi.org/10.1111/aos.13157>.
- [30] J.E. Grunwald, M. Pistilli, G. Ying, M.G. Maguire, E. Daniel, D.F. Martin, Growth of Geographic Atrophy in the Comparison of Age-related Macular Degeneration Treatments Trials, *Ophthalmology*. 122 (2015) 809–816. <https://doi.org/10.1016/j.optha.2014.11.007>.
- [31] M. Aumailley, M. Gurrath, G. Müller, J. Calvete, R. Timpl, H. Kessler, Arg-Gly-Asp constrained within cyclic pentapeptides Strong and selective inhibitors of cell adhesion to vitronectin and laminin fragment P1, *FEBS Letters*. 291 (1991) 50–54. [https://doi.org/10.1016/0014-5793\(91\)81101-D](https://doi.org/10.1016/0014-5793(91)81101-D).
- [32] R. Haubner, R. Gratias, B. Diefenbach, S.L. Goodman, A. Jonczyk, H. Kessler, Structural and Functional Aspects of RGD-Containing Cyclic Pentapeptides as Highly Potent and Selective Integrin $\alpha V/\beta 3$ Antagonists, *J. Am. Chem. Soc.* 118 (1996) 7461–7472. <https://doi.org/10.1021/ja9603721>.
- [33] C. Kumar, Integrin $\alpha v\beta 3$ as a Therapeutic Target for Blocking Tumor-Induced Angiogenesis, *CDT*. 4 (2003) 123–131. <https://doi.org/10.2174/1389450033346830>.
- [34] Z. Guo, B. He, H. Jin, H. Zhang, W. Dai, L. Zhang, H. Zhang, X. Wang, J. Wang, X. Zhang, Q. Zhang, Targeting efficiency of RGD-modified nanocarriers with different ligand intervals in response to integrin $\alpha v\beta 3$ clustering, *Biomaterials*. 35 (2014) 6106–6117. <https://doi.org/10.1016/j.biomaterials.2014.04.031>.
- [35] X. Montet, M. Funovics, K. Montet-Abou, R. Weissleder, L. Josephson, Multivalent Effects of RGD Peptides Obtained by Nanoparticle Display, *J. Med. Chem.* 49 (2006) 6087–6093. <https://doi.org/10.1021/jm060515m>.
- [36] K. Pollinger, R. Hennig, A. Ohlmann, R. Fuchshofer, R. Wenzel, M. Breunig, J. Tessmar, E.R. Tamm, A. Goepferich, Ligand-functionalized nanoparticles target endothelial cells in retinal capillaries after systemic application, *Proceedings of the National Academy of Sciences*. 110 (2013) 6115–6120. <https://doi.org/10.1073/pnas.1220281110>.
- [37] R. Hennig, A. Ohlmann, J. Staffel, K. Pollinger, A. Haunberger, M. Breunig, F. Schweda, E.R. Tamm, A. Goepferich, Multivalent nanoparticles bind the retinal and choroidal vasculature, *Journal of Controlled Release*. 220, Part A (2015) 265–274. <https://doi.org/10.1016/j.jconrel.2015.10.033>.
- [38] B. Heurtault, P. Saulnier, B. Pech, J.-E. Proust, J.-P. Benoit, A novel phase inversion-based process for the preparation of lipid nanocarriers, *Pharmaceutical Research*. 19 (2002) 875–880. <https://doi.org/10.1023/A:1016121319668>.

-
- [39] B. Saliou, O. Thomas, N. Lautram, A. Clavreul, J. Hureauux, T. Urban, J.-P. Benoit, F. Lagarce, Development and in vitro evaluation of a novel lipid nanocapsule formulation of etoposide, *European Journal of Pharmaceutical Sciences*. 50 (2013) 172–180. <https://doi.org/10.1016/j.ejps.2013.06.013>.
- [40] P. Rafiee, J. Heidemann, H. Ogawa, N.A. Johnson, P.J. Fisher, M.S. Li, M.F. Otterson, C.P. Johnson, D.G. Binion, Cyclosporin A differentially inhibits multiple steps in VEGF induced angiogenesis in human microvascular endothelial cells through altered intracellular signaling, *Cell Communication and Signaling*. 2 (2004) 3. <https://doi.org/10.1186/1478-811X-2-3>.
- [41] C. Esposito, A. Fornoni, F. Cornacchia, N. Bellotti, G. Fasoli, A. Foschi, I. Mazzucchelli, T. Mazzullo, L. Semeraro, A. Dal Canton, Cyclosporine induces different responses in human epithelial, endothelial and fibroblast cell cultures, *Kidney Int*. 58 (2000) 123–130. <https://doi.org/10.1046/j.1523-1755.2000.00147.x>.
- [42] B.A. Nacev, J.O. Liu, Synergistic Inhibition of Endothelial Cell Proliferation, Tube Formation, and Sprouting by Cyclosporin A and Itraconazole, *PLoS ONE*. 6 (2011) e24793. <https://doi.org/10.1371/journal.pone.0024793>.
- [43] G. Shah, F.A. Middleton, K.L. Gentile, S. Tripathi, D. Bruch, K.G. Maier, D.S. Kittur, Cyclosporine Inhibition of Angiogenesis Involves the Transcription Factor HESR1, *Journal of Surgical Research*. 149 (2008) 171–176. <https://doi.org/10.1016/j.jss.2008.03.016>.
- [44] A. Carmo, lia, J. Cunha-Vaz, G. A. Carvalho, L. P, M.C. Lopes, Effect of cyclosporin-A on the blood-retinal barrier permeability in streptozotocin-induced diabetes, *Mediators of Inflammation*. 9 (2000) 243–248. <https://doi.org/10.1080/09629350020025764>.
- [45] B.A. Nacev, P. Grassi, A. Dell, S.M. Haslam, J.O. Liu, The Antifungal Drug Itraconazole Inhibits Vascular Endothelial Growth Factor Receptor 2 (VEGFR2) Glycosylation, Trafficking, and Signaling in Endothelial Cells, *Journal of Biological Chemistry*. 286 (2011) 44045–44056. <https://doi.org/10.1074/jbc.M111.278754>.
- [46] C.R. Chong, J. Xu, J. Lu, S. Bhat, D.J. Sullivan, J.O. Liu, Inhibition of Angiogenesis by the Antifungal Drug Itraconazole, *ACS Chem. Biol*. 2 (2007) 263–270. <https://doi.org/10.1021/cb600362d>.
- [47] R. Del Carratore, A. Carpi, P. Beffy, V. Lubrano, L. Giorgetti, B.E. Maserti, M.A. Carluccio, M. Simili, G. Iervasi, S. Balzan, Itraconazole inhibits HMEC-1 angiogenesis, *Biomedicine & Pharmacotherapy*. 66 (2012) 312–317. <https://doi.org/10.1016/j.biopha.2011.11.004>.
- [48] R. Auerbach, Vascular endothelial cell differentiation: organ-specificity and selective affinities as the basis for developing anti-cancer strategies, *International Journal of Radiation Biology*. 60 (1991) 1–10. <https://doi.org/10.1080/09553009114551401>.

- [49] R. Auerbach, R. Lewis, B. Shinnars, L. Kubai, N. Akhtar, Angiogenesis Assays: A Critical Overview, *Clin Chem.* 49 (2003) 32–40. <https://doi.org/10.1373/49.1.32>.
- [50] M.L. Ponce, Tube formation: an in vitro matrigel angiogenesis assay, in: S. Martin, C. Murray (Eds.), *Angiogenesis Protocols*, 2nd ed., Humana Press, a part of Springer Science + Business Media, LLC, 2009: pp. 183–188.
- [51] I. Arnaoutova, H.K. Kleinman, In vitro angiogenesis: endothelial cell tube formation on gelled basement membrane extract, *Nat Protoc.* 5 (2010) 628–635. <https://doi.org/10.1038/nprot.2010.6>.
- [52] I. Arnaoutova, J. George, H.K. Kleinman, G. Benton, The endothelial cell tube formation assay on basement membrane turns 20: state of the science and the art, *Angiogenesis.* 12 (2009) 267–274. <https://doi.org/10.1007/s10456-009-9146-4>.
- [53] S. Dias, K. Hattori, Z. Zhu, B. Heissig, M. Choy, W. Lane, Y. Wu, A. Chadburn, E. Hyjek, M. Gill, D.J. Hicklin, L. Witte, M. a. S. Moore, S. Rafii, Autocrine stimulation of VEGFR-2 activates human leukemic cell growth and migration, *J Clin Invest.* 106 (2000) 511–521. <https://doi.org/10.1172/JCI8978>.
- [54] G. Carpentier, M. Martinelli, J. Courty, I. Cascone, Angiogenesis Analyzer for ImageJ, in: Centre de Recherche Public Henri Tudor (Ed.), *Proceedings of the ImageJ User and Developer Conference, CRP, Mondorf-les-Bains, Luxembourg, 2012*: pp. 198–201.
- [55] D.-A. Lacorre, E.S. Baekkevold, I. Garrido, P. Brandtzaeg, G. Haraldsen, F. Amalric, J.-P. Girard, Plasticity of endothelial cells: rapid dedifferentiation of freshly isolated high endothelial venule endothelial cells outside the lymphoid tissue microenvironment, *Blood.* 103 (2004) 4164–4172. <https://doi.org/10.1182/blood-2003-10-3537>.
- [56] J. Bednarz, H.A. Weich, A.R. Schrenck, K. Engelmann, Expression of Genes Coding Growth Factors and Growth Factor Receptors in Differentiated and Dedifferentiated Human Corneal Endothelial Cells:, *Cornea.* 14 (1995) 372–381. <https://doi.org/10.1097/00003226-199507000-00005>.
- [57] T. Thum, A. Haverich, J. Borlak, Cellular dedifferentiation of endothelium is linked to activation and silencing of certain nuclear transcription factors: implications for endothelial dysfunction and vascular biology, *The FASEB Journal.* 14 (2000) 740–751. <https://doi.org/10.1096/fasebj.14.5.740>.
- [58] K.L. Taylor, A.M. Henderson, C.C.W. Hughes, Notch Activation during Endothelial Cell Network Formation in Vitro Targets the Basic HLH Transcription Factor HESR-1 and Downregulates VEGFR-2/KDR Expression, *Microvascular Research.* 64 (2002) 372–383. <https://doi.org/10.1006/mvre.2002.2443>.

-
- [59] A. Fischer, N. Schumacher, M. Maier, M. Sendtner, M. Gessler, The Notch target genes Hey1 and Hey2 are required for embryonic vascular development, *Genes Dev.* 18 (2004) 901–911. <https://doi.org/10.1101/gad.291004>.
- [60] M. Bohley, A. Haunberger, A.M. Goepferich, Intracellular availability of poorly soluble drugs from lipid nanocapsules, *European Journal of Pharmaceutics and Biopharmaceutics*. 139 (2019) 23–32. <https://doi.org/10.1016/j.ejpb.2019.03.007>.
- [61] P.C. Brooks, A.M.P. Montgomery, M. Rosenfeld, R.A. Reisfeld, T. Hu, G. Klier, D.A. Cheresh, Integrin $\alpha\beta 3$ antagonists promote tumor regression by inducing apoptosis of angiogenic blood vessels, *Cell*. 79 (1994) 1157–1164. [https://doi.org/10.1016/0092-8674\(94\)90007-8](https://doi.org/10.1016/0092-8674(94)90007-8).
- [62] K. Meerovitch, F. Bergeron, L. Leblond, B. Grouix, C. Poirier, M. Bubenik, L. Chan, H. Gourdeau, T. Bowlin, G. Attardo, A novel RGD antagonist that targets both $\alpha\beta 3$ and $\alpha 5\beta 1$ induces apoptosis of angiogenic endothelial cells on type I collagen, *Vascular Pharmacology*. 40 (2003) 77–89. [https://doi.org/10.1016/S1537-1891\(02\)00339-7](https://doi.org/10.1016/S1537-1891(02)00339-7).
- [63] K.L. DeCicco-Skinner, G.H. Henry, C. Cataisson, T. Tabib, J.C. Gwilliam, N.J. Watson, E.M. Bullwinkle, L. Falkenburg, R.C. O’Neill, A. Morin, J.S. Wiest, Endothelial cell tube formation assay for the in vitro study of angiogenesis, *J Vis Exp.* (2014) e51312. <https://doi.org/10.3791/51312>.
- [64] A.N. Stratman, M.J. Davis, G.E. Davis, VEGF and FGF prime vascular tube morphogenesis and sprouting directed by hematopoietic stem cell cytokines, *Blood*. 117 (2011) 3709–3719. <https://doi.org/10.1182/blood-2010-11-316752>.
- [65] D. Stone, M. Phaneuf, N. Sivamurthy, F.W. LoGerfo, W.C. Quist, A biologically active VEGF construct in vitro: Implications for bioengineering-improved prosthetic vascular grafts, *J. Biomed. Mater. Res.* 59 (2002) 160–165. <https://doi.org/10.1002/jbm.1229>.
- [66] E. Chavakis, B. Riecke, J. Lin, T. Linn, R.G. Bretzel, K.T. Preissner, M. Brownlee, H.-P. Hammes, Kinetics of integrin expression in the mouse model of proliferative retinopathy and success of secondary intervention with cyclic RGD peptides, *Diabetologia*. 45 (2002) 262–267. <https://doi.org/10.1007/s00125-001-0727-z>.

Supporting information

Pretests without LNC treatment were performed to determine the optimal experimental conditions for tube formation assays with HDMEC. Therefore, 10,000 to 50,000 cells per well were seeded on Matrigel and images were taken after 12, 16, 20 and 24 h of incubation with 50 ng/ml VEGF (Figure 5A). Different tube formation parameters, like the number of junctions and meshes and the total length of formed tubes, were analyzed. As all parameters had similar tendencies for the tested seeding densities and time points, total tube length was used for further analysis. For 10,000 cells/well no tube formation occurred. 20,000 and 30,000 cells/well led to well-defined tube networks for which the automatic analysis with the tube formation analyzer tool for ImageJ produced reliable results. With higher seeding densities of 40,000 or 50,000 cells/well, cells grew in a confluent layer instead of forming defined tubes. The automatic analysis was not accurate for 10,000, 40,000 and 50,000 cells/well, as tubes and meshes were assumed in areas where no tube formation was visible or cells were confluent.

In the next step, 20,000 and 30,000 cells/well were used to test which duration of VEGF stimulation (50 ng/ml) had the highest effect on tube formation (Figure 5B and C). In both seeding densities, cells started to build a confluent cell layer in the beginning. The holes in this layer grew over time, resulting in an increasingly defined tube network (Figure 5C). For 30,000 cells/well, the cell layer was still too dense to show actual tubes after 12 h of incubation. In contrast, cells started to form tubes after 6 to 8 h, when only 20,000 cells were seeded per well. The biggest difference between VEGF-stimulated and unstimulated cells was observed after 8 - 10 h of incubation for 20,000 cells/well.

When the experiment was repeated with a new cell batch with 10,000 and 15,000 cells per well, cells were too dense for tube formation analysis and no effect of VEGF was observable (Figure 6A and B). Therefore, 5,000 and 8,000 cells of the new cell batch were tested and 100 ng/ml VEGF were added to stimulate tube formation. With these seeding densities, more defined tubes were achieved, but tube formation was not as pronounced as with the first batch and no difference was measurable between VEGF-stimulated and unstimulated cells (Figure 6C and D).

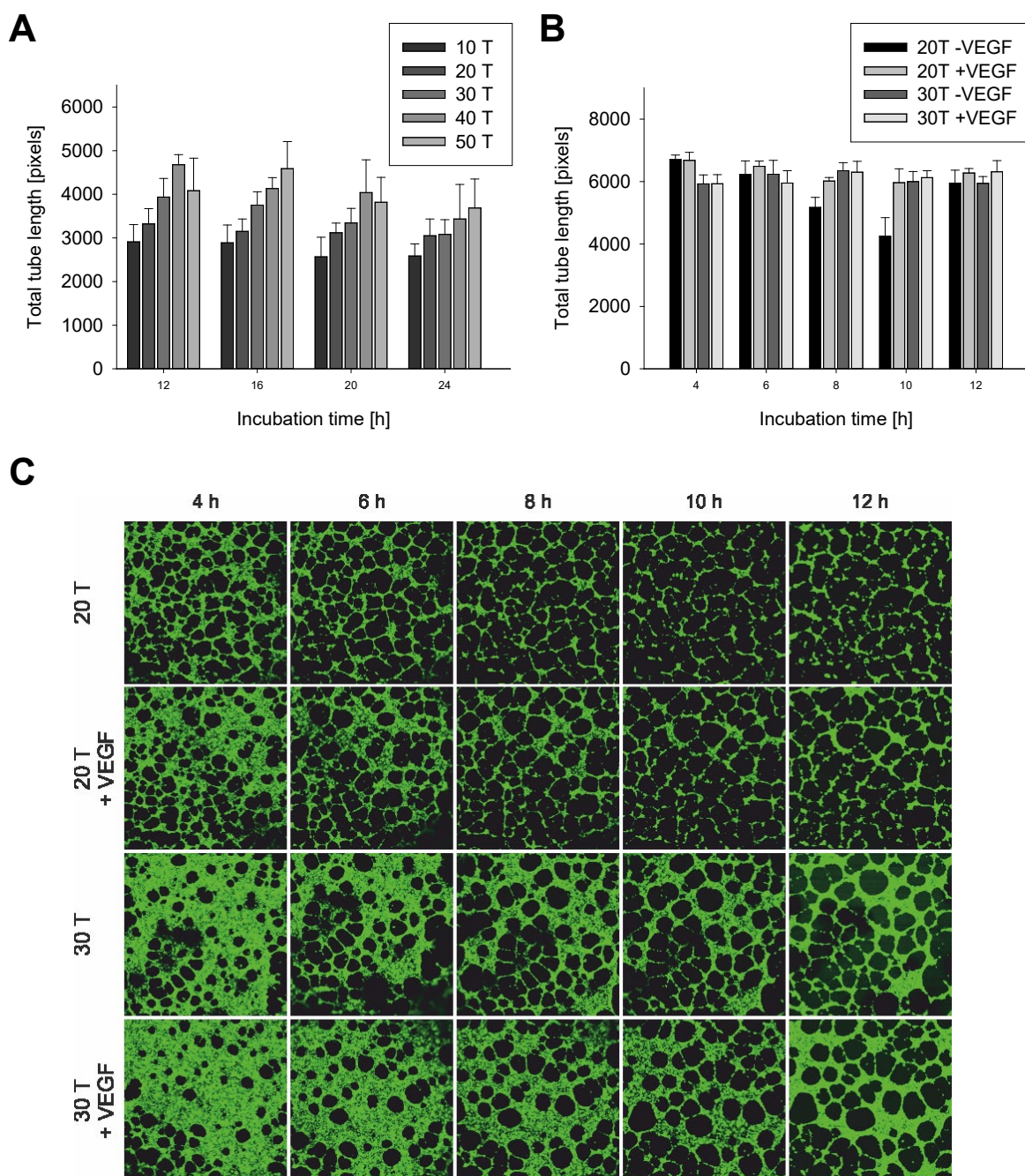


Figure 5: Pretests to find the optimal experimental conditions for further tube formation assays. Tube formation with 10,000 to 50,000 cells/well (with 50 ng/ml VEGF) was observed 12, 16, 20 and 24 h after seeding. 20,000 and 30,000 cells/well led to the most defined tube networks and tube formation was decreasing over time (A). A second tube formation assay with 20,000 and 30,000 cells/well and without VEGF stimulation (50 ng/ml) was conducted. The highest impact of VEGF was observed with 20,000 cells/well after 8 – 10 h of incubation (B and C). The images are showing an area of 2.5 x 2.5 mm each.

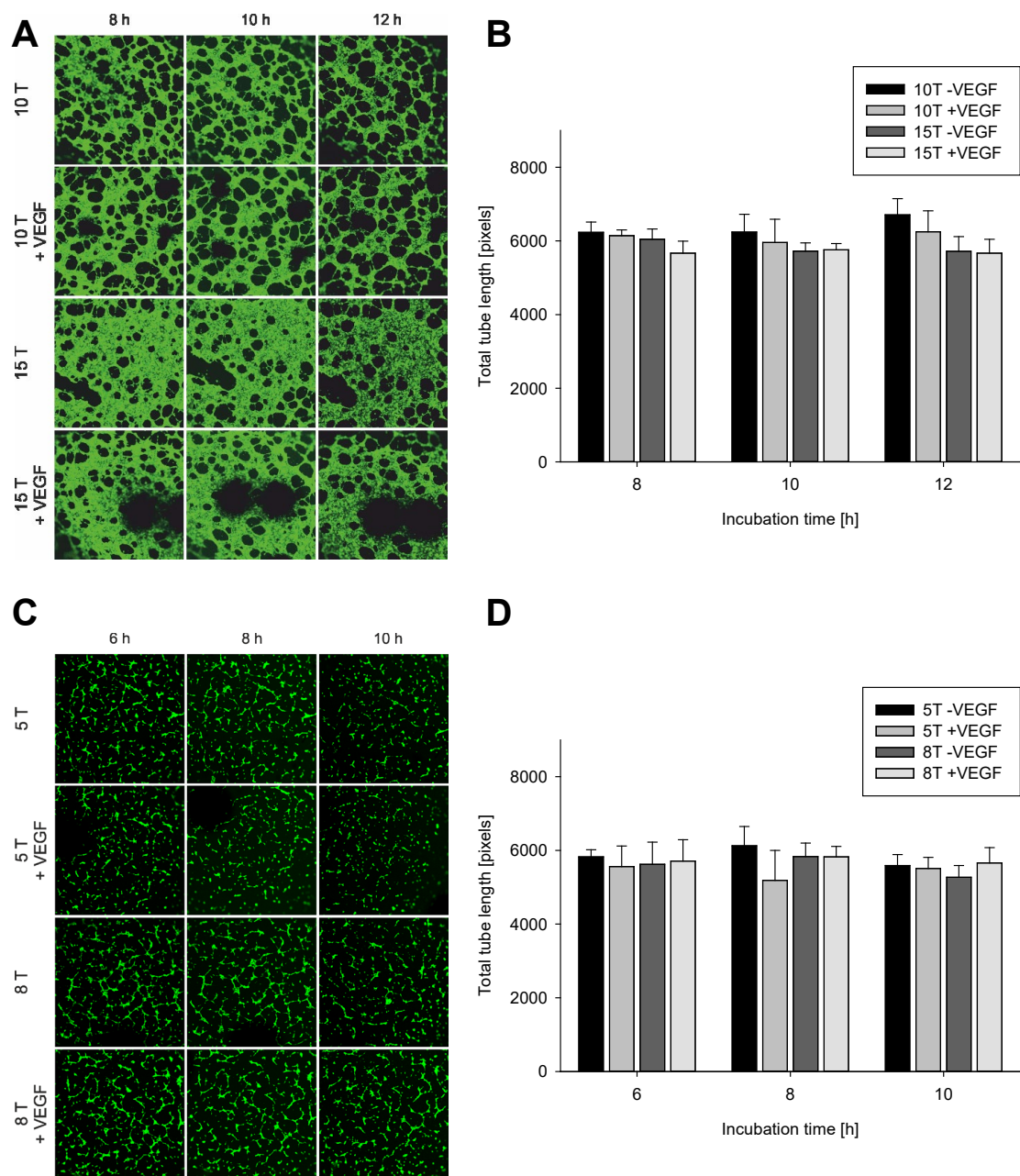


Figure 6: Tube formation pretests with second batch of HDMEC. Cells from this batch grew much faster, resulting in confluent cell layers with 10,000 and 15,000 cells/well with and without the presence of 50 ng/ml VEGF (A). The automatic analysis of the total tube length was not accurate, as cells were too dense (B). With 5,000 and 8,000 cells/well, more defined tubes were achieved (C) but no effect of stimulation with 100 ng/ml VEGF was measurable (D). The images are showing an area of 2.5 x 2.5 mm each.

Antiproliferative effect of drug-loaded
LNC in a mouse model of retinal
neovascularization

Abstract

Pathological retinal neovascularization is characteristic for the proliferative form of diabetic retinopathy, as well as for retinopathy of prematurity. The current standard of care for these diseases are retinal ablative therapy with laser photocoagulation, or the intravitreal injection of anti-VEGF agents, like bevacizumab, ranibizumab or aflibercept. However, both therapies are associated with potential severe adverse effects, often cannot stop disease progression or, especially in case of retinopathy of prematurity, come along with high recurrence rates. Therefore, an innovative nanoparticle formulation was designed for the therapy of neovascular eye diseases. For this purpose, lipid nanocapsules were loaded with cyclosporin A and itraconazole, which have formerly been shown to exhibit synergistic antiproliferative effects. A cyclic RGD-peptide was used as surface modification to enhance the accumulation of nanoparticles in endothelial cells of the proliferative vasculature. The nanocapsules were administered to mice intravenously via injection into the retrobulbar venous plexus. The systemic availability was confirmed with fluorescently labelled nanocapsules, and the detectability in blood, liver and retinal vessels was investigated. In a second step, the effect of drug-loaded lipid nanocapsules was tested in a mouse model of oxygen-induced retinopathy. A significant reduction of pathological neovascularizations was achieved after a single injection with these nanoparticles, proofing their great therapeutic potential.

6.1 Introduction

While diabetic retinopathy (DR) is the leading cause of vision loss in working-age adults [1,2], retinopathy of prematurity (ROP) is one of the major reasons for avoidable blindness in children globally. In 2010, approximately 170,000 preterm babies worldwide developed some degree of ROP [3] and the number of vision-threatening DR has been estimated to rise to 56.3 million by 2030 [1,2]. In both diseases, neovascularizations sprouting from the retinal vasculature are pivotal driving forces for disease progression. The newly formed vessels are typically leaky, causing edema and vitreous hemorrhage, they can induce retinal detachment due to tractional stress and, therefore, lead to vision impairment and blindness [4–6].

DR as well as ROP are commonly treated with laser photocoagulation or the intravitreal injection of anti-VEGF agents, like the VEGF-antibodies bevacizumab and ranibizumab or the soluble VEGF-receptor aflibercept [7–12]. However, these treatment options can cause severe adverse effects, like cataract, hemorrhage, constriction of the visual field or myopia [13–15]. Additionally, DR progression can often not be stopped [8] and the recurrence rates in ROP remain high [11,16]. Against this background, there is a high demand for new therapeutic options. Over the last three decades, a variety of nanoparticulate formulations has found its way into clinical application, especially in cancer therapy [17]. As there are physiological parallels between the proliferative vasculature in tumors and in retinopathies [18], nanoparticles might also open the door to new therapies in this field. Our group has already demonstrated, that accumulation of nanoparticles in healthy retinal vessels is achievable with RGD-peptides as targeting moieties [19]. These peptides bind to the $\alpha_v\beta_3$ -integrin, which is highly upregulated in proliferative endothelial cells [20–22]. Therefore, it can be reasonably assumed that the particle accumulation is further increased in eyes with pathological neovascularization. Also the enhanced vascular permeability of the newly formed vessels might further promote nanoparticle deposition [23,24].

We chose cyclosporin A (CsA) and itraconazole as antiangiogenic cargo for our nanoparticles. Both drugs have been shown to exert synergistic effects [25] and their intracellular targets make them ideal candidates for a cell-specific delivery by integrin-binding nanocarriers. Additionally, CsA could thwart the inflammation that essentially contributes to the angiogenesis and increased vasopermeability in DR [26] as well as in ROP [27].

In a first step, it was demonstrated that RGD-decorated nanoparticles significantly accumulate in the retinal vasculature after systemic application. The therapeutic effect of the drug-loaded nanocapsules was then investigated in a mouse model of oxygen-induced retinopathy (OIR). After a single injection of RGD-nanoparticles loaded with CsA and itraconazole, the formation of pathological blood vessels was significantly reduced. These results suggest that this novel therapeutic approach might be a valuable option for the treatment or even the prevention of neovascular diseases of the eye in the future and could, therefore, be a promising tool for the global fight against vision loss.

6.2 Materials

Miglyol®812 (medium-chain triglycerides (MCT)) was purchased from Caesar&Loretz, Hilden, Germany. Solutol®HS 15 (Poly(ethylene glycol (PEG))₁₅-12-hydroxy-stearate with about 30% free PEG) and Lipoid S75-3 (soy lecithin with 70% phosphatidylcholine) were kindly provided by BASF, Ludwigshafen, Germany, and Lipoid, Ludwigshafen, Germany, respectively. 1,1'-Dioctadecyl-3,3',3'-tetramethylindodicarbocyanine perchlorate (DiD oil) was obtained from Thermo Fisher Scientific (life technologies), Waltham, USA (MA). 1,2-distearoyl-sn-glycero-3-phosphoethanolamine-N-[maleimide-PEG-2000] (DSPE-PEG-Mal) ammonium salt was purchased from Avanti Polar Lipids, Alabaster, USA (AL). Cyclo-(Arg-Gly-Asp-D-Phe-Cys) acetate salt (c(RGDfC)) was obtained from Bachem Distribution Service, Weil am Rhein, Germany. Cyclosporin A (CsA) was a kind gift of Pharma Stulln, Stulln, Germany. Itraconazole was purchased from Fagron, Barsbüttel, Germany. Fluorescein isothiocyanate (FITC)-dextran (2000 kDa) was obtained from TdB Labs, Uppsala, Sweden. All other chemicals were purchased from Sigma Aldrich, Taufkirchen, Germany. Ultrapure water was obtained from a Milli-Q water purification system from Millipore, Billerica, USA (MA).

6.3 Methods

6.3.1 Preparation of LNC

The preparation of LNC was conducted in accordance with Heurtault et al. [28] with slight modifications. Therefore, a mixture of 60% NaCl solution (1% in water), 1.5% Lipoid, 17.8% Solutol and 20.7% MCT was subjected to three heating and cooling cycles in which the

phase inversion temperature was passed in each step. In the last cycle, the 2.5-fold amount of water at room temperature was added during the phase inversion to obtain stable LNC. For fluorescence labelling, 1.4 (OIR-experiments) or 2.8 mg DiD per 100 mg LNC were added to the mixture before the phase inversion process. The resulting preparations were filtered through a 0.22 µm poly(ether sulfone) syringe filter prior to further use. The concentration of LNC in the preparations was calculated to be 106 - 107 mg/ml.

6.1.1 Loading of LNC with cyclosporin A and itraconazole

For drug-loaded LNC (CsIt-LNC), CsA was first dissolved in MCT at a concentration of 4.25 mg CsA per gram MCT. Itraconazole was dissolved in methanol and added to the LNC ingredients Solutol, MCT with CsA, Lipoid and fluorescence dye. The mixture was kept at 75°C for 30 min to evaporate the methanol. Afterwards, NaCl 1% solution was added and the LNC were prepared in the phase-inversion process described above. The concentration of drugs in the final preparation was 0.14 µg itraconazole and 2.3 µg CsA per mg LNC.

6.1.2 Coupling of DSPE-PEG-Mal with c(RGDfC) and post-insertion into LNC

A 1 mg/ml solution of c(RGDfC) in Dulbecco's phosphate buffered saline (DPBS) was added to DSPE-PEG-Mal (12 mg/ml in DPBS) in a molar ratio of 2:1 and shaken for 2 h protected from light. For post-insertion of the modified phospholipid into the LNC shell, the nanoparticles were added in a ratio of 1:40 (c(RGDfC):LNC) and the mixture was incubated for 3 h at 37°C. Subsequently, the post-inserted LNC (RGD-LNC or RGD-CsIt-LNC) were cooled down in an ice water bath for 5 min.

The nanocapsules had a diameter of about 50 nm (Z-Average) before surface modification, measured by dynamic light scattering with a Zetasizer Nano ZS (Malvern Instruments, Herrenberg, Germany). Their diameter increased in the single digit nanometer range due to post-insertion. Their polydispersity index stayed below 0.05, indicating that no aggregation occurred.

6.1.3 Animal experiments

The mice used for the experiments described below were bred in-house in the animal facility of the University of Regensburg. Animal experiments were carried out in accordance with the national and institutional guidelines and were approved by the local authority (Regierung von Unterfranken,

reference number: 55.2-2532-2-363) and the Animal Care and Use Committee (Tierschutzausschuss) of the University of Regensburg.

6.1.4 Detection of LNC in tissue homogenates

Three adult mice were killed by cervical dislocation and their livers were removed. Half of each liver served as control for background fluorescence. The other part was injected with LNC without further modifications. The livers were cut in parts of 80 to 100 mg and homogenized together with 1 ml DPBS per 100 mg tissue using an Ultra-Turrax homogenizer (IKA Labortechnik, Staufen, Germany). Homogenate samples of 150 μ l were transferred into a well-plate with a direct displacement pipette, and fluorescence spectra at an excitation wavelength of 635 nm were recorded with an LS 55 fluorimeter (Perkin Elmer LAS, Rodgau-Jügesheim, Germany).

6.1.5 Retrobulbar injection of LNC in mice

The systemic availability and accumulation of RGD-LNC in the retina was investigated 1 h and 24 h after intravenous application. Therefore, eight mice at postnatal day 14 (P14) were anesthetized with inhalatory isoflurane and 10 μ l fluorescent RGD-LNC were injected into the retrobulbar venous plexus of each eye (0.3 mg total dose per mouse). Six mice were killed 1 h and three mice were killed 24 h after the injection by cervical dislocation, and blood was collected. The eyes were enucleated, fixed in 4% paraformaldehyde (PFA) for 2 h and washed with DPBS, before retinal whole mounts were prepared. Therefore, the eye cups were dissected, the anterior part was removed, and four radial cuts were made in the retinae to allow flatmounting with Mowiol mounting medium (Carl Roth, Karlsruhe, Germany). The specimens were examined by laser scanning microscopy with a Zeiss Axiovert 200 microscope combined with an LSM 510 laser-scanning device using a 40x Plan-Neofluar (NA 1.3) oil immersion objective (Zeiss, Jena, Germany). Nanoparticle fluorescence was excited at 633 nm and recorded using a long-pass emission filter at 650 nm. Tissue autofluorescence was excited with a 488 nm laser and detected by using a 505 to 530 nm bandpass filter. For image acquisition and processing AIM 4.2. (Zeiss, Jena, Germany) was used. LNC fluorescence was displayed in red. Liver homogenates were prepared as described above. LNC fluorescence in blood and liver homogenates was excited at 640 nm and recorded at 680 nm with an Omega FLUOstar plate reader (BMG Labtech, Ortenberg, Germany). Nine uninjected mice served as control and their liver and blood were used as blanks for the respective fluorescence measurements.

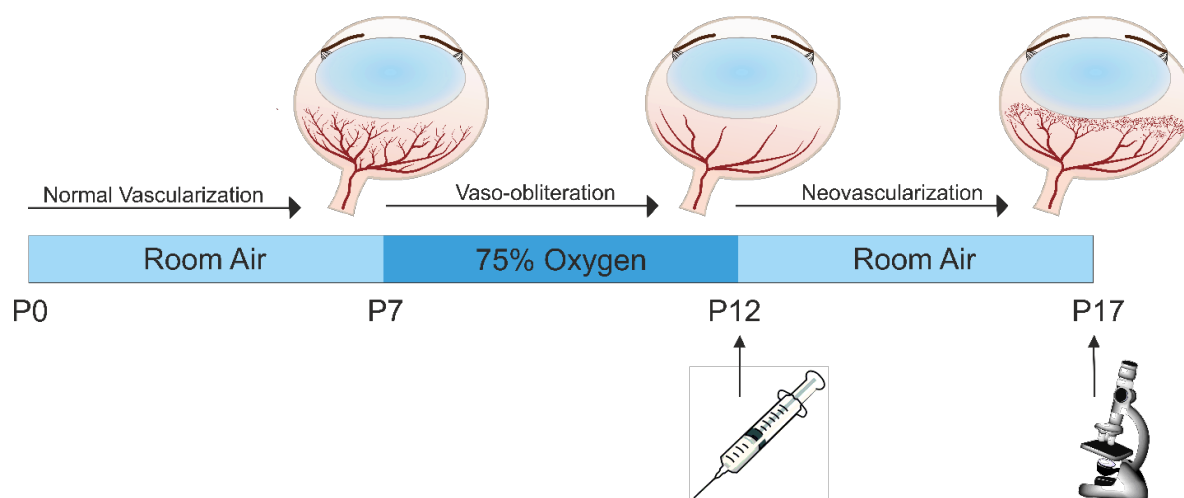


Figure 1: Schematic illustration of the retinal development and interventions in the OIR model (modified from [29]). During the first 6 days, mouse pups were kept in normal room air, enabling a physiological vascular development. From P7 until P12, the litters were exposed to 75% oxygen. This leads to the suppression of angiogenic factors, like VEGF, and results in a loss of retinal vessels. The pups were put back into normal atmosphere on P12 and LNC were injected in the treatment groups. As a result of oxygen deficiency and induced overexpression of angiogenic factors, pathological neovascularizations with leaky and tufting vessels are formed over the next days. Mice were sacrificed at P17 for subsequent analysis of retinal flatmounts.

6.1.6 Mouse model of oxygen-induced retinopathy

Figure 1 gives an overview over the changes in the retinal vasculature and the interventions in the OIR model. The Mouse pups (129/SV) with their mothers were exposed to hyperoxia with 75% oxygen from P7 to P12, to induce vaso-obliteration as first phase of OIR [29]. The animals were then returned to room air, the pups were randomly allocated to the RGD-CsIt-LNC, RGD-LNC or the control group. It was ensured that there was no significant difference in weight and weight gain between the treatment groups before and after the oxygen treatment, as these factors are known to influence the extent of oxygen-induced retinopathy [30,31]. In the nanoparticle treatment groups, LNC were administered by retrobulbar injection of 10 μ l LNC per eye in short-term anesthesia using inhalatory isoflurane. The total dose of LNC was 0.1 mg for each mouse pup in the RGD-LNC or RGD-CsIt-LNC group. On P17, mice were deeply anesthetized by intraperitoneal injection of 20 - 30 μ l of 7.5% Ketamin and 0.5% Xylazin and perfused through the left ventricle with 5% FITC-dextran in Tris-buffered saline. The eyes were enucleated and fixed in 4% PFA for 1 h. Retinal whole mounts were prepared as described above and fluorescence images were obtained with an Axio Imager Z1 equipped with a Plan-Neofluar 10x/0.30 M27 objective (Carl Zeiss

Microscopy, Jena, Germany). For quantitative analysis the total area of the flat-mounted retina, the area of the avascular zone as well as the area of tufting and vascular tortuosity (tuft area) were determined [29] using the Zen Software (Carl Zeiss Microscopy, Jena, Germany).

6.1.7 Statistical analysis

If not stated otherwise, data are expressed as mean \pm standard deviation. Graphical analysis and outlier tests were performed with Origin 2016. Other statistical analysis was conducted with SigmaPlot 12.0. In the animal experiments, n represents the number of animals. When both retinæ from one mouse were analyzed, the mean result was used for statistical analysis. The number of retinæ r included in the analysis is given in brackets after n ($n = n(r)$).

6.2 Results and discussion

6.2.1 Detection of LNC in tissue homogenates

The nanoparticles used in this work were labelled with lipophilic fluorescent dyes to enable concentration determination after surface modification and to allow for detection in body tissues. One of the applied detection methods was fluorescence microscopy, which gives an important insight into the interaction of nanoparticles with cells and into their exact location in tissues. But, on the other hand, it provides only little information about the actual concentration of particles in different tissues and, only small tissue samples can be considered for the analysis instead of whole organs [32].

There are numerous methods for the quantification of nanoparticles in body tissues, for example the extraction of encapsulated drugs and the subsequent quantification by HPLC with a suitable detection method [33] or the quantification of specific elements in inorganic nanoparticles by inductively coupled plasma mass spectrometry [34]. The extraction of drugs for further quantification is a process which has to be developed and validated carefully. On the one hand, the substance of interest needs to be extracted as completely as possible and, on the other hand, other compounds that might interfere with the detection need to be removed.

The quantification of fluorescence in tissue homogenates without previous extraction with solvents is, therefore, very appealing, but it might be hindered by quenching effects or tissue autofluorescence [32,35]. The excitation and emission maxima of DiD are located approximately

at 644 and 665 nm, respectively. This long-wave emission can pass through tissues and, can therefore be detected without prior extraction.

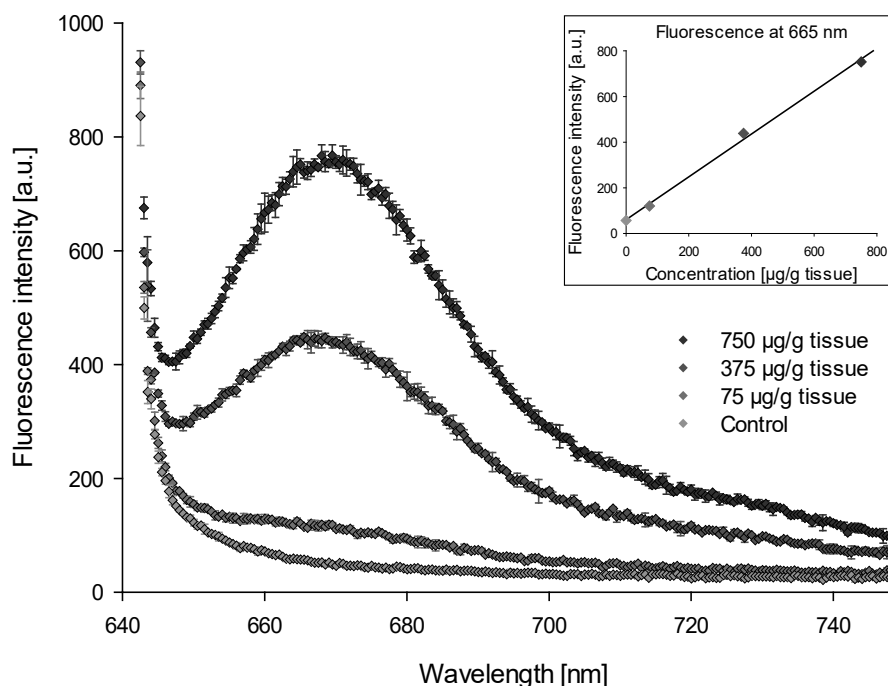


Figure 2: Fluorescence spectra of liver homogenates spiked with different concentrations of LNC at an excitation wavelength of 635 nm. The fluorescence of DiD ($\lambda_{em} = 665$ nm) is clearly detectable and there is no significant tissue autofluorescence that might interfere with DiD detection. The fluorescence intensity at 665 nm corresponds linearly with the LNC concentration (inset).

To make sure that the detection is indeed not hampered by the surrounding matrix, liver as model tissue was spiked with different doses of LNC. The fluorescence spectra of the spiked and control liver homogenates are shown in Figure 2. No significant background fluorescence of the control tissue was measured at the emission maximum of DiD ($\lambda_{em} = 665$ nm) and there was a linear correlation between the calculated LNC concentration per gram tissue and the measured fluorescence intensity (inset in Figure 2). Therefore, the direct measurement of DiD fluorescence in tissue homogenates was used for LNC quantification in the further experiments.

6.1.1 Accumulation of LNC in retinal vessels 24 h after retrobulbar injection

Retro-orbital injection into the retrobulbar venous plexus is an alternative to more common injection sites, like the tail vein or the jugular vein, and is advantageous especially in young or highly pigmented mouse pups. It can be conducted in inhalatory short-term anesthesia and without

surgical procedure [36]. Because successful administration of nanoparticles was crucial for the investigation of their therapeutic potential, the systemic availability after the retrobulbar injection was tested. One hour after administration of 0.3 mg RGD-LNC, the concentration of LNC in the collected blood samples was $101 \pm 39 \mu\text{g/ml}$ ($n = 5$). One mouse was excluded from the analysis, as not enough blood could be collected. These data proof the systemic availability of LNC after retrobulbar injection. The mouse pups had a mean weight of 6 g and the blood volume of adult mice is assumed to be about 80 to 96 ml/kg [37,38]. Although these values might not apply exactly to mouse pups at that age, their total blood volume can be roughly estimated from them to be about 0.5 to 0.6 ml. Therefore, approximately one fifth of the injected dose was remaining in the circulation after one hour. This is comparable with the results of Hoarau et al. for PEGylated lipid nanocapsules with a similar PEG-length and amount [39].

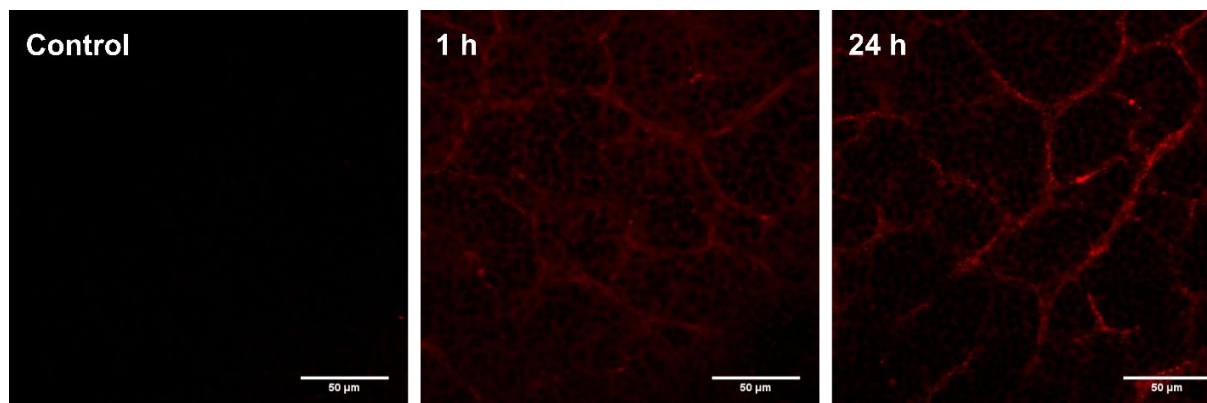


Figure 3: Example images of retina specimens of a control mouse (no injection) versus animals 1 h and 24 h after injection of 0.3 mg fluorescent RGD-LNC. After 1 h of circulation, LNC are already detectable in the retinal vessels. After 24 h LNC fluorescence in the retina has further increased, despite the decreased LNC concentration in the systemic circulation. This shows that RGD-LNC significantly accumulate in retinal vessels.

LNC were also detectable in the retinal whole mounts at this time point, but no pronounced accumulation was observed here (Figure 3). As the blood was not removed from the organs before microscopy, the presence of LNC in retinal vessels might also be attributed to the high LNC concentration in the general circulation at this time point. A high blood half-life is advantageous for a targeted therapy, as it gives the nanoparticles the chance for specific interaction with the receptor of interest before they are cleared from the circulation. Therefore, it is a promising sign that one hour after administration the nanoparticle concentration in the blood is still relatively high.

After 24 hours from administration, an accumulation of RGD-LNC in the retinal vessels was clearly observed (Figure 3). The LNC concentration in the blood had dropped to only $6 \pm 4 \mu\text{g/ml}$ ($n = 3$) at this time point, so the LNC fluorescence observed in the retinal whole mounts was most likely not originating from the blood remaining in the vessels. The LNC concentration in the liver was determined to be $156 \pm 11 \mu\text{g/g}$ tissue. A high accumulation in the liver is typical for the biodistribution of nanoparticles [40]. Nevertheless, the accumulation of RGD-modified LNC in the retinal vessels as a pivotal requirement for their therapeutic application was clearly proven in this experiment.

6.1.2 RGD-CsIt-LNC significantly reduce tufting in the mouse model of OIR

The exposure to increased oxygen levels in the phase from P7 to P12 suppresses the physiological production of proangiogenic factors and consequently leads to a retinal vessel loss. As a result, when mice are brought back to room air, there is a lack of oxygen in the retina and proangiogenic factors are overexpressed. This leads to pathological vessel growth at the edge of the avascular zone with dilated, leaky vessels that are sprouting into the vitreous body (tufting). The extent of pathological neovascularizations increases from P12 to P17 (Figure 1), before the tufting starts to regress and the vasculature normalizes again [11,41,42]. The area of the avascular zone (AVZ) as well as the area of tufting and vascular tortuosity (tufts) can be determined after perfusion with FITC-dextran and can be assessed in relation to the total retinal area.

Seven pups were treated with RGD-CsIt-LNC, four mice were injected with RGD-LNC without drug loading and eight mice were in the control group without treatment. Some of the retina specimens had to be excluded from the analysis due to insufficient perfusion or because the central area of retinae was damaged during preparation which hinders the correct measurement of the AVZ area. One animal from the RGD-CsIt-LNC group was excluded from statistical analysis as a significant outlier (Grubbs test, $p < 0.05$) but is represented in Figure 4D and E. In the RGD-LNC group, only one mouse (two retinae) could be analyzed and, therefore, this group was not taken into account for statistical analysis and two-tailed t-test was performed to compare the RGD-CsIt-LNC with the control group.

Regarding the avascular area (Figure 4B and D), no significant difference between these two groups was observed ($p = 0.16$). The AVZ proportion of the total area was $2.81\% \pm 1.91\%$ for the control group ($n = 6(11)$) and $1.42\% \pm 0.63\%$ ($n = 6(12)$) in the RGD-CsIt-LNC group. After

RGD-LNC treatment, the AVZ proportion was 1.88% ($n = 1(2)$). According to this result, the treatment had no effect on the revascularization of the retina. VEGF is an important physiological factor for the development and recovery of retinal vessels [43] and although its inhibition can reduce pathological neovascularization, this might come at the cost of a delayed reperfusion of

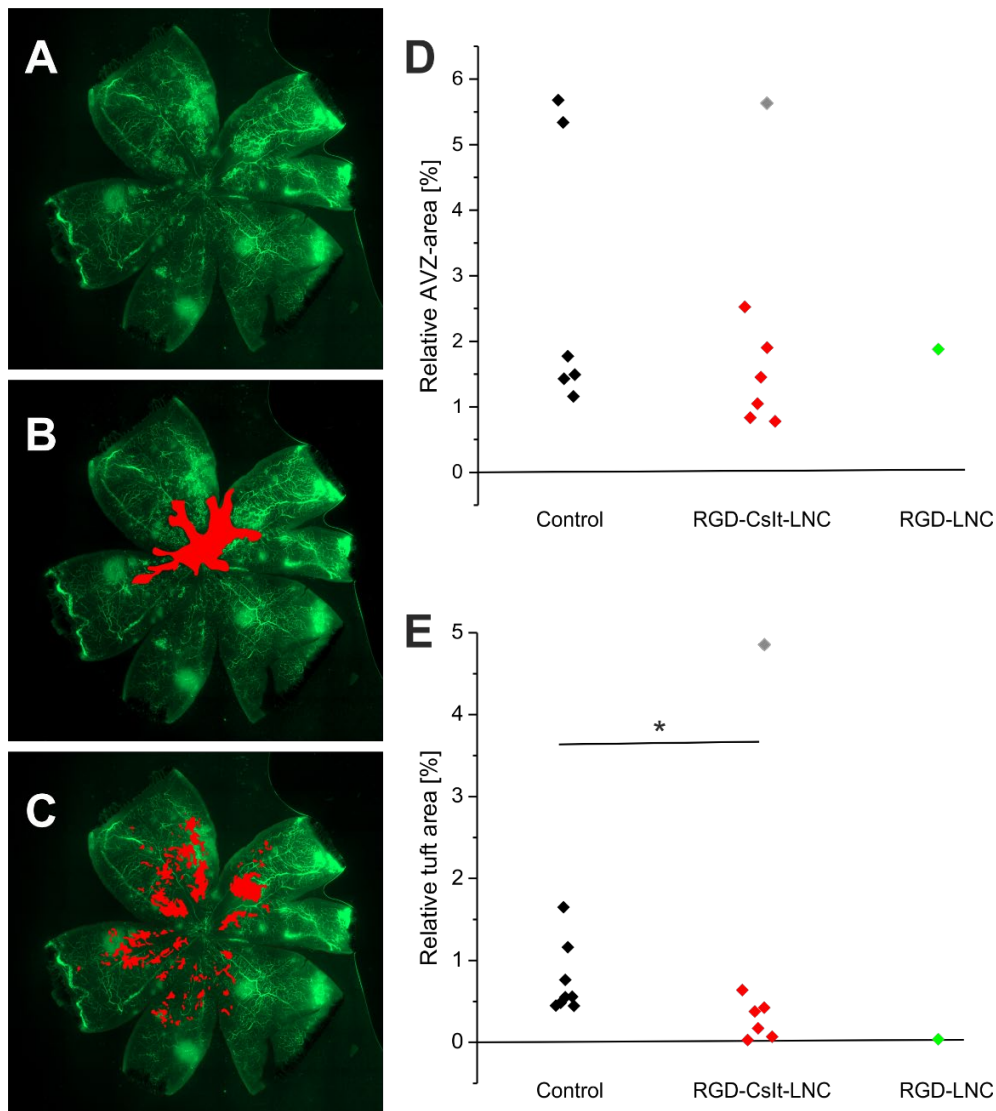


Figure 4: Representative image of a retinal flatmount with FITC-dextran perfused vasculature (green) (A-C). The avascular zone (B) and the areas of pathological neovascularization with dilatated and tufting vessels (C) were quantified in relation to the total retinal area (D, E). There was no significant difference in the relative area of the avascular zone between RGD-CsIt-LNC-treated mice and the untreated control group (D), but RGD-CsIt-LNC significantly reduced the area of tufting (E). Statistical significance (*) in the difference between the RGD-CsIt-LNC group and the control group was assessed by two-tailed t-test ($p < 0.05$). One data point (gray) was excluded as significant outlier (Grubbs test, $p < 0.05$).

avascular zones [44]. Keeping this in mind, it is promising that the LNC treatment had no such side effects and the avascular area was not increased compared to control mice. In another study, aflibercept did not accelerate the recovery of retinal vessels until P17, but the treated mice showed a better vascularization on P25 than untreated controls [45]. A later time point of analysis might, therefore, reveal more details about the influence of the nanoparticle treatment on the retinal recovery.

The tuft area in contrast, as shown in Figure 4C and E, was significantly reduced from $0.76\% \pm 0.40\%$ ($n = 8(15)$) in the control group to $0.28\% \pm 0.22\%$ by treatment with RGD-CsIt-LNC ($n = 6(12)$; p -Value 0.033). The relative tuft area in the RGD-LNC-treated pups was 0.04% ($n = 1(2)$). These results show that RGD-CsIt-LNC are capable of reducing the pathological neovascularization significantly. As no statistical comparison to the RGD-LNC treatment was possible, it needs to be further evaluated whether the improvement of the vascular status is a result solely of the cyclosporin A-itraconazole combination or also an effect of the integrin ligand c(RGDfC). This RGD-peptide itself is known to exert antiproliferative effects [46–48] and might, therefore, contribute to the inhibition of neovascularizations.

6.2 Conclusion

After the accumulation of RGD-modified quantum dots in retinal vessels has already been shown by Pollinger et al., it could be proven in this work that also RGD-conjugated lipid nanocapsules are capable of targeting the retinal vasculature. A high proportion of LNC, which carried the c(RGDfC)-peptide on their surface, was still circulating in the systemic blood flow one hour after the injection. The nanoparticles showed pronounced accumulation in the retinal vessels, but also in the liver, 24 h after administration. It was demonstrated in a mouse model of oxygen-induced retinopathy that a single injection of RGD-LNC loaded with cyclosporin A and itraconazole significantly reduced the development of tufting and vasodilatation without hampering retinal reperfusion. The respective contribution of the RGD-peptide, cyclosporin A, itraconazole and the combination of both should be further investigated to optimize this therapy. The presented results already rise hope that an effective therapy for proliferative DR and ROP without the need for destructive laser ablation or intravitreal injections is possible.

6.3 References

- [1] D.S.W. Ting, G.C.M. Cheung, T.Y. Wong, Diabetic retinopathy: global prevalence, major risk factors, screening practices and public health challenges: a review, *Clinical & Experimental Ophthalmology*. 44 (2016) 260–277. <https://doi.org/10.1111/ceo.12696>.
- [2] D.R. Whiting, L. Guariguata, C. Weil, J. Shaw, IDF Diabetes Atlas: Global estimates of the prevalence of diabetes for 2011 and 2030, *Diabetes Research and Clinical Practice*. 94 (2011) 311–321. <https://doi.org/10.1016/j.diabres.2011.10.029>.
- [3] A.L. Solebo, L. Teoh, J. Rahi, Epidemiology of blindness in children, *Arch Dis Child*. 102 (2017) 853–857. <https://doi.org/10.1136/archdischild-2016-310532>.
- [4] P. Sapienza, J.-S. Joyal, J.C. Rivera, E. Kermorvant-Duchemin, F. Sennlaub, P. Hardy, P. Lachapelle, S. Chemtob, Retinopathy of prematurity: understanding ischemic retinal vasculopathies at an extreme of life, *J Clin Invest*. 120 (2010) 3022–3032. <https://doi.org/10.1172/JCI42142>.
- [5] P. Sapienza, D. Hamel, Z. Shao, J.C. Rivera, K. Zaniolo, J.S. Joyal, S. Chemtob, Proliferative retinopathies: Angiogenesis that blinds, *The International Journal of Biochemistry & Cell Biology*. 42 (2010) 5–12. <https://doi.org/10.1016/j.biocel.2009.10.006>.
- [6] R.N. Frank, Diabetic retinopathy, *N Engl J Med*. 350 (2004) 48–58. <https://doi.org/10.1056/NEJMr021678>.
- [7] G. P. Giuliani, Diabetic Retinopathy: Current and New Treatment Options, *Current Diabetes Reviews*. 8 (2012) 32–41. <https://doi.org/10.2174/157339912798829188>.
- [8] A.W. Stitt, T.M. Curtis, M. Chen, R.J. Medina, G.J. McKay, A. Jenkins, T.A. Gardiner, T.J. Lyons, H.-P. Hammes, R. Simó, N. Lois, The progress in understanding and treatment of diabetic retinopathy, *Progress in Retinal and Eye Research*. 51 (2016) 156–186. <https://doi.org/10.1016/j.preteyeres.2015.08.001>.
- [9] S.E. Mansour, D.J. Browning, K. Wong, H.W. Flynn, A.R. Bhavsar, The Evolving Treatment of Diabetic Retinopathy, *Clin Ophthalmol*. 14 (2020) 653–678. <https://doi.org/10.2147/OPTH.S236637>.
- [10] M.E. Hartnett, Retinopathy of Prematurity: Evolving Treatment With Anti-Vascular Endothelial Growth Factor, *Am J Ophthalmol*. 218 (2020) 208–213. <https://doi.org/10.1016/j.ajo.2020.05.025>.
- [11] M.E. Hartnett, Advances in understanding and management of retinopathy of prematurity, *Surv Ophthalmol*. 62 (2017) 257–276. <https://doi.org/10.1016/j.survophthal.2016.12.004>.
- [12] S.G. Schorr, H.-P. Hammes, U.A. Müller, H.-H. Abholz, R. Landgraf, B. Bertram, The prevention and treatment of retinal complications in diabetes, *Deutsches Ärzteblatt Online*. (2016). <https://doi.org/10.3238/arztebl.2016.0816>.

-
- [13] K.D. Tran, L.A. Cernichiaro-Espinosa, A.M. Berrocal, Management of Retinopathy of Prematurity—Use of Anti-VEGF Therapy, *The Asia-Pacific Journal of Ophthalmology*. 7 (2018) 56–62. <https://doi.org/10.22608/APO.2017436>.
- [14] M.M. Popovic, P. Nichani, R.H. Muni, K. Mireskandari, N.N. Tehrani, P.J. Kertes, Intravitreal antivascular endothelial growth factor injection versus laser photocoagulation for retinopathy of prematurity: A meta-analysis of 3,701 eyes, *Surv Ophthalmol*. (2020). <https://doi.org/10.1016/j.survophthal.2020.12.002>.
- [15] T. Moutray, J.R. Evans, N. Lois, D.J. Armstrong, T. Peto, A. Azuara-Blanco, Different lasers and techniques for proliferative diabetic retinopathy, *Cochrane Database Syst Rev*. 3 (2018) CD012314. <https://doi.org/10.1002/14651858.CD012314.pub2>.
- [16] M.J. Sankar, J. Sankar, P. Chandra, Anti-vascular endothelial growth factor (VEGF) drugs for treatment of retinopathy of prematurity, *Cochrane Database Syst Rev*. 1 (2018) CD009734. <https://doi.org/10.1002/14651858.CD009734.pub3>.
- [17] A.C. Anselmo, S. Mitragotri, Nanoparticles in the clinic: An update, *Bioengineering & Translational Medicine*. 4 (2019) e10143. <https://doi.org/10.1002/btm2.10143>.
- [18] E.J. Battegay, Angiogenesis: mechanistic insights, neovascular diseases, and therapeutic prospects, *J Mol Med*. 73 (1995) 333–346. <https://doi.org/10.1007/BF00192885>.
- [19] K. Pollinger, R. Hennig, A. Ohlmann, R. Fuchshofer, R. Wenzel, M. Breunig, J. Tessmar, E.R. Tamm, A. Goepferich, Ligand-functionalized nanoparticles target endothelial cells in retinal capillaries after systemic application, *Proceedings of the National Academy of Sciences*. 110 (2013) 6115–6120. <https://doi.org/10.1073/pnas.1220281110>.
- [20] R.B. Brem, S.G. Robbins, D.J. Wilson, L.M. O'Rourke, R.N. Mixon, J.E. Robertson, S.R. Planck, J.T. Rosenbaum, Immunolocalization of integrins in the human retina, *Invest Ophthalmol Vis Sci*. 35 (1994) 3466–3474.
- [21] S.G. Robbins, R.B. Brem, D.J. Wilson, L.M. O'Rourke, J.E. Robertson, I. Westra, S.R. Planck, J.T. Rosenbaum, Immunolocalization of integrins in proliferative retinal membranes, *Invest Ophthalmol Vis Sci*. 35 (1994) 3475–3485.
- [22] M. Friedlander, C.L. Theesfeld, M. Sugita, M. Fruttiger, M.A. Thomas, S. Chang, D.A. Cheres, Involvement of integrins alpha v beta 3 and alpha v beta 5 in ocular neovascular diseases, *Proc Natl Acad Sci U S A*. 93 (1996) 9764–9769. <https://doi.org/10.1073/pnas.93.18.9764>.
- [23] J.L. Perry, K.G. Reuter, J.C. Luft, C.V. Pecot, W. Zamboni, J.M. DeSimone, Mediating Passive Tumor Accumulation through Particle Size, Tumor Type, and Location, *Nano Lett*. 17 (2017) 2879–2886. <https://doi.org/10.1021/acs.nanolett.7b00021>.

- [24] E. Karathanasis, L. Chan, L. Karumbaiah, K. McNeeley, C.J. D’Orsi, A.V. Annapragada, I. Sechopoulos, R.V. Bellamkonda, Tumor Vascular Permeability to a Nanoprobe Correlates to Tumor-Specific Expression Levels of Angiogenic Markers, *PLOS ONE*. 4 (2009) e5843. <https://doi.org/10.1371/journal.pone.0005843>.
- [25] B.A. Nacev, J.O. Liu, Synergistic Inhibition of Endothelial Cell Proliferation, Tube Formation, and Sprouting by Cyclosporin A and Itraconazole, *PLoS ONE*. 6 (2011) e24793. <https://doi.org/10.1371/journal.pone.0024793>.
- [26] M. Capitão, R. Soares, Angiogenesis and Inflammation Crosstalk in Diabetic Retinopathy, *J Cell Biochem*. 117 (2016) 2443–2453. <https://doi.org/10.1002/jcb.25575>.
- [27] O. Dammann, Inflammation and Retinopathy of Prematurity, *Acta Paediatr*. 99 (2010) 975–977. <https://doi.org/10.1111/j.1651-2227.2010.01836.x>.
- [28] B. Heurtault, P. Saulnier, B. Pech, J. Proust, J. Benoit, A novel phase inversion-based process for the preparation of lipid nanocarriers, *Pharmaceutical Research*. 19 (2002) 875–880. <https://doi.org/10.1023/A:1016121319668>.
- [29] K.M. Connor, N.M. Krah, R.J. Dennison, C.M. Aderman, J. Chen, K.I. Guerin, P. Sapieha, A. Stahl, K.L. Willett, L.E.H. Smith, Quantification of oxygen-induced retinopathy in the mouse: a model of vessel loss, vessel regrowth and pathological angiogenesis, *Nat Protoc*. 4 (2009) 1565–1573. <https://doi.org/10.1038/nprot.2009.187>.
- [30] C.B. Kim, P.A. D’Amore, K.M. Connor, Revisiting the mouse model of oxygen-induced retinopathy, *Eye Brain*. 8 (2016) 67–79. <https://doi.org/10.2147/EB.S94447>.
- [31] A. Stahl, J. Chen, P. Sapieha, M.R. Seaward, N.M. Krah, R.J. Dennison, T. Favazza, F. Bucher, C. Löfqvist, H. Ong, A. Hellström, S. Chemtob, J.D. Akula, L.E.H. Smith, Postnatal Weight Gain Modifies Severity and Functional Outcome of Oxygen-Induced Proliferative Retinopathy, *Am J Pathol*. 177 (2010) 2715–2723. <https://doi.org/10.2353/ajpath.2010.100526>.
- [32] A. Ostrowski, D. Nordmeyer, A. Boreham, C. Holzhausen, L. Mundhenk, C. Graf, M.C. Meinke, A. Vogt, S. Hadam, J. Lademann, E. Rühl, U. Alexiev, A.D. Gruber, Overview about the localization of nanoparticles in tissue and cellular context by different imaging techniques, *Beilstein J. Nanotechnol*. 6 (2015) 263–280. <https://doi.org/10.3762/bjnano.6.25>.
- [33] K. Alhareth, C. Vauthier, C. Gueutin, G. Ponchel, F. Moussa, HPLC quantification of doxorubicin in plasma and tissues of rats treated with doxorubicin loaded poly(alkylcyanoacrylate) nanoparticles, *Journal of Chromatography B*. 887–888 (2012) 128–132. <https://doi.org/10.1016/j.jchromb.2012.01.025>.
- [34] A. Elsaesser, A. Taylor, G.S. de Yanés, G. McKerr, E.-M. Kim, E. O’Hare, C.V. Howard, Quantification of nanoparticle uptake by cells using microscopical and analytical techniques, *Nanomedicine*. 5 (2010) 1447–1457. <https://doi.org/10.2217/nnm.10.118>.

- [35] M. Monici, Cell and tissue autofluorescence research and diagnostic applications, in: *Biotechnology Annual Review*, Elsevier, 2005: pp. 227–256. [https://doi.org/10.1016/S1387-2656\(05\)11007-2](https://doi.org/10.1016/S1387-2656(05)11007-2).
- [36] T. Yardeni, M. Eckhaus, H.D. Morris, M. Huizing, S. Hoogstraten-Miller, Retro-orbital injections in mice, *Lab Animal*. 40 (2011) 155–160. <https://doi.org/10.1038/labon0511-155>.
- [37] R.W. Barbee, B.D. Perry, R.N. Re, J.P. Murgo, Microsphere and dilution techniques for the determination of blood flows and volumes in conscious mice, *American Journal of Physiology-Regulatory, Integrative and Comparative Physiology*. 263 (1992) R728–R733. <https://doi.org/10.1152/ajpregu.1992.263.3.R728>.
- [38] A.C. Riches, J.G. Sharp, D.B. Thomas, S.V. Smith, Blood volume determination in the mouse, *The Journal of Physiology*. 228 (1973) 279–284. <https://doi.org/10.1113/jphysiol.1973.sp010086>.
- [39] D. Hoarau, P. Delmas, David, Stéphanie, E. Roux, J.-C. Leroux, Novel Long-Circulating Lipid Nanocapsules, *Pharm Res*. 21 (2004) 1783–1789. <https://doi.org/10.1023/B:PHAM.0000045229.87844.21>.
- [40] Y.-N. Zhang, W. Poon, A.J. Tavares, I.D. McGilvray, W.C.W. Chan, Nanoparticle–liver interactions: Cellular uptake and hepatobiliary elimination, *Journal of Controlled Release*. 240 (2016) 332–348. <https://doi.org/10.1016/j.jconrel.2016.01.020>.
- [41] F.M. Mutlu, S.U. Sarici, Treatment of retinopathy of prematurity: a review of conventional and promising new therapeutic options, *Int J Ophthalmol*. 6 (2013) 228–236. <https://doi.org/10.3980/j.issn.2222-3959.2013.02.23>.
- [42] C. Lange, C. Ehlken, A. Stahl, G. Martin, L. Hansen, H.T. Agostini, Kinetics of retinal vaso-obliteration and neovascularisation in the oxygen-induced retinopathy (OIR) mouse model, *Graefes Arch Clin Exp Ophthalmol*. 247 (2009) 1205–1211. <https://doi.org/10.1007/s00417-009-1116-4>.
- [43] N. Ferrara, Role of vascular endothelial growth factor in regulation of physiological angiogenesis, *Am J Physiol Cell Physiol*. 280 (2001) C1358–C1366. <https://doi.org/10.1152/ajpcell.2001.280.6.C1358>.
- [44] C.C. Tokunaga, K.P. Mitton, W. Dailey, C. Massoll, K. Roumayah, E. Guzman, N. Tarabishy, M. Cheng, K.A. Drenser, Effects of Anti-VEGF Treatment on the Recovery of the Developing Retina Following Oxygen-Induced Retinopathy, *Invest. Ophthalmol. Vis. Sci*. 55 (2014) 1884–1892. <https://doi.org/10.1167/iovs.13-13397>.
- [45] S.M. Amin, A. Gonzalez, J. Guevara, C. Bolch, L. Andersen, W.C. Smith, S. Agarwal-Sinha, Efficacy of Aflibercept Treatment and Its Effect on the Retinal Perfusion in the Oxygen-Induced Retinopathy Mouse Model of Retinopathy of Prematurity, *ORE*. 64 (2021) 91–98. <https://doi.org/10.1159/000509380>.

- [46] P.C. Brooks, A.M.P. Montgomery, M. Rosenfeld, R.A. Reisfeld, T. Hu, G. Klier, D.A. Cheresh, Integrin $\alpha v \beta 3$ antagonists promote tumor regression by inducing apoptosis of angiogenic blood vessels, *Cell*. 79 (1994) 1157–1164. [https://doi.org/10.1016/0092-8674\(94\)90007-8](https://doi.org/10.1016/0092-8674(94)90007-8).
- [47] K. Meerovitch, F. Bergeron, L. Leblond, B. Grouix, C. Poirier, M. Bubenik, L. Chan, H. Gourdeau, T. Bowlin, G. Attardo, A novel RGD antagonist that targets both $\alpha v \beta 3$ and $\alpha 5 \beta 1$ induces apoptosis of angiogenic endothelial cells on type I collagen, *Vascular Pharmacology*. 40 (2003) 77–89. [https://doi.org/10.1016/S1537-1891\(02\)00339-7](https://doi.org/10.1016/S1537-1891(02)00339-7).
- [48] E. Chavakis, B. Riecke, J. Lin, T. Linn, R.G. Bretzel, K.T. Preissner, M. Brownlee, H.-P. Hammes, Kinetics of integrin expression in the mouse model of proliferative retinopathy and success of secondary intervention with cyclic RGD peptides, *Diabetologia*. 45 (2002) 262–267. <https://doi.org/10.1007/s00125-001-0727-z>.

Summary and conclusion

7.1 Summary

Non-physiological angiogenesis is a mutual complication of the proliferative forms of diabetic retinopathy (DR), age-related macular degeneration (AMD) and retinopathy of prematurity (ROP), and can lead to severe vision loss or even blindness. There is a great unmet need for more efficient and at the same time less invasive therapies for these diseases (**Chapter 1**).

The focus of this thesis was on the development of a nanoparticulate system for the targeted therapy of proliferative diseases of the posterior eye segment. This was realized with lipid nanocapsules (LNC) as versatile carriers for lipophilic drugs and a cyclic RGD-peptide as targeting motif to deliver cyclosporin A (CsA) and itraconazole (Itra) directly to their side of action (**Chapter 2**). CsA and Itra show promising synergistic antiangiogenic properties *in vitro*, but due to off-target side effects the free drugs are unlikely to make their way into the therapeutic portfolio for proliferative DR, AMD or ROP. The specific transport to proliferating endothelial cells by nanoparticles could help to overcome these obstacles.

LNC are highly appealing as nanocarriers, as they can be prepared in a solvent-free process with various sizes and surface modifications. Size and surface charge are known to essentially determine a nanoparticle's fate in the body. In this context, it was an important step in the present work to reveal the exact relation between LNC diameter and the ratio of surfactant and lipid phase in the LNC composition. With this knowledge, particles with defined diameters between approximately 20 and 100 nm could be precisely prepared. Additionally, it was shown that the surface charge of LNC can be switched to positive values by the introduction of an aminated poly(ethylene glycol) (PEG)-cetyl/stearyl alcohol. This might enhance the particle uptake into cells but was shown to come at the cost of a higher toxicity and was, therefore, not used in the further development of therapeutic LNC. A complete and stable encapsulation of CsA and Itra in LNC was achieved (**Chapter 3**).

The endothelial-cell specific targeting with LNC was realized by the conjugation of cyclo(RGDfC) to a PEGylated phospholipid and subsequent post-insertion into the LNC shell. The extent of RGD-grafting under different reaction conditions was evaluated, and it was demonstrated that previous chemical reduction of the peptide with tris(2-carboxyethyl)phosphine is not necessary and can even hamper the reaction. Utilizing the effect of fluorescence resonance energy transfer (FRET), it could be shown that once post-inserted, the phospholipid stays stably

anchored in the LNC shell. This is crucial for the peptide to fulfill its targeting task after systemic application. It was demonstrated *in vitro* that RGD-grafted LNC are massively taken up into endothelial cells, especially in the presence of serum, and that this enhanced cellular interaction does not adversely affect the tolerability of LNC (**Chapter 4**).

In the next step the effects of RGD-modified and drug-loaded lipid nanocapsules on endothelial cells were investigated *in-vitro*. RGD-LNC were able to completely inhibit vascular endothelial growth factor (VEGF)-induced proliferation even without encapsulated drugs, confirming that the c(RGDfC)-peptide not only enables the internalization into the target cells, but also exerts a therapeutic effect. Loading of LNC with Itra and CsA could not further enhance this effect on cultured cells. Also, the influence on the expression of hairy/enhancer of split-related protein 1 (HEY-1) and the angiogenesis associated migratory cell protein (AAMP), two markers for the intracellular effects of CsA and Itra, respectively, was unexpectedly low. One reason might be an insufficient drug release from LNC. But it needs to be kept in mind that, although *in-vitro* models are undoubtedly useful to gather information about the potential of a new therapeutic approach, their outcome highly depends on the specific experimental conditions. Especially in the tube formation model, a poor reproducibility obstructed significant results (**Chapter 5**).

Additionally, *in-vitro* models cannot fully represent the complex pathological mechanisms of proliferative eye diseases and the role of nanoparticle biodistribution so far. For this reason, the *in-vivo* distribution and therapeutic effect of LNC was further investigated in animal experiments. It was demonstrated that RGD-LNC strongly accumulate in the retinal vessels after intravenous administration. A mouse-model of oxygen-induced retinopathy was utilized to mimic the pathological process of retinal neovascularization. In this model, a single injection of RGD-LNC loaded with cyclosporin A and itraconazole significantly reduced the development of tufting and vasodilatation without impeding retinal reperfusion (**Chapter 6**).

7.2 Conclusion

This work underlines the potential of LNC as carrier platform for diverse therapies due to their versatile possibilities for size and surface charge adjustment and functionalization. It was confirmed that RGD-grafted LNC are a highly promising approach for the treatment of proliferative ophthalmic diseases. The RGD-peptide enables a targeted accumulation in proliferating endothelial cells and RGD-LNC have been demonstrated to be capable of blocking VEGF-induced cell proliferation. They were shown to be massively taken up into endothelial cells *in vitro* and to strongly accumulate even in healthy retinal vessels *in vivo*. This allows active ingredients to be delivered selectively to pathological neovascularizations while avoiding side-effects on off-target tissues. For the combination of CsA and Itra, this is highly appealing. The drugs were successfully co-encapsulated in LNC. The downside of this stable encapsulation is that the therapeutic effect of drug-loaded LNC might be hampered by an insufficient drug release. Nevertheless, a single injection of drug-loaded RGD-LNC significantly reduced pathological vessel growth in oxygen-induced retinopathy. These results underpin that RGD-modified nanoparticles bear great potential as innovative therapy for neovascular ophthalmic diseases.

Appendix

Abbreviations

AAMP	angiogenesis associated migratory cell protein
AGE	advanced glycation end products
AMD	age-related macular degeneration
ANOVA	analysis of variance
AVZ	avascular zone
basal medium	Endothelial Cell Basal Medium MV
BRB	blood retina barrier
BSA	bovine serum albumin
c(RGDfC)	cyclic arginine-glycine-aspartate-D-phenylalanine-cysteine peptide
CLSM	confocal laser scanning microscopy
CNV	choroidal neovascularization
cryo-TEM	cryogenic transmission electron microscopy
CsA	cyclosporin A
CsIt	combination of cyclosporin A and itraconazole
CsIt-LNC	lipid nanocapsules loaded with cyclosporin A and itraconazole
CTGF	connective tissue growth factor
cyclo(RGDfN(Me)V)	cyclic arginine-glycine-aspartate-D-phenylalanine-N-methylvaline peptide
DCM	dichloromethane
DCP	deep capillary plexus
DEE	diethyl ether
DiD	1,1'-dioctadecyl-3,3,3',3'-tetramethylindodicarbocyanine
DiI	1,1'-Dioctadecyl-3,3,3',3'-tetramethylindocarbocyanine
DiO	3,3'-dioctadecyloxacarbocyanine

DLS	dynamic light scattering
DMSO	dimethyl sulfoxide
DNA	deoxyribonucleic acid
DPBS	Dulbecco's phosphate buffered saline
DR	diabetic retinopathy
DSPE	distearoyl-sn-glycero-phosphoethanolamine
DSPE-mPEG	1,2-distearoyl-sn-glycero-3-phosphoethanolamine-N-[methoxy(PEG)-2000]
DSPE-PEG-Mal	1,2-distearoyl-sn-glycero-3-phosphoethanolamine-N-[maleimide(polyethylene glycol)-2000]
DTT	dithiothreitol
EDTA	ethylenediamine-tetraacetate
EMEM	Eagle's Minimum essential Medium
FACS	flow cytometry (fluorescence-activated cell sorting)
FCS	fetal calf serum
FRET	fluorescence resonance energy transfer
GAPDH	glyceraldehyde 3-phosphate dehydrogenase
GCL	ganglion cell layer
GCLP	ganglion cell layer plexus
growth medium	Endothelial Cell Growth Medium MV
HDMEC	human dermal microvascular endothelial cells
HESR-1 / HEY-1	hairy/enhancer of split-related protein 1
HPLC	high pressure liquid chromatography
iBRB	inner blood retina barrier
IC50	half-maximal inhibitory concentration
ICP	intermediate capillary plexus

INL	Inner nuclear layer
IPL	inner plexiform layer
IS	photoreceptor inner segments
Itra	itraconazole
LPC	laser photocoagulation
LNC	lipid nanocapsules
MCT	medium-chain triglycerides
mPEG-LNC	lipid nanocapsules post-inserted with DSPE-mPEG
MPS	mononuclear phagocyte system
MTT	3-(4,5-dimethylthiazol-2-yl)-2,5-diphenyl tetrazolium bromide
MWCO	molecular weight cut off
NFAT	nuclear factor of activated T-cells
NFL	nerve fiber layer
NFLP	nerve fiber layer plexus
NMR	nuclear magnetic resonance
NTA	nanoparticle tracking analysis
NV	neovascularization
oBRB	outer blood retina barrier
OIR	oxygen-induced retinopathy
ONL	outer nuclear layer
OPL	outer plexiform layer
OS	photoreceptor outer segments
PCR	polymerase chain reaction
PDI	polydispersity index
PDT	photodynamic therapy

PEG	poly(ethylene glycol)
PI	post insertion
qPCR	quantitative polymerase chain reaction
RGD	arginine-glycine-aspartate peptide
RGD-CsIt-LNC	lipid nanocapsules modified with RGD and loaded with cyclosporin A and itraconazole
RGD-LNC	lipid nanocapsules with RGD-modification
RNA	ribonucleic acid
ROP	retinopathy of prematurity
RPCP	radial peripapillary capillary plexus
RPE	retinal pigment epithelium
RT-PCR	reverse transcription PCR
S	Sympatens
SA	Sympatensamine
SAMSA-fluorescein	5-((2-(and-3)-S-(acetylmercapto) succinoyl) amino) fluorescein
SVC	superficial vascular complex
TCEP	tris(2-carboxyethyl)phosphine
THF	tetrahydrofuran
TRIS	Tris(hydroxymethyl)aminomethane
UV	ultraviolet
VEGF	vascular endothelial growth factor
VEGFR-2	vascular endothelial growth factor receptor 2
Z-Av	Z-Average

Curriculum Vitae

Personal Information

Name	Alexandra Maria Ławrowska, née Haunberger
Date of birth	19 th July 1989
Place of birth	Pfarrkirchen
Nationality	German

Professional Training, Scientific Education and Work Experience

Since 01/2018	Pharmacist, University Hospital Regensburg
01/2014 – 01/2018	PhD candidate, Department of Pharmaceutical Technology, University of Regensburg
12/2014 – 02/2018	Pharmacist at Marien Apotheke Seubersdorf
12/2013	Licensure as Pharmacist, Regensburg
05/2013 – 10/2013	Practical Training Marien-Apotheke Lappersdorf
11/2012 – 04/2013	Practical Training University Hospital Regensburg
2008 – 2013	Studies of Pharmacy, University of Regensburg

School Education

06/2008	Abitur (General qualification for university entrance)
1999 – 2008	Grammar School, Karl-von-Closen-Gymnasium, Eggenfelden
1995 – 1999	Primary School, Mitterskirchen

List of Publications

Peer-reviewed Publications

A. Haunberger, A. Goepferich, Nanoparticles Targeting Retinal and Choroidal Capillaries In Vivo, in: B.H.F. Weber, T. Langmann (Eds.), Retinal Degeneration: Methods and Protocols, Springer, New York, NY, 2019: pp. 391–404. https://doi.org/10.1007/978-1-4939-8669-9_25.

M. Bohley, A. Haunberger, A.M. Goepferich, Intracellular availability of poorly soluble drugs from lipid nanocapsules, European Journal of Pharmaceutics and Biopharmaceutics. 139 (2019) 23–32. <https://doi.org/10.1016/j.ejpb.2019.03.007>.

R. Hennig, S. Kuespert, A. Haunberger, A. Goepferich, R. Fuchshofer, Cyclic RGD peptides target human trabecular meshwork cells while ameliorating connective tissue growth factor-induced fibrosis, J Drug Target. 24 (2016) 952–959. <https://doi.org/10.3109/1061186X.2016.1163709>.

R. Hennig, A. Ohlmann, J. Staffel, K. Pollinger, A. Haunberger, M. Breunig, F. Schweda, E.R. Tamm, A. Goepferich, Multivalent nanoparticles bind the retinal and choroidal vasculature, Journal of Controlled Release. 220, Part A (2015) 265–274. <https://doi.org/10.1016/j.jconrel.2015.10.033>.

Conference Abstracts and Poster Presentations

A. Haunberger, A. Goepferich, Precise adjustment of size and surface charge of lipid nanocapsules, 2nd European Conference on Pharmaceutics, Krakow, Poland, 2017.

A. Haunberger, A. Goepferich, Delivery system for the targeting of ocular neovascularizations, DPhG Annual Meeting, Munich, Germany, 2016.

Acknowledgements

At this point I would like to express my gratitude to all those who have supported me over the last years and who contributed to the completion of this thesis.

First and foremost, I would like to sincerely thank my supervisor Prof. Dr. Achim Göpferich for giving me the opportunity to be part of his research group and to work on this project. I am deeply grateful for his continued enthusiasm, inspiring ideas, insightful discussions and his patience. Furthermore, I want to express my thanks for the opportunity to attend several national and international conferences.

I offer my thanks to Prof. Dr. Miriam Breunig and Dr. Ferdinand Brandl for their extremely valuable scientific input and Prof. Dr. Barbara Braunger and her research group for the advice and support with animal experiments.

Moreover, I would like to thank my colleagues in the research group of the Department of Pharmaceutical Technology for the scientific exchange, constant motivation, and positive working atmosphere. Of course, I am also grateful for the good times we spent together outside the lab and the ongoing friendship I share with many of them. Special thanks go to

- Dr. Manuel Gregoritz and Dr. Kathrin Gregoritz for inspiring conversations, productive gym sessions and their friendship.
- Dr. Robert Hennig for the introduction into cell culture and nanoparticle modification and for being a very pleasant lab mate with a good taste in music.
- Sebastian Beck for the warm lab atmosphere, his uncomplicated manner and authentic character.
- Dr. Michael Backofen for his HPLC expertise, and for always being eager to organize social events after work.
- Dr. Johanna Lempp and Dr. Michaela Stretz for sharing the trouble and joy of research with me and for motivation through tough times.
- Sabine Hofmeister for her very helpful and reliable lab assistance.
- Marilena Bohley who continued this project with extraordinary dedication.

Further thanks go to Eva Wrobel for her support in organizational matters, and to Renate Liebl, Viktoria Eismann, Andrea Blaimer, Angelika Berie, Silvia Babl, Edith Schindler, and Stefan Kolb

for their technical assistance and advice in practical matters. Moreover, I thank Margit Schimmel for her assistance with the electron microscopy.

The financial support from the German Research Foundation (DFG, Grant GO 565/18-1) for this project is gratefully acknowledged.

My warmest thanks go to my husband Robert for his constant encouragement, patience, and the inspiring scientific conversations beyond the boundaries of our respective scientific fields.

Finally, I want to express my deep gratitude towards my family for their unconditional love and support. Most of all, I would like to thank my parents, who have encouraged my curiosity about nature from childhood on and have always believed in me.

Statement in Lieu of an Oath

I hereby confirm that I have written this thesis on my own and that I have not used any other media or materials than the ones referred to in this thesis.

Regensburg,

.....

Alexandra Ławrowska